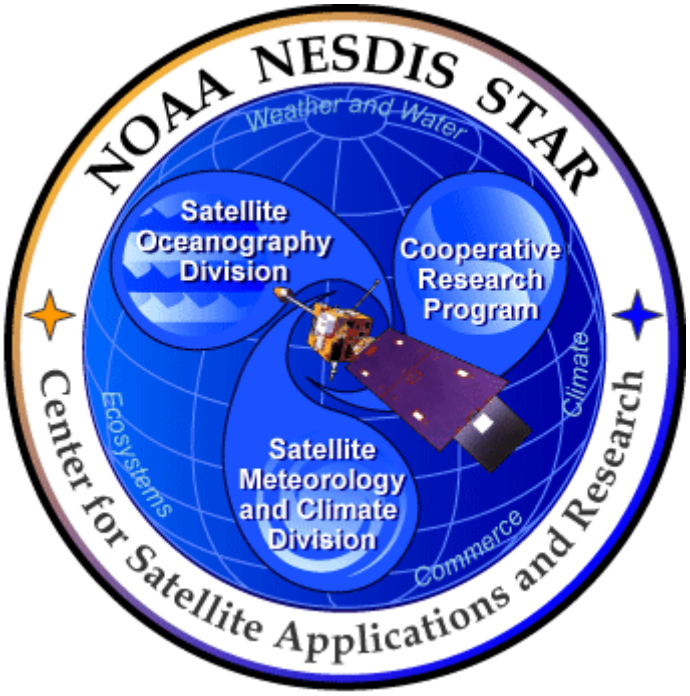

NOAA NESDIS
CENTER for SATELLITE APPLICATIONS and RESEARCH

Enterprise Algorithm Theoretical Basis Document For Derived Motion Winds

Jaime Daniels, NOAA/NESDIS/STAR
Wayne Bresky, Andrew Bailey, Americo Allegrino, IMSG, Inc.
Steve Wanzong, Chris Velden, Howard Berger, UW/CIMSS

Version 4.2
June 2024

TABLE OF CONTENTS

LIST OF FIGURES

LIST OF TABLES

LIST OF ACRONYMS

ABI – Advanced Baseline Imager
AIADD – Algorithm Interface and Ancillary Data Description
AIT – Algorithm Integration Team
AQC - Automatic Quality Control
ASCII - American Standard Code for Information Interchange
ATBD – Algorithm Theoretical Basis Document
AVHRR - Advanced Very High-Resolution Radiometer
AWG – Algorithm Working Group
CC – Cross Correlation
CONUS – Continental United States
CRTM – Community Radiative Transfer Model
CTP – Cloud-top Pressure
NWP – Numerical Weather Prediction
DMW – Derived Motion Winds
DMWA – Derived Motion Winds Algorithm
EE – Expected Error
EUMETSAT - European Organization for the Exploitation of Meteorological Satellites.
FD – Full Disk
F&PS – Functional and Performance Specification
FPM – Focal Plane Module
GFS – Global Forecast System
GOES – Geostationary Operational Environmental Satellite
GPO – GOES-R Program Office
IGFOV – Instantaneous Geometric Field of View
INR – Image Navigation and Registration
IO – Input/Output
IR – Infrared
JPSS – Joint Polar Satellite System
LWIR – Longwave Infrared
LZA – Local Zenith Angle
METOP - Meteorological Operational Satellite
MRD – Mission Requirements Document
MSG – Meteosat Second Generation
MODIS - Moderate Resolution Imaging Spectroradiometer
MVD – Mean Vector Difference
MSFC – Marshall Space Flight Center
NASA – National Aeronautics and Space Administration
NCSA – National Center for Super Computing Applications
NCEP – National Centers for Environmental Prediction
NESDIS – National Environmental Satellite, Data, and Information Service
NOAA – National Oceanic and Atmospheric Administration
NPP – National Polar-Orbiting Partnership
NWP – Numerical Weather Prediction
OSDPD – Office of Satellite Data Processing and Distribution

PDF – Probability Distribution Function
PG – Product Generation
PORD – Performance Operational Requirements Document
QC – Quality Control
QI – Quality Indicator
RAOB – Radiosonde Observation
RMSE – Root Mean Square Error
SD – Standard Deviation
SDR - Sensor Data Records
SEVIRI – Spinning Enhanced Visible Infrared Imager
SOI – Successive Order of Interaction
SSD – Sum of Squared Differences
STAR – Center for Satellite Applications and Research
SWIR – Shortwave Infrared
TELL – Tracking Error Lower Limit
TOA – Top of Atmosphere
TRR – Test Readiness Review
VAGL - Vendor Allocated Ground Latency
VIS – Visible
WRF – Weather Research and Forecasting

1 INTRODUCTION

1.1 Purpose of This Document

The derived motion wind Algorithm Theoretical Basis Document (ATBD) provides a description of and the physical basis for the estimation of atmospheric wind from observations from instruments in satellites that NESDIS uses on an operational basis to fulfill its mission. These include the Advanced Baseline Imager (ABI) flown on the GOES-R series of NOAA geostationary meteorological satellites, the Visible Infrared Imaging Radiometer Suite (VIIRS) flown on National Aeronautics and Space Administration's (NASA) Suomi National Polar-orbiting Partnership (NPP) meteorological satellite and NOAA's Joint Polar Satellite System (JPSS) series of polar orbiting satellites, the Advanced Himawari Imager (AHI) flown on the Himawari series of Japan's Meteorological Agency's (JMA) geostationary meteorological satellites, and the Advanced Very High Resolution Radiometer (AVHRR) flown on EUMETSAT's Meteorological Operational Satellite (MetOP) series of polar orbiting satellites. The Derived Motion Wind Algorithm (DMWA) estimates not only the speed and direction of identified tracers (clouds and/or moisture gradients), but also their height in the atmosphere. This document also provides details on the performance of the DMW products as measured against correlative wind measurements from other observing systems.

1.2 Who Should Use This Document

The intended users of this document are those interested in understanding the physical basis of the algorithms and how to use the output of this algorithm to optimize the use of the derived motion wind output for a particular application. This document also provides information useful to anyone maintaining or modifying the original algorithm.

1.3 Inside Each Section

This document is broken down into the following main sections.

System Overview: Provides relevant details of the DMWA system and gives a brief description of the products generated by the algorithm.

Algorithm Description: Provides a detailed description of the DMWA including its physical basis, its input and its output.

Algorithm Outputs and Verification: Provides a description of the output data and verification of retrieved winds performance using correlative data sources.

Practical Considerations: Provides a description of algorithm programming and quality control considerations.

Assumptions and Limitations: Provides an overview of the current limitations of the approach and gives the plan for overcoming these limitations with further algorithm development.

1.4 Related Documents

- GOES-R Functional and Performance Specification (F&PS) Document
- GOES-R Ground Segment Mission Requirements Document (MRD)
- Joint Polar Satellite System (JPSS) Level 1 Requirements Document Supplement (L1RDS)
- Joint Polar Satellite System (JPSS) JPSS Level 1 Requirements - J2 Follow-On Document
- Joint Polar Satellite System (JPSS) National Environmental Satellite, Data, and Information Service (NESDIS) Environmental Satellite Processing Center (ESPC)
- Requirements Document (JERD) Volume 2: Science Requirements Document

1.5 Revision History

Version 0.1 of this document was created by members of the GOES-R winds algorithm development team and its intent to accompany the delivery of the version 1.0 derived motion winds algorithm to the GOES-R AWG Algorithm Integration Team (AIT). (May 2008)

Version 0.2 of this document was created by members of the GOES-R winds algorithm development team and its intent is to accompany the delivery of the version 3.0 derived motion winds algorithm to the GOES-R AWG Algorithm Integration Team (AIT). (June 2009)

Version 1.0 of this document was created by Jaime Daniels, Wayne Bresky, and Steve Wanzong in response to internal AWG review items. This version of the ATBD still accompanies the version 3.0 of the derived motion winds algorithm to the GOES-R AWG AIT. (September 30, 2009)

Version 1.1 of this document was created by Jaime Daniels, Wayne Bresky, and Steve Wanzong and its intent is to accompany the delivery of the version 4.0 derived motion winds algorithm to the GOES-R AWG Algorithm Integration Team (AIT). (June 2010)

Version 1.2 of this document was created by Jaime Daniels, Wayne Bresky, and Steve Wanzong and its intent is to accompany the delivery of the version 5.0 derived motion winds algorithm to the GOES-R AWG Algorithm Integration Team (AIT). (August 2010)

Version 2.0 of this document was created by Jaime Daniels, Wayne Bresky, and Steve Wanzong in response to internal AWG and STAR review items. This version of the ATBD still accompanies the version 5.0 of the derived motion winds algorithm to the GOES-R AWG AIT. (September 2010)

Version 2.1 of this document was created by Jaime Daniels, Wayne Bresky, and Steve Wanzong to reflect corrections/additional information as a result of technical interactions the winds team had with AER over the past year. (July 2012)

Version 3.1 of this document was created by Jaime Daniels, Wayne Bresky, and Steve Wanzong to update the section on the gross forecast difference test and the cloud top band 8 height assignment method.

Version 3.2 of this document was created by Jaime Daniels, Wayne Bresky, and Steve Wanzong to detail the changes made to the algorithm to mitigate the impacts of the GOES-17 ABI Focal Plane Module (FPM) warming on the quality and generation of the G-17 wind products.

Version 3.3 of this document was created by Jaime Daniels, Andrew Bailey and Americo Allegrino to update the outputs and verification section replacing pre-launch proxy data outputs (SEVERI and Simulated GOES-R data) with current operational data from GOES-16 and 17.

Version 4.0 of this document was created by Jaime Daniels and Andy Bailey to update early sections of this ATBD to capture all geostationary and low earth orbiting satellites and instruments that the DMWA is applied to operationally at NOAA. This version also captures descriptions of the very latest updates to the DMWA and is considered the Enterprise version of the DMW Algorithm Theoretical Basis Document (ATBD).

Version 4.1 of this document was created by Andy Bailey to update algorithm changes related to Satellite Zenith Angle and the addition of a QI (with no forecast term), ‘QINF,’ to the algorithm output. This version captures descriptions of the very latest updates to the DMWA and is considered the Enterprise version of the DMW Algorithm Theoretical Basis Document (ATBD).

Version 4.2 of this document was created by Andy Bailey to include VIIRS shortwave infrared polar winds.

2 OBSERVING SYSTEM OVERVIEW

This section will describe the products generated by NESDIS' Enterprise Derived Motion Winds Algorithm (DMWA) and the requirements it places on the operational sensors.

2.1 Products Generated

The DMWA employs a sequence of images to arrive at an estimate of atmospheric motion for a set of targeted tracers viewed in selected spectral bands. These targets include well defined cloud edges or moisture gradients. Tables 1 provides the specifications for the derived motion winds product for each of the sensors used operationally at NESDIS.

Table 1: Requirements for the Derived Motion Winds Product

Derived Motion Winds	**Specification**
Geographic Coverage	***ABI:*** Full Disk, CONUS, Mesoscale ***AHI:*** Full Disk ***VIIRS:*** Poleward of 55 degrees latitude ***AVHRR-3:*** Poleward of 55 degrees latitude
Vertical Resolution	Cloud Motion Vector winds: At cloud tops; Clear-Sky Water Vapor winds: 200 mb
Horizontal Resolution	***ABI:*** FD: 38km; CONUS: 38km; Meso: 38km ***AHI:*** FD: 38 km ***VIIRS:*** 19km ***AVHRR-3:*** 19 km
Mapping Accuracy	***ABI:*** 0.5 pixel ***AHI:*** 0.5 pixel ***VIIRS:*** 0.4 km (at NADIR); 1.5km (Edge of Scan) ***AVHRR-3:*** 0.5km
Measurement Range	Speed: 0-300 kts (3- 155 m/s) & Direction: 0 to 360 degrees
Measurement Accuracy	Mean Vector Difference: 7.5 m/s
Refresh Rate/Coverage Time	***ABI (Mode 6):*** FD: "60 mins (based on a single set of 3 sequential images 5 or more minutes apart); CONUS: 15 mins; Meso: 5 minutes ***ABI (Flex Mode 3)***: FD: "60 mins (based on a single set of 3 sequential images 15 minutes apart) ***ABI (Mode 4):*** FD: "60 mins (based on a single set of 3 sequential images 5 or more minutes apart); CONUS: 15 mins (subsected from FD); Meso (subsected from FD): 5 minutes ***AHI:*** 10 mins ***VIIRS:*** Orbit (101 mins) ***AVHRR-3:*** Orbit (101 mins)

VAGL (Mode 3 or 6)	***ABI:*** 806s ***AHI:*** 30 min ***VIIRS:*** 120 mins ***AVHRR-3:*** 120 mins
Measurement Precision	4.2 m/sec
Product Qualifiers	
Temporal Coverage	Day and night
Product Extent	Quantitative out to at least 70 degrees LZA and qualitative beyond
Cloud Cover Conditions	Clear conditions down to feature of interest associated with threshold accuracy
Product Statistics	Over specified geographic area

2.2 Instrument Characteristics

The DMW algorithm will be applied to an array of GOES-R Series ABI, Himawari Series AHI, S-NPP and JPSS Series VIIRS, or Metop Series AVHRR-3 pixels belonging to a target scene to be tracked in time. Tables 2a-d summarize the channels used by the DMWA.

Table 2a. ABI Channel numbers, associated wavelengths, resolution, and channels used by the DMWA.

Channel Number	*Central Wavelength (um)*	*Nominal subsatellite IGFOV (km)*	*Used in DMWA*
1	0.47	1	
2	0.64	0.5	✓
3	0.86	1	
4	1.38	2	
5	1.61	1	
6	2.26	2	
7	3.9	2	✓
8	6.15	2	✓
9	7.0	2	✓
10	7.4	2	✓
11	8.5	2	
12	9.7	2	
13	10.35	2	
14	11.2	2	✓
15	12.3	2	
16	13.3	2	

Table 2b. AHI channel numbers, associated wavelengths, resolution, and channels used by the DMWA algorithm.

Channel Number	*Central Wavelength (um)*	*Nominal subsatellite IGFOV (km)*	*Used in DMWA*
1	0.47	1	
2	0.51	1	
3	0.64	0.5	✓
4	0.86	1	
5	1.61	2	
6	2.26	2	
7	3.9	2	✓
8	6.24	2	✓
9	6.94	2	✓
10	7.34	2	✓
11	8.59	2	
12	9.64	2	
13	10.41	2	
14	11.24	2	✓
15	12.38	2	
16	13.28	2	

Table 2c. VIIRS channel numbers, associated wavelengths, resolution, and channels used by the DMWA algorithm.

Channel Number	*Central Wavelength (um)*	*Nominal subsatellite IGFOV (km)*	*Used in DMWA*
M1	0.412	0.75	
M2	0.445	0.75	
M3	0.488	0.75	
M4	0.555	0.75	
M5	0.672	0.75	
M6	0.746	0.75	
M7	0.865	0.75	
M8	1.240	0.75	
M9	1.378	0.75	
M10	1.61	0.75	
M11	2.25	0.75	✓
M12	3.7	0.75	
M13	4.05	0.75	
M14	8.55	0.75	
M15	10.763	0.75	✓

M16	12.013	0.75	
DNB	0.7	0.75 (across full scan)	
I1	0.64	0.375	
I2	0.865	0.375	
I3	1.61	0.375	
I4	3.74	0.375	
I5	11.45	0.375	

Table 2d. AVHRR-3 channel numbers, associated wavelengths, resolution, and channels used by the DMWA algorithm.

Channel Number	*Central Wavelength (um)*	*Nominal subsatellite IGFOV (km)*	*Used in DMWA*
1	0.630	1.08	
2	0.865	1.08	
3a	1.610	1.08	
3b	3.740	1.08	
4	10.8	1.08	✓
5	12.0	1.08	

3 ALGORITHM DESCRIPTION

A complete description of the DMWA algorithm at the current level of maturity (which will improve with each revision) is provided in this section.

3.1 Algorithm Overview

The enterprise DMWA is based on the DMWA developed for the GOES-R ABI instrument (Bresky et al, 2013, Daniels et al, 2012). There are four basic steps involved in the process of generating DMWs for any satellite instrument:

Step 1: Obtain a set of at least three precisely calibrated, navigated and co-registered images (ie., L1b data) in a selected spectral channel.

Under nominal instrument operating conditions, this step is straightforward with the only conditions being the satellite, instrument channel, image times, and image sectors or granules to use. The GOES-17 operating conditions, however, are not considered nominal due to the ABI cooling system anomaly (Wang et al, 2020). As a

result, the following DMWA mitigations are exercised when generating winds from GOES-17 ABI observations:

- Read the ABI maximum Focal Plane Module (FPM) temperatures from the input L1b data (all three tracking images) and compare the warmest of the three values to a band-dependent FPM temperature threshold established for ABI bands 7-16.
- If the ABI maximum FPM temperature associated with any of the three images exceeds the temperature threshold for that band, the DMWA processing is terminated after the creation of an output file with zero good winds.
- In the case of band 14, if the FPM temperature threshold is exceeded for any of the three images, a backup set of band 13 images may be used as a replacement, provided the maximum FPM temperature is below the specified ABI band 13 FPM temperature threshold.

Step 2: Locate and select a set of suitable target scenes in the middle image domain

A target scene is represented by an NxN array of pixels that defines a suitable feature in the image whose movement can be tracked in time. The size of this array is a function of the spatial and temporal resolution of the imagery and the scale of the intended feature to be tracked. Both cloudy and clear target scenes are selected by the DMWA. One of the challenges of deriving atmospheric motion winds operationally from satellites is to determine and utilize imagery taken at frequencies appropriate to the scales resolvable by operational numerical weather prediction systems, while at the same time, meeting production demands that require routine full disk coverage.

Step 3: For each image pair in the image triplet, use a correlation algorithm to derive the motion most representative for the target scene

When tracking cloudy target scenes, a correlation algorithm is used in conjunction with a nested tracking algorithm where the following steps are performed:

- Apply the correlation algorithm to smaller sub-targets within each target scene in order to derive a set of local motion vectors for each target scene
- Analyze the local motion field with a cluster analysis algorithm in order to extract the dominant motion within the target scene.
- Assign a height to the derived winds using pixel level information (obtained from running a precursor cloud algorithm) from the dominant cluster.

When tracking moisture gradients in clear target scenes, the nested tracking algorithm is disabled and the following steps performed:

- Assign a height to the tracer using a cold sample of pixels.
- Apply the correlation algorithm to the entire target in order to arrive at a motion vector
- Average the vectors derived from each of the image pairs to arrive at the final set of DMWs

Step 4: Perform quality control on the DMWs and assign quality indicators to each of the DMWs.

Quality control of retrieved DMWs is done via the application of numerous target selection, feature tracking, and height assignment error checks and via calculation of quality indicators for each retrieved DMW. The

In addition to the DMW quality control procedures described above, the DMWA captures mitigation processing conditions when processing winds from the GOES-17 ABI. More specifically, the winds product Data Quality Flag (DQF) captures the DMWA mitigation condition for band selection used in the feature tracking step and the mitigation condition taken by the upstream cloud height algorithm to produce cloud heights (used to assign heights to DMWs).

3.2 Processing Outline

In order to estimate motion, one must have a sequence of images separated by some, preferably fixed and relatively short, time interval. The DMW algorithm described here uses a sequence of three images to compute a pair of vector displacements (one for an earlier time step and one for a later time step) that are averaged to obtain the final motion estimate. The DMWA uses the middle image to perform the initial feature targeting, then searches the before and after images for traceable (coherent) features to derive motion estimates.

For geostationary satellite winds processing the image sectors are fixed with coverage defined by FD, CONUS, or Meso sectors. For low earth orbiting satellites polar winds processing, three sequential orbital images (remapped to a polar stereographic projection) are used and winds are generated in the area where these three orbits overlap. Figure 1 illustrates the overlap (gray area) area associated with three sequential orbits where winds can be generated.

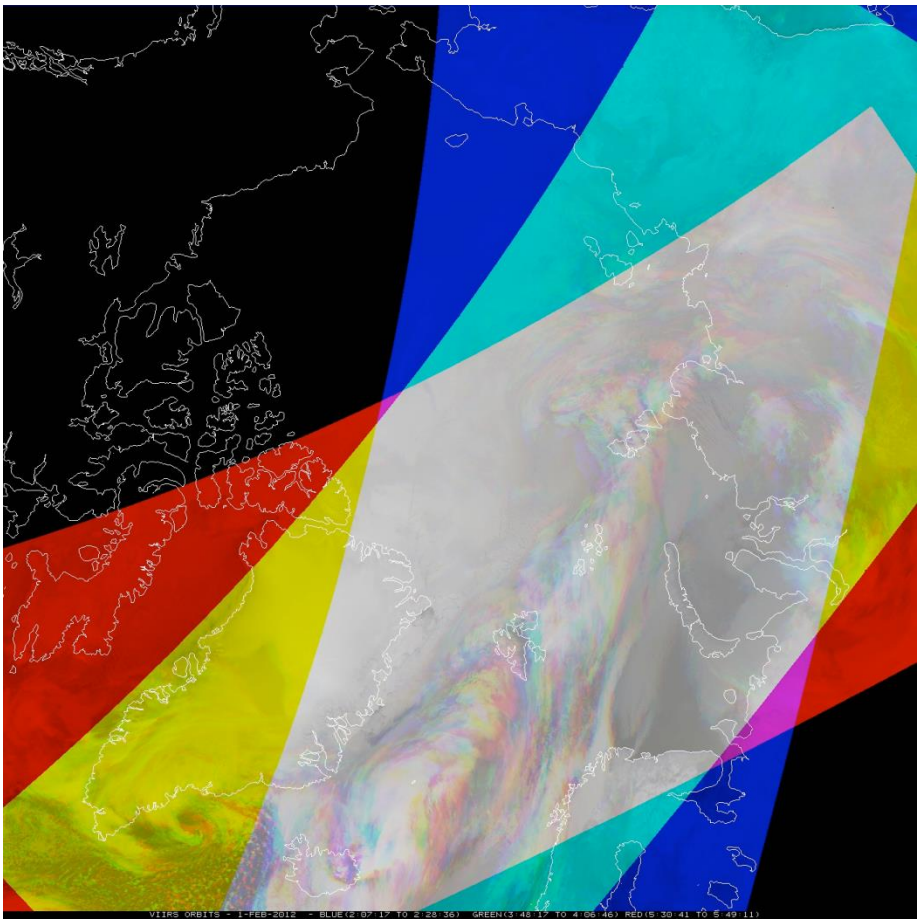
Figure 1. Three sequential orbits used in polar winds processing. The gray region represents the overlap in three sequential orbits where the polar winds can be derived.

The basic processing outline for the DMWA is summarized in Figure 2. The algorithm is designed to run on segments of data provided by the framework and consisting of multiple scan lines. Processing begins after a data buffer containing the brightness temperature values from three consecutive images is filled. The data buffer also contains output from the cloud mask and cloud height algorithms (coincident with the time of the middle image of the image triplet) which must execute before the DMWA.

Once the data buffer is full, the middle portion of the buffer is divided into small "target" scenes NxN pixels and each scene is analyzed to determine if it is a suitable tracer. Only the brightness temperature field from the middle image time is processed for targets and it is these targets that will be tracked over time to derive the motion. Processing only the middle portion of the buffer allows for the features to drift over time but still remain within the domain of the buffer. Within each target scene, the algorithm locates the strongest 2-D gradient in the brightness temperature field and re-centers the NxN target scene at this location. A brightness temperature gradient threshold is used to prevent target selection on very weak gradients.

After the target scene is re-centered on the maximum gradient, tests are performed to determine whether or not the scene would be a suitable tracer. These tests eliminate target

scenes that lack the gradients necessary to track reliably while also removing scenes that are suspected to contain multiple cloud layers.

If a potential tracer makes it through the target quality control, a search region, much larger in size than the target scene, is defined in each of the tracking images. At this point, depending on the channel being processed, one of two tracking strategies is employed. Both strategies use the Sum of Squared Differences (SSD) similarity measure to locate the target scene in the preceding and succeeding images.

When processing cloud-top features from the 0.65, 3.9, 6.2, or 11.2um channels, a tracking strategy called nested tracking is used to estimate motion. In this approach, a small 5x5 pixel box is "nested" within the outer target scene and a local motion vector is derived at each interior pixel. A 2-pixel offset is used near the boundary of the outer target scene. The field of local motion vectors that results is then analyzed with a cluster analysis algorithm to find the dominant motion. The dominant motion is computed by averaging the displacements associated with the largest motion cluster found by using a cluster analysis algorithm. The wind vector is then assigned a representative height after examining the cloud top pressure or brightness temperatures associated with the pixels in the largest cluster. When processing the visible, SWIR or LWIR channels, a median cloud top pressure is found by examining the cloud-top pressure values of all pixels in the largest cluster. When processing one of the three water vapor channels the height assignment process is slightly different. Here, the water vapor channel brightness temperature values are examined and a median temperature is found from the pixels in the largest cluster. The median brightness temperature is then compared to a GFS forecast temperature profile to find the pressure where the two values agree. The pressure at which these two values agree serves as the representative height of the derived motion wind.

When processing the clear sky portions of a water vapor (6.2um, 7.0um or 7.3um) image, the strategy for tracking features is more conventional. For these cases, the target is assigned a height before it is tracked. The height is computed using a sample of pixels from the coldest portion of the scene. After the target is assigned a height, a search is performed to find the closest match of the target in the preceding and succeeding images in the image triplet. This conventional approach produces a single motion vector associated with the motion of the entire target scene.

Both tracking approaches use a forecast wind (from the center of the target scene) to locate and place the center of the search region in the next image. This practice of using the forecast to "guide" the search serves two purposes. First, it reduces the number of "false positives" in the tracking step. Secondly, it minimizes the computational expense of the search.

During the tracking process, correlation thresholds are applied to screen out false positives. When nested tracking is employed, only matching scenes possessing a correlation score of 0.8 or higher (1.0 is perfect) are allowed to influence the final

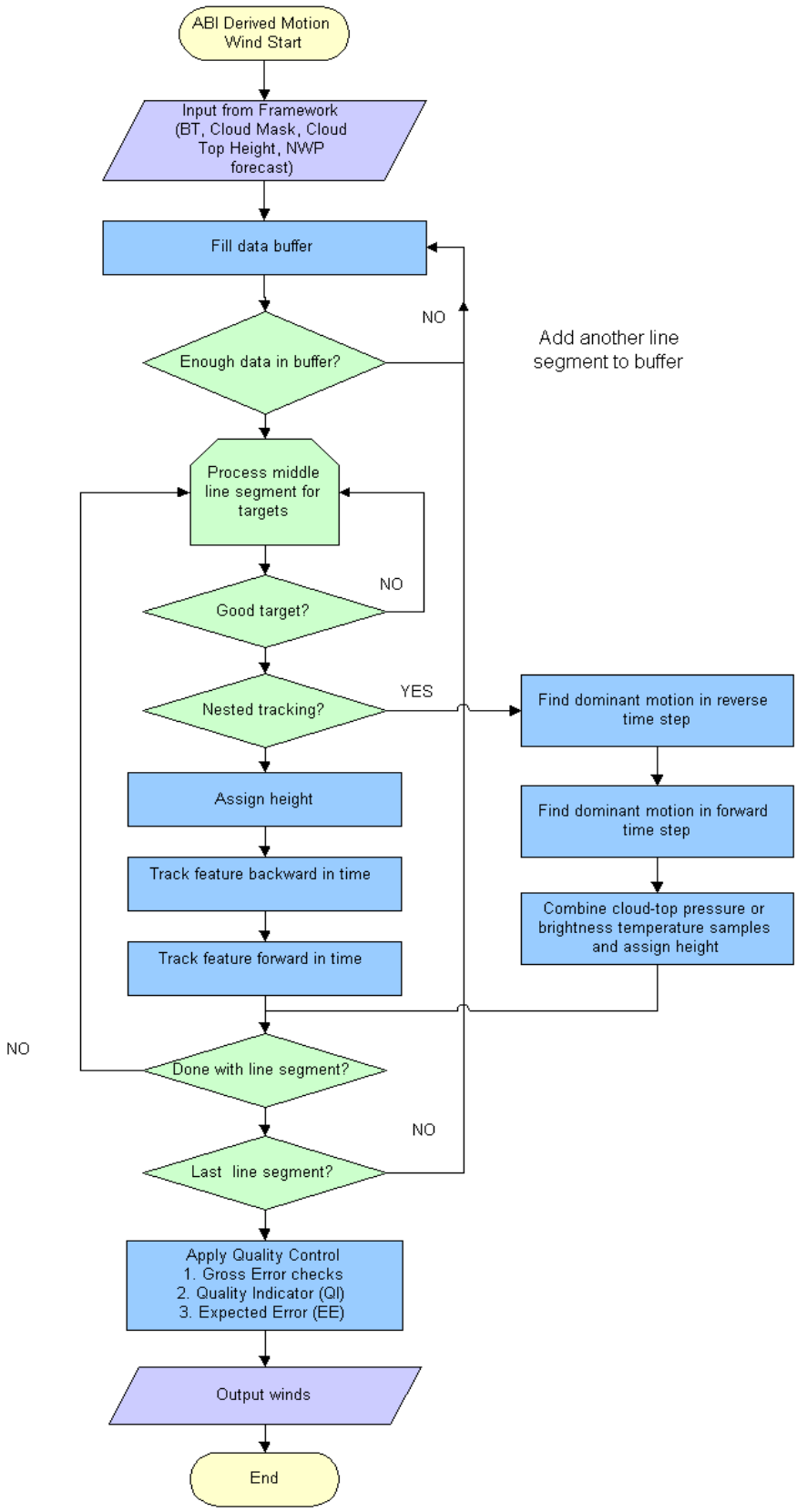

Figure 2. High Level Flowchart of the Derived Motion Wind Algorithm.

solution. For conventional tracking, where nested tracking is not invoked and the larger target scene is tracked, the correlation threshold is reduced to 0.6.

Two sub-vectors are generated in the tracking process, one vector for the backward time step and one vector for the forward time step. Accelerations between sub-vectors exceeding a user defined threshold (5 or 10 m/s depending on band) are not permitted (vectors are discarded). In addition, gross errors in the height assignment and tracking estimates are removed by comparing the satellite-derived motion wind to a numerical forecast wind and discarding those satellite-derived wind vectors which differ significantly from the forecast wind. These gross error thresholds are band-dependent.

Once the last line segment is processed, the entire set of derived winds undergoes a more rigorous quality control process. Two related algorithms will make up the Automatic Quality Control (AQC) of the GOES-R DMW processing. The first one is the quality indicator (QI), based on work done at EUMETSAT (Holmlund, 1998). The second is the Expected Error (EE) principles developed at the Bureau of Meteorology, Australia (LeMarshall et al. 2004).

As noted in Section 3.1, special mitigation processing takes place when G17 data is processed to generate winds. This begins with extracting the maximum ABI FPM temperature from each of the three tracking images and comparing them to the appropriate ABI FPM temperature threshold. Winds processing is terminated if the threshold is exceeded and an empty output file is created with zero good winds. The G17 ABI band-dependent FPM threshold temperatures are shown in Table 4.

Table 4. G17 focal plane temperature thresholds used by the DMW algorithm.

Channel Number	**Center Frequency (μm)**	**Temperature threshold (K)**
7	3.89	150
8	6.17	93
9	6.93	93
10	7.34	90.5
13	10.33	100
14	11.2	93

In addition to checking the focal plane temperatures of the tracking images, the DMW algorithm also checks to see if the upstream cloud height algorithm is using a mitigated set of channels to derive the cloud height instead of the nominal bands (14, 15 and 16). When this occurs, the DMW algorithm uses the mitigated cloud heights, but flags every wind with a unique product quality value (DQF= -2). Because the threshold temperature for band 13 is higher than the threshold for band 14, the algorithm allows band 13 to be used as a backup to band 14 if the maximum focal plane temperature is below the band 13 threshold. When a set of band 13 images is used in place of band 14 this condition is indicated by a unique product quality value (DQF= -1).

It should be noted that the visible band (ABI band 2) from G-17 is not impacted by the ABI focal plane warming issue so tracking is unaffected for this band. However, because the visible winds rely on cloud heights from the upstream cloud height algorithm, their quality can be impacted by the use of a mitigated set of channels to assign the height.

3.3 Algorithm Input

This section describes the input needed to process the DMWs. While the DMWA uses information at the pixel level (e.g., cloud mask, cloud height), the derived motion is representative of a group of pixels (i.e., a scene within a target box of size NxN pixels). The DMWA is currently designed to process winds only after a data buffer has been filled with brightness temperature data from all three images in the tracking sequence. Cloud height and cloud mask information for the middle image time is also required. The buffer must be large enough to capture the motion of features up or down in the image. Consequently, the DMWA processes only a portion of the buffer (a middle strip the same width as the target box size) for suitable tracers. Processing proceeds from west to east until the satellite zenith angle exceeds 70º, the earth edge is encountered or no more elements exist in the line segment. The process is repeated until the number of lines remaining in the line segment is smaller than the number of lines that make up the target scene. At this point the extra lines are saved in the buffer and control is returned to the framework until the next line segment is read into memory. The following sections describe the actual input needed to run the DMWA.

3.3.1 Primary Sensor Data

The list below contains the primary sensor data to be used by the DMWA. By primary sensor data, we mean information that will be derived solely from the ABI observations and geolocation information. The sensor data is used at it original resolution.

- Calibrated and navigated radiances for ABI channel 14 (11.2um) for the middle image time of the loop sequence.
- Calibrated and navigated reflectances (percent) for ABI channel 2 (0.64um) and brightness temperatures for ABI channels 7 (3.9um), 8 (6.15um), 9 (7.0um), 10 (7.4um), and 14 (11.2um) for three consecutive images.
- G-17 maximum focal plane temperature

3.3.2 Ancillary Data

The following list briefly describes the ancillary data required to run the DMWA. By ancillary data, we mean data that will require information not included in the ABI observations or geolocation data.

Land mask / Surface type

A land mask file is needed such that each ABI pixel can be classified as being over land or water. The details of the dataset that contains this information and the procedure for spatially mapping it to the ABI are described in detail in the Algorithm Interface and Data Description (AIADD) Document.

DMWA configuration file

A configuration file is needed to set six variables within the DMWA processing algorithm:

- GOES-R ABI channel number – Channel number to use for feature tracking
- Time step between images
- Target box size – In pixel space
- Nested tracking flag – to enable or disable nested tracking.
- Expected Error (EE) filter flag
- Clear-sky WV flag – to enable or disable clear sky processing.

Numerical Weather Prediction (NWP) Forecast Data

Short-term forecast temperature and wind data on pressure surfaces from National Centers for Environmental Prediction's (NCEP) Global Forecast System (GFS) model are used to calculate target heights and for calculating model shear and model temperature gradients used in the Expected Error algorithm described in Section 3.4.2.4.2. Details concerning the preprocessing of NWP forecast data can be found in the AIADD Document.
Short-term GFS forecast wind profiles are also used to center the search box on the predicted locations of targeted features being tracked in the first and last images of the loop sequence

Expected Error Coefficients File

A set of regression coefficients corresponding to a number of predictors used to compute the Expected Error quality flag that is appended to each DMW that is computed. The details of this approach are described in Section 3.4.2.4.2.

3.3.3 Derived Data

This section lists the input data that must be derived before the DMWA is executed. The output of several upstream cloud product algorithms from the GOES-R AWG cloud team are used in the DMWA derivation process and include the following:

Cloud Mask

The cloud mask is used by the DMWA as part of the cloud amount test when selecting which target scenes to process. It is also used to screen out pixels that do not have a cloud top pressure associated with them.

Cloud top pressure, cloud top pressure quality, and cloud top temperature

This information is used by the DMWA to assign a representative height to the target scene being tracked.

Cloud top height and temperature error estimates

Low level inversion flag

This information is used by the DMWA to assign a representative height to the scene being tracked within a GFS model designated low-level inversion.

Solar zenith angle

This information is used by the DMWA to determine day/night pixels.

Satellite zenith angle

This information is used by the DMWA to determine geographic coverage limits based on the sensor viewing angle.

3.4 Theoretical Description

3.4.1 Physics of the Problem – Estimation of atmospheric flow from motions in sequential satellite imagery

This section discusses the theory behind the challenge of estimating atmospheric flow from motions in sequential satellite imagery. Atmospheric motion is determined through the tracking of features in time. Identifying features to be tracked is the first step in the process. These features can be clouds, or in the case of clear-sky conditions, moisture gradients.

The DMWA uses the ABI visible and infrared observations shown in Table 3 to extract atmospheric motion. The choice of spectral band will determine the intended target (cloud or moisture gradient) to be tracked, its height in the atmosphere, as well as the scale of its motion. Historically, the coverage of operational GOES DMWs is diurnally consistent in the mid- to upper tropospheric levels (100–600 hPa) through the use of the mid-wave (6.7um – 7.3um) water vapor channels and longwave (10.7um) infrared

(LWIR) channel for deriving vectors. In the lower levels (600–950 hPa), DMWs are provided by a combination of the visible (VIS) and IR channels, depending on the time of day. During daylight imaging periods, the VIS channel usually provides superior low-level tracer detection than the LWIR channel due to its finer spatial resolution and decreased susceptibility to attenuation by low-level moisture. During night-time imaging periods, the shortwave (3.9um) infrared (SWIR) channel compliments the LWIR channel to derive DMWs. The SWIR channel is a slightly "cleaner" window channel than the LWIR (less WV attenuation), making it more sensitive to warmer (lower tropospheric) temperature features (Dunion and Velden, 2002). The SWIR channel is also not as sensitive as the LWIR channel to cirrus clouds that may obscure low-level cloud tracers. These two characteristics make it a superior channel for producing low level DMWs at night.

As described previously, each target is an NxN array of instrument measurements (scene) that encapsulate a suitable feature whose movement is tracked in time. The size of this array is a function of both the spatial and temporal resolution of the imagery and the scale of the intended feature to be tracked. Generally speaking, a small target box yields a noisier motion field than one generated with a larger target box. Conversely, if the target scene is too large, the algorithm will tend to measure the mean flow of the pixels in the target scene (i.e. a spatial average of several motions) rather than the intended instantaneous wind at a single point. These considerations need to be kept in mind when choosing the optimal target box size.

3.4.1.1 Target Selection

The objectives of the target selection process are to select high quality target scenes that: i) capture the intended target (i.e., clouds or clear-sky water vapor gradient), ii) contain sufficient contrast, and iii) do not contain a mix of multi-layered clouds. Target scenes that possess these characteristics are more amenable to precision tracking and height assignment that result in more accurate atmospheric wind estimates.

Target scenes are centered at pixel locations where the magnitude of the brightness temperature gradient is large. In other words, these target scenes are centered over cloud edges or tight moisture gradients in clear-sky conditions. To assure that only high quality targets are selected, all potential target scenes first undergo a spatial coherence and cluster analysis (Coakley & Bretherton, 1982) check. The primary goal of this analysis is to identify the presence of a coherent signal in the target scene that indicates a dominant single layer cloud in the target scene. The spatial-coherence method attempts to identify the presence of cloud layers in each target scene by identifying the portions of the region that exhibit a high degree of local uniformity in the pixel-level emitted radiances. A high degree of uniformity will exist for regions that are cloud-free or for regions completely covered by cloud at a uniform height. For targets that are not completely covered by clouds, the emitted radiances can vary significantly from one pixel to the next.

3.4.1.1.1 Spatial Coherence and Cluster Analysis Methods

The starting point for spatial-coherence and cluster analysis methods is the model of a well-defined, single-layered system of clouds situated over a relatively uniform background. What is meant by the term "well-defined" and "relatively uniform" will be explained below. The emitted radiance observed by a radiometer viewing such a system is given by

$$I = (1 - C)I_{cs} + C(\varepsilon_{cld}I_{cld} + t_{cld}I_{cs}) \quad (1)$$

where I is the emitted radiance, C is the fractional cloud cover for the field of view, I_{cs} is the radiance associated with the cloud-free portion of the field of view, i.e. the radiance observed when C = 0. ε_{cld} is the mean effective emissivity associated with the cloud layer, t_{cld} is the mean transmissivity, and I_{cld} is the radiance that would be observed for overcast regions, i.e. C = 1, if the clouds were black at the wavelength of observation. The emitted radiance, I, is assumed to be at an infrared (IR) window wavelength so that downward emission above the cloud can be neglected. Likewise, the surface is assumed to be black at the wavelength of observation so that all radiation incident on the surface is absorbed, especially that emitted downward by the cloud. It is assumed that no radiation is reflected by the surface. Over a relatively small region the emission of the clear-sky background, I_{cs}, and the height of the cloud layer, and therefore I_{cld}, are assumed to have little variance. That is, the effects of variations in the thermal emissions associated with the clear-sky background and the height of the cloud layer are small when compared with the effects caused by variations in the fractional cloud cover and the cloud optical properties. If these conditions are met, the background is said to be relatively uniform and the layer is said to be well-defined. From (1), the variance of the radiances under such conditions is given by:

$$(I-\bar{I})^2 = [(C-\bar{C})I_{cs} + (C\varepsilon_{cld} - \overline{C\varepsilon_{cld}})I_{cld} + (Ct_{cld} - \overline{Ct_{cld}})I_{cs}]^2 \quad (2)$$

The variances of emitted radiances over small areas spanning several image pixels is the key to identifying the portions of a region that are cloud-free or overcast by clouds in a well-defined layer. The variance approaches zero when the mean cloud cover in a region approaches zero. If the mean cloud cover is zero, then the fractional cover in every pixel is also zero (i.e. $C = \overline{C} = 0$). Where the clouds become sufficiently extensive so that several image pixels are overcast, then for analogous reasons, the variance approaches zero because $C = \overline{C} = 1$. Often when cloud systems become sufficiently extensive that they cover several image pixels, they also become opaque. A notable exception can be cirrus. For opaque, overcast clouds the variance again becomes zero because $t^i_{cld} = t_{cld} = 0$ and $\varepsilon^i_{cld} = \varepsilon_{cld} = \varepsilon_{cldmax.}$, where, t_{cld} is the cloud transmissivity and ε_{cldmax} is the emissivity that the clouds obtain when they become opaque (i.e., where r_{cldmax} is the reflectivity). When pixels become overcast with opaque clouds, the variance in emitted radiances also becomes zero. When pixels become overcast by semitransparent clouds, like cirrus, pixel-to-pixel variations in the cloud optical properties, i.e. ε_{cld} and t_{cld}, prevent the variance from dropping to zero. Because clouds appear to vary incoherently on the ~1 km × 1 km scale available to current satellite imagers, (2) indicates that variances in the emitted

radiances for regions that are covered by several image pixels will be nonzero when the region contains broken cloud. The variability will be caused partly by differences in the fractional cloud cover from pixel to pixel and partly by variations in the average cloud optical properties from pixel to pixel. The spatial-coherence method identifies pixels that are overcast by layered clouds where the clouds become opaque, and pixels that are cloud-free by relying on the near-zero variances in emitted radiances for localized collections, or clusters, of the pixels. Collections of pixels that are partly covered by clouds or are overcast by clouds that are semitransparent invariably exhibit relatively larger variances. The application of a simple threshold on the variance of emitted radiances over local sub-regions within each target scene is performed as part of the target selection process in order to identify coherent pixels representative of cloud features and the surface.

The cluster analysis method is designed to filter out hard to track multi-layered cloud scenes. It is related to the spatial coherence method in that it starts with the same radiance information (mean and standard deviation values for small sub-regions of the target box), but takes the analysis further to determine if more than one cloud layer is present in the target scene. This analysis involves constructing a histogram of pixel level radiance values within the target scene and then identifying the clusters of warm and cold samples that are assumed to correspond to the surface and the elevated cloud layer, respectively. A second cloud layer is assumed to exist in the target scene if more than a pre-determined percentage (20%) of the radiance values fall outside of the two clusters of warm and cold samples. If a second cloud layer is determined to exist, the target scene is rejected as a suitable target for feature tracking.

Further details about how both of these tests are applied are provided in Section 3.4.2.1.1

3.4.1.2 Feature Tracking

If a target scene survives the selection criteria, then attempts to track this target in the image sequence can commence. Feature tracking involves coherent tracking of clouds or water vapor features over a specified time interval. A key assumption made in this process is that cloud or water vapor features are passive tracers that move with the ambient wind flow. Of course, it is understood that cloud tracers (in particular) are not always passive. There may be growth, decay, or change in cloud top height over the time interval being assessed. Further complicating matters is the fact that some clouds do not move with the wind (i.e. wave clouds) while others track with the wind at a level lower than cloud top (i.e. marine cumulus). Therefore, it is important to apply robust quality control to remove retrieved DMWs that are in error as a result of these complicating factors (discussed in Section 3.4.2.4).

Clouds grow and decay with lifetimes that vary with their size and location (i.e., land versus ocean). To be effectively tracked, the lifetime of the tracer must be at least as long as the time interval of the image sequence used. The resolution of the imagery is also an important consideration when tracking features in satellite imagery. Merill (1989) and

Schmetz et al. (1993) discuss this at length. It is important that the size of the target scene (spatial resolution) is consistent with the temporal resolution of the imagery in order to capture the scale of the intended feature being tracked. For example, estimation of low level winds over land is improved by using smaller target scenes and higher temporal resolution imagery. Early work by Hamada (1983) suggested that the temporal resolution of images should be less than 15 minutes in order to accommodate the short lifetime and rapid deformation of cloudy tracers over land. Shenk (1991) suggested that the temporal resolution needed to properly track low level cumulus over land was in the range of 10 minutes to less than a minute. More recently, Velden et al. (2000) experimented with special GOES-10 rapid scan imagery to determine the optimal temporal resolution to use for different spectral channels. A general finding, that was not unexpected, was that a higher number of high quality winds can be derived with decreasing time intervals and increasing spatial resolution.

A critical factor that has a significant impact on the quality of the derived winds, especially at higher temporal resolutions, is the image registration; that is, the stability of the image-to-image navigation. If the stability of the image-to-image navigation is poor for an image sequence, the result will be added noise to the tracking process and poor quality DMWs. Furthermore, use of imagery with high temporal resolution, but coarse spatial resolution, can result in poor quality DMWs. This is especially true for small tracer displacements (i.e., low wind speeds) where image registration uncertainties will dominate the resulting true displacements.

Jedlovek and Atkinson (1998) discuss the development of a Tracking Error Lower Limit (TELL) parameter, $\mathfrak{I}$, that provides guidance for understanding the trade-offs between spatial and temporal resolution for varying image registration performances. The TELL parameter is given by:

$$\mathfrak{I} = (\mathfrak{R} + \rho/2)/t \tag{3}$$

where: $\mathfrak{R}$ is the image registration accuracy, ρ is the image spatial resolution, and *t* is the image separation interval. Figure 3 shows the magnitude of the TELL parameter for various values of the image registration accuracy and image separation.

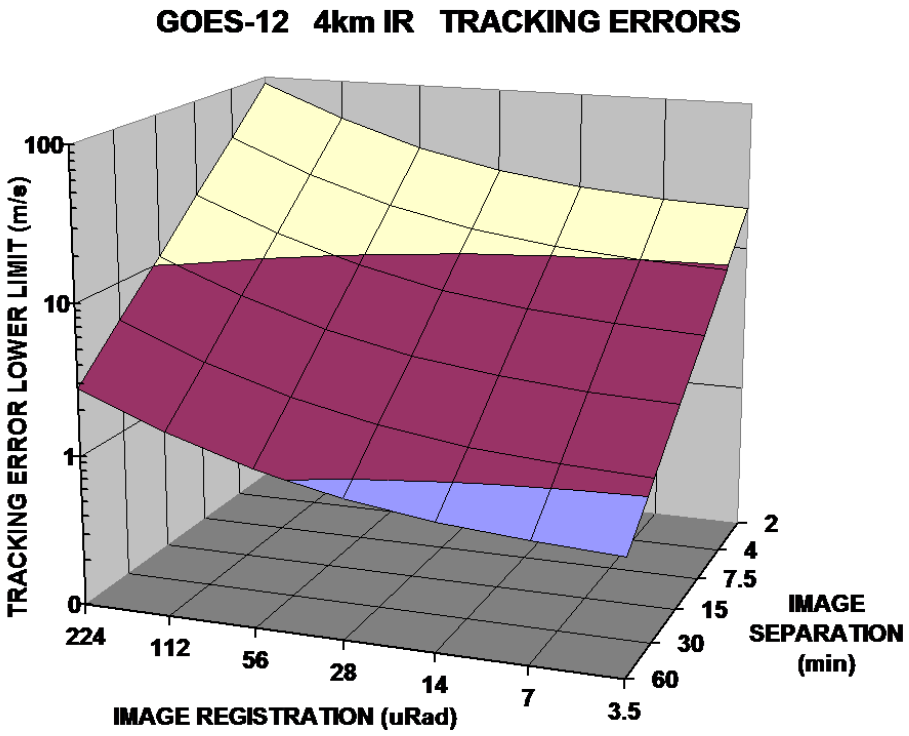

Figure 3. Tracking Error Lower Limit (TELL) is a function of image registration accuracy and image separation time. (Jedlovek and Atkinson, 1998)

Small values of TELL (small wind errors) are achieved with good image registration, high resolution data, and relatively large image separation times. However, for atmospheric applications where trackable features change considerably over a short period of time, large separation intervals are not desirable, making values of image resolution and registration accuracy critical parameters in DMW accuracy.

3.4.1.3 Target Height Assignment

Assigning a representative height to each cloudy target is achieved by processing pixel-level cloud heights, derived via the GOES-R ABI cloud height algorithm, within the target scene. A detailed description of the GOES-R ABI cloud height algorithm can be found in the GOES-R ABI Cloud Height Algorithm Theoretical Basis Document. For clear-sky water vapor targets, NCEP GFS forecast temperature profiles are used as ancillary data and compared to brightness temperatures calculated from the clear-sky water vapor channel brightness temperatures. The pressure height is determined as the level where the brightness temperature fits the forecast temperature.

Target height assignment is considered to be the major source of error for DMWs. A perfectly tracked feature can be rendered useless if it is assigned to the wrong level in the atmosphere. There is also the consideration of how well the final wind actually represents the local wind field at a singular location, height (level) and time. Some clouds do not

move with the wind while others follow the wind at a level lower than the cloud top. Additionally, DMWs tend to represent the movement of a layer of the atmosphere, as opposed to the movement of the atmosphere at a particular level (Velden and Bedka 2009).

3.4.2 Mathematical Description

The GOES-R DMWA approach to derive an individual vector consists of the following general steps, each of which is described in detail in the following sections.

- Locate and select a suitable target in second image (middle image; time=t_0) of a prescribed image triplet
- Assign an estimated representative height to the target
- Use a pattern matching algorithm to locate the target in the earlier and later image. Track the target backward in time (to first image; time=t-Δt) and forward in time (to third image; time=t+Δt) and compute corresponding displacement vectors. Compute the mean vector displacement from the two displacement vectors and assign this final DMW to time = t_0.
- Perform quality control procedures on the DMW to edit out or flag suspect vectors. Compute and append quality indicators to each DMW

3.4.2.1 Target Selection

Targets are selected from the middle image of the sequence. The size of each target scene will depend on the channel being processed and the scale of the motion being estimated. The target scene is traditionally a square with sides of equal length (in pixels). Table 5 summarizes the target scene size and image time separation interval to be employed for each instrumental channel used to derive DMWs. It should be noted that the horizontal resolution of the DMW product is driven by the size of the target scene used.

Table 5. Summary of target scene sizes and image time intervals that should be used to derive DMWs for pertinent instrument channels.

Channel Number	Target Scene Size (Image lines x elements)	Image Time Interval (mins)
ABI		
2	15x15	Full disk: 5, 10, or 15 CONUS: 5 Mesoscale: 5
7	15x15	Full disk: 5, 10, or 15 CONUS: 5 Mesoscale: 5
8 (cloudy targets) ---------- 8 (Clear targets)	15x15	Full disk: 5, 10, or 15 CONUS: 5 Mesoscale: 5 ---------- FD, CONUS, Mesoscale: 30
9	15x15	FD, CONUS, Mesoscale: 30
10	15x15	FD, CONUS, Mesoscale: 30
14	19x19	Full disk: 5, 10, or 15 CONUS: 5 Mesoscale: 5
AHI		
3	15x15	Full disk: 10
7	15x15	Full disk: 10
8 (cloudy targets) ---------- 8 (Clear targets)	15x15	Full disk: 10 ---------- Full Disk: 30
9	15x15	Full Disk: 30
10	15x15	Full Disk: 30
14	19x19	Full disk: 10
VIIRS		
M11	15x15	Orbital: 101
M15	19x19	Orbital: 101
AVHRR-3		
4		Orbital: 101

Before the target selection process begins, the brightness temperature gradient magnitude for each pixel location is computed from equation (4).

$$Gradient_{Line,Element} = \sqrt{\{\sum_{k=-2}^{k=2}(W_k)(BT_{Ele\,+\,k,\,Line})\}^2 + \{\sum_{k=-2}^{k=2}(W_k)(BT_{Ele,\,Line\,+\,k})\}^2} \quad (4)$$

where: $W_k = \{-1/12, 8/12, 0, -8/12, 1/12\}$; for k= -2 to 2

BT is the pixel level channel brightness temperature
Ele refers to an image column
Line refers to an image row

Figure 4 shows an example of a brightness temperature gradient image (right side) derived from brightness temperatures (left side) for the GOES-12 imager. The dark areas on the right side of Figure 3 indicate locations where the magnitudes of the brightness temperature gradients are large. These locations exist on the edges of clouds and in the interior of cloud systems where cloud structure exists. It is in these locations where potential acceptable targets are expected to be found. The white boxes shown on the left-side of Figure 3 show the original target scene locations and the yellow dots show the location of the maximum gradient magnitude in each of these target scenes. The center of every target scene is then repositioned at the pixel containing the maximum gradient magnitude. If the same gradient value occurs in multiple pixels within a target scene, then the first occurrence of the maximum gradient value is the one chosen. The repositioned target scenes are shown in green. The intent of repositioning the target scene at the

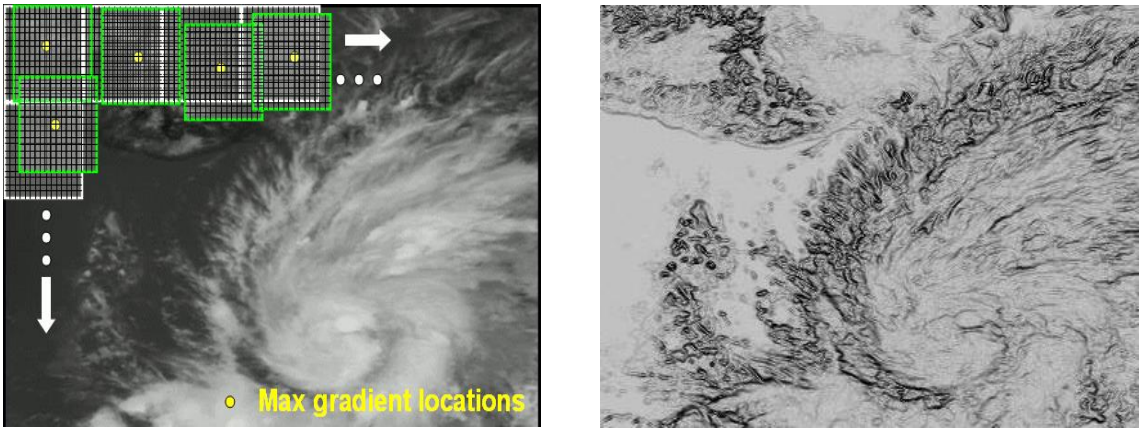

Figure 4. Image of 11um brightness temperature (left) and the 11um brightness temperature gradient (right). The white boxes show the target scenes at their original locations. The green boxes show the target scenes which have been repositioned at the pixel location containing the maximum brightness temperature gradient as indicated by the yellow dot.

3.4.2.1.1 Target Selection Tests

All of the potential target scenes undergo a series of quality control tests to determine if the target is a suitable tracer. These 'target selection' tests are described below. If a target fails any one of these tests, the target is determined to be a non-suitable tracer and is

flagged. Each failure is associated with a unique "flag" value which is saved in the DMW output file. These values are shown in Table 6.

Table 6. Derived Motion Winds Algorithm Failure Codes.

Derived Motion Wind Quality Control Codes	
Data Quality Flag (DQF)	**Definition**
-3	Good wind, but an alternative channel (band 13) used for feature tracking and an alternative set of channels used for the determination of cloud-top height/AMV height
-2	Good wind, but an alternative set of channels used for the determination of cloud-top height/AMV height assignment
-1	Good wind, but an alternative channel used for feature tracking
0	Good wind
Internal Quality Flag Failure Codes	**Definition**
1	Maximum gradient below acceptable threshold
2	Target located on earth edge or Satellite Zenith Angle greater than 70º
3	Cloud amount failure (less than 10% cloud cover for cloud track winds or greater than 0% cloud cover for water vapor clear-sky winds)
4	Median pressure failure
5	Bad or missing brightness temperature in target scene
6	Multiple cloud layers present
7	Target scene too coherent (not enough structure for reliable tracking)
8	Tracking correlation below 0.6 (not used for nested tracking)
9	u-component acceleration greater than 10 m/s (5 m/s for visible)
10	v-component acceleration greater than 10 m/s (5 m/s for visible)
11	u- and v- component accelerations greater than 10 m/s (5 m/s for visible)
12	Derived wind slower than 3 m/s
13	Target scene too close to day/night terminator (visible and SWIR only)
14	Median pressure used for height assignment outside acceptable pressure range (channel dependent)
15	Match found on boundary of search region
16	Gross difference from forecast wind (channel dependent)
17	Median pressure (used for height assignment) of largest cluster for first image pair is too different from median pressure of largest cluster for second image pair – only valid for nested tracking
18	Search region extends beyond domain of data buffer
19	Expected Error (EE) too high
20	Missing data in search region
21	No winds are available for the clustering algorithm
22	No clusters were found
Catastrophic Failures	
Invalid time interval	
Temporal data not available	
Line segment swath too small (must contain at least the same number of lines as target box size specified in the Winds Configuration File.	
Search region size is less than the target scene size	

maximum gradient is twofold. First, it focuses the target scene on a strong feature that is expected to be effectively tracked over time. Secondly, it establishes a link between pixels containing the feature being tracked and the pixels contributing to its height assignment (discussed later). Repositioning of the target scenes can result in an irregular spatial distribution of target scenes, and hence, an irregular spatial distribution of the DMW product. The white arrows indicate the direction of the image processing, which begins at the top left of the image and moves left to right along the image and then downwards.

Table 6 describes every possible failure code from the initial target selection step through the final QC process. Because target selection is the first step in the AMV derivation process the tests associated with it are described first. The target selection tests are applied in the following order:

1. Zero gradient check
2. Proximity to day/night terminator check
3. Earth edge test (no space pixels allowed)
4. Satellite zenith angle test
5. Fractional cloud cover/clear sky test
6. Note: when processing the upper-level water vapor channel for clear-sky tracers pixels with low-level clouds (CTP >= 600 mb) are considered clear.
7. Contrast test – channel dependent
8. Channel validity test

Quality control check #6 is the extent of target QC for WV processing

Additional target QC performed for visible, SWIR and LWIR winds:

9. Spatial coherence check
10. Multi-layer cloud check

If a target scene fails test #1 the next adjacent target box is processed.
If a target fails any of the 2-10 tests the box is shifted by ½ the width of the target box.

Zero gradient Test

If the maximum gradient found in the target scene is zero the target is discarded and the next adjacent box is processed.

Contrast Test

Each target scene is required to contain sufficient contrast, which is computed from the range of channel measurements (brightness temperature or reflectance percent) within the target scene. The contrast threshold used is channel dependent and is the product of the contrast constant (shown in Table 7) and the ratio of the target scene size used (see Table 5) and the nominal target scene size (7 or 15).

Table 7. Contrast constants and thresholds used for target selection.

Channel Number	Contrast Constant	Contrast Threshold
ABI		
2	12% (reflectance)	12%
7	3K	6.43K
8 (clear-sky)	1K	1K
8 (cloud-top)	2K	2K
9	1K	1K
10	1K	1K
14	4K	5.07K
AHI		
3	12% (reflectance)	12%
7	3K	6.43K
8 (clear-sky)	1K	1K
8 (cloud-top)	2K	2K
9	1K	1K
10	1K	1K
14	4K	5.07K
VIIRS		
M11	2K	2K
M15	4K	5.07K
AVHRR-3		
4	4K	5.07K

Earth Edge Test

All pixels within the target scene must have valid earth navigation associated with it. If any pixel within the target scene is determined to be located in space (i.e., off the earth edge) the target scene fails, and is flagged. The space mask provided by the framework is used for this purpose. It is assumed that a space mask will be passed down by the framework to the L2 product algorithm level for use by the various algorithms.

Satellite Zenith Angle Test

If the target is determined to be located at a sensor viewing angle greater than 70º, the target scene fails and is flagged as off the earth edge.

Fractional Cloud Cover Test

The clear-sky mask product associated with each pixel is used to classify the target scene as cloudy or clear. When the intent is to track clouds, a minimum threshold of 10% is used to determine whether the target scene is cloudy or clear. In other words, if at least 10% of the pixels in a target scene are deemed as being cloudy or probably cloudy, then the target scene is classified as cloudy. When the intent is to track clear-sky water vapor features, then a minimum threshold of 0% is used to determine whether the target scene is cloudy or clear. In other words, every pixel in the target scene must be deemed clear for this target scene to be deemed a suitable clear-sky water vapor target. An exception is made, however, when the upper-level water vapor band (6.15 um) is used to track clear-sky moisture gradient features. Because this band senses radiation only from the middle and upper layers of the atmosphere, any pixel which is clear above a low-level cloud is considered clear instead of cloudy. In practice, a pressure threshold of 600 hPa is used to identify the low cloud. In other words, a cloudy pixel assigned a cloud-top pressure greater than 600 hPa is considered to be clear instead of cloudy. This exception is made to increase the coverage of these winds.

The cloudy or clear designation given to the target scene has implications on the target selection tests (described in sections 3.4.2.1.1-3.4.2.1.3) and/or thresholds used as well as which algorithm is used to assign a height to the target (described in section 3.4.2.2).

Channel Validity Test

The channel brightness temperature or reflectance percent of each pixel in a target scene is checked to ensure its value falls within a valid range. The valid range of reflectance percent for a visible channel is 1-200. For the IR channels, the valid range of brightness temperature is 150-340K. If the channel brightness temperature or percent of any pixel in the target scene falls outside the valid range the target fails and is flagged.

Spatial Coherence Test

The spatial coherence test is applied when winds are being generated from cloudy target scenes.

Originally proposed by Coakley and Bretherton (1982), the spatial coherence method utilizes the local spatial structure (local mean and standard deviation) of the IR-window radiance field to determine the radiances associated with cloud-free and completely cloud-covered fields of view and to infer the radiances associated with partially filled fields of view. In the context of the DMW algorithm, the method is first used to filter out target scenes that are too uniform to track reliably, and second, to filter out scenes that may contain multiple cloud layers. For both purposes it is necessary to compute the local mean and standard deviation of the radiance field derived from 3x3 sub-regions within the larger target box. The mean and standard deviation values are computed for the entire line segment (with data surrounding the target box). Near the edges these values are computed with however many pixels are available.

After computing the mean and standard deviation radiance values for all possible 3x3 pixel sub-regions in the target box, a standard deviation threshold (1.0 Wm^{-2} sr^{-1} um^{-1}) is applied that results in a "filtered" or coherent sample. The standard deviation threshold value is chosen arbitrarily with consideration given to the range of possible data values expected in the imagery. The resulting "filtered" or coherent sample represents either cloud-free or completely cloud-covered pixels from the less-coherent sample that is likely to include partially filled fields of view. If more than 80% of the total number of 3x3 pixel sub-regions within the target scene have a standard deviation below the defined threshold, the scene is deemed to be too coherent and it fails to be a viable target for subsequent feature tracking. Target scenes that contain a mixture of cloud-free and cloud-covered pixels exhibit a characteristic arch shape as shown in Figure 5.

Multi-Layer Cloud Test

The multi-layer cloud test is applied when winds are being generated from cloudy target scenes.

Target scenes that contain multiple cloud layers in them can be difficult to track since clouds at different levels of the atmosphere may be moving in different directions and/or speeds. Furthermore, the assignment of a representative cloud height in these situations is difficult given the existence of clouds at different levels of the atmosphere.

In order to avoid these troublesome target scenes, the filtered sample from the spatial coherence approach described above is used in a cluster analysis approach in order to identify the possible existence of multiple cloud layers. The basic idea behind the method is to use the local mean and standard deviation information to identify clusters of points sharing common characteristics (such as mean radiance and low variance). If more than two clusters (one of which is implicitly assumed to be the surface in clear sky conditions) is found in a target box then the scene is rejected. The key concept of this approach is that peaks in the frequency histogram can be described by Gaussian distribution functions (Simmer et al., 1982; Rossow et al., 1985; Nieman et al., 1993).

Using the filtered sample, the method starts by identifying the peak in the 1-D histogram of local mean IR radiance values. A Gaussian curve is then fitted to the peak of the histogram and all points falling within +/- 3 standard deviations of the peak value are added to the dominant cluster sample. Likewise, a second Gaussian is fitted to the "cold peak" of the histogram and the cold cluster is identified. Lastly, the total number of points falling within the dominant and cold clusters is summed and compared to the total number of points in the filtered sample. If the total number of points from both clusters is less than 80% of the original filtered sample it is assumed that a third, unidentified, cluster exists (in theory representing another cloud layer) and the target is rejected. The example shown in Figure 6 is for a target scene that was partly filled by a single cloud layer.

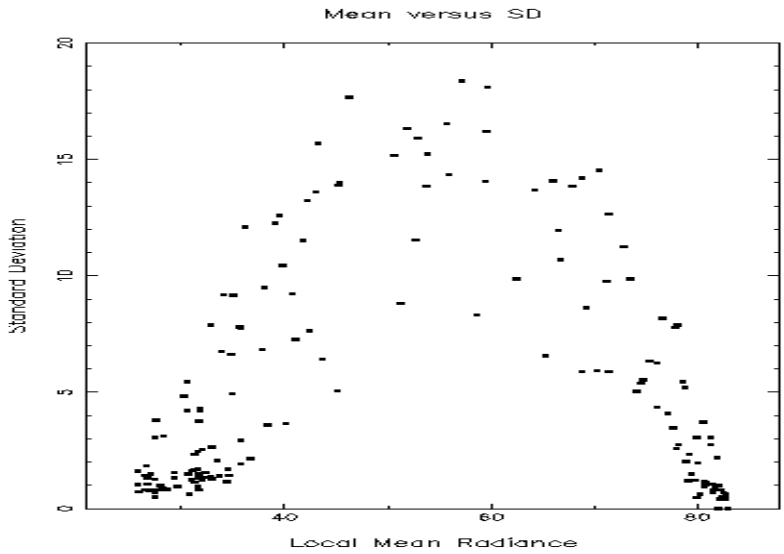

Figure 5. Scatter diagram of window channel IR local mean radiance and standard deviation values for a single target scene. Each point in the figure represents a 3x3 array of pixels constructed from 4-km GOES IR radiance data. The cluster of points near 80 is associated with clear sky while the cluster near 30 is associated with a single cloud layer. The points in the arch represent partly filled fields of view.

The step by step procedure for the above procedure is defined below:

1. Construct histogram of radiance values from 0 to 199 using bin width of 1.

2. Estimate the variance using a two point method (one end point is always the peak frequency) for the three bins closest to the peak (Note: if there is more than one peak the first one is selected) on the LHS with the formula:

$$variance_i = \frac{\left(\overline{x}_i - \overline{x}_{peak}\right)^2}{2\ln\left(\frac{f_i}{f_{peak}}\right)} \tag{5}$$

Where x is the bin value (i.e., radiance), f is the number of points in the bin (i.e., frequency),

$$\overline{x}_i = \frac{x_{i-1} + x_i}{2} \tag{6}$$

and

$$\overline{x}_{peak} = \frac{x_{peak-1}+x_{peak}}{2} \quad (7)$$

NOTE: If f_i is 0 then the variance is set to a value of 0.

3. Average the three variance estimates to obtain the final variance for the LHS half curve.

$$\overline{variance}_{LHS} = \frac{1}{3}\sum_{i=1}^{3} variance_i \quad (8)$$

NOTE: If the computed variance is greater than 25 it is set to a value of 25. Also, only non-zero variance values are used to compute the average. This means any bin having a zero count will not be used in the average.

4. Repeat steps 2 and 3 for the three bins closest to the peak on the RHS of peak frequency.

5. Compute the full Gaussian curve using LHS and RHS variance values. The full Gaussian spans the interval ±5 standard deviations about the peak frequency and is computed using:

$$f_{Gauss} = f_{peak} exp\left[-\frac{(\overline{x}_i-\overline{x}_{peak})^2}{2(\overline{variance}_{LHS,RHS})}\right] \quad (9)$$

NOTE: If the exponent is less than -10.0 it is set to a value of 0.0.

6. Find peak frequency of 5 coldest non-zero clusters and repeat steps 2 to 5 for the cold peak.

7. Total the number of pixels engulfed by the two Gaussian curves according to the following rules:

   ±1 standard deviation of peak, sum up all histogram points
   ±1 to 3 standard deviations of peak, sum up points in Gaussian histogram (from step 5)
   Do not count pixels outside this range

8. If the total number of points from both clusters is less than 80% of the original filtered sample, it is assumed that a third, unidentified cluster, exists and the target

scene is flagged. DMWA assigns QC_Flag=6 to the processed target scene and moves to the next target scene.

Note: If the cold peak corresponds with the overall peak this implies a single cloud layer exists in the target scene. This would be an acceptable target.

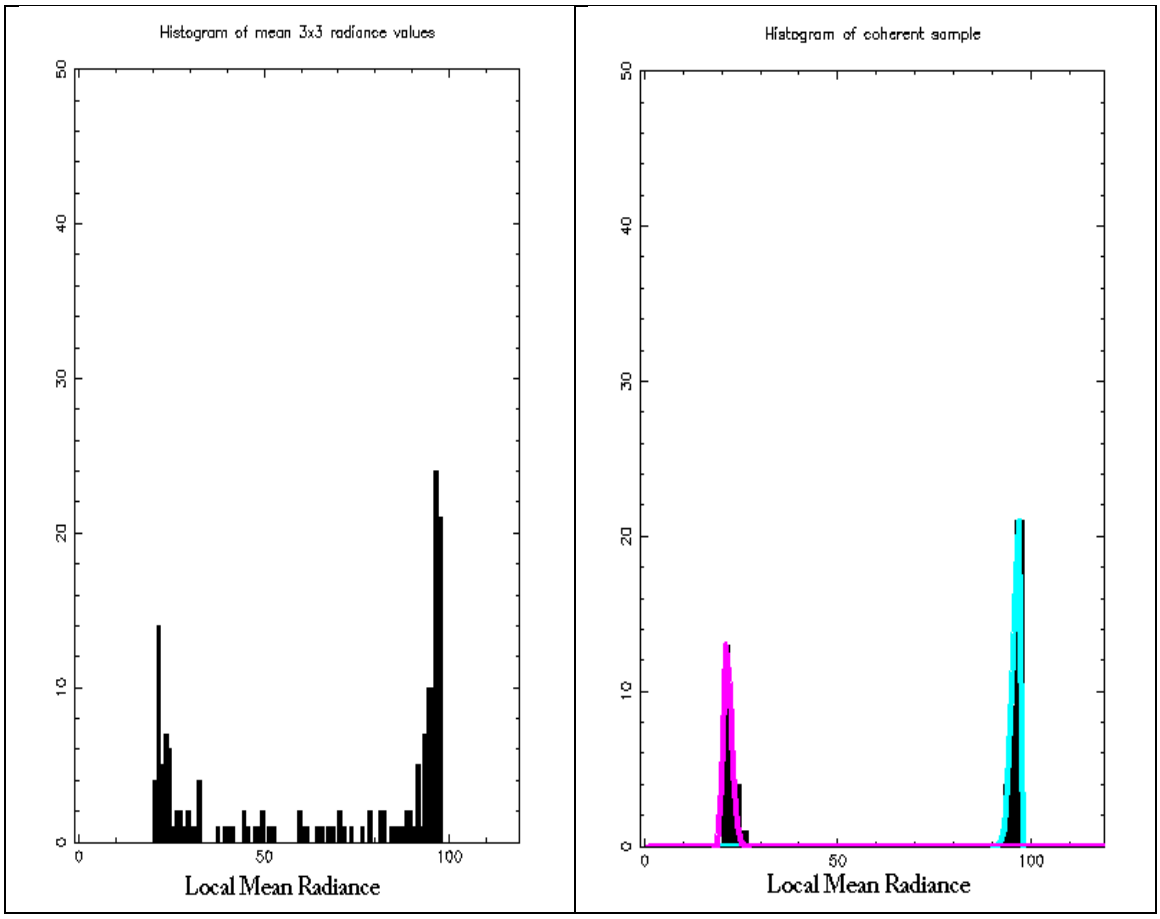

Figure 6. Histogram plots of local mean infrared radiance values for a single target scene: (Left) For the entire target scene, (Right) Filtered sample with Gaussian curves fitted to the peaks. The peak on the left is associated with a single cloud layer.

Day/Night Terminator Test

The Day/Night terminator test is applied when winds are generated from visible (0.64um) or SWIR (3.9um) bands.

When the VIS or SWIR band is being used, a test is invoked in order to avoid the day/night terminator. If the VIS channel is being used, then the solar zenith angle of the center pixel of the target scene must be less than or equal to 80^{o} for the target to be

deemed a suitable target. If the SWIR channel is being used, then the solar zenith angle of the center of the target scene cannot be less than 90^{o} or greater than 200^{o} for the target scene to be deemed a suitable target.

3.4.2.2 Feature Tracking

Correlation-based methods are commonly used to track cloud and clear-sky water vapor features in image sequences. A widely used correlation approach to feature tracking is the Sum of Squared Differences (SSD). This correlation method, like all others, aims to locate a target scene, at some time t, in a larger search scene at some earlier or later time. This process is illustrated in Figure 7. A similarity criterion is computed that measures the correlation between the target and search area pixel scenes in the two images. In the DMW algorithm a feature or target is selected from the middle of three images and is tracked backwards and forwards in time, thus generating two displacements. These two displacements are then averaged to generate an average wind vector that is taken to

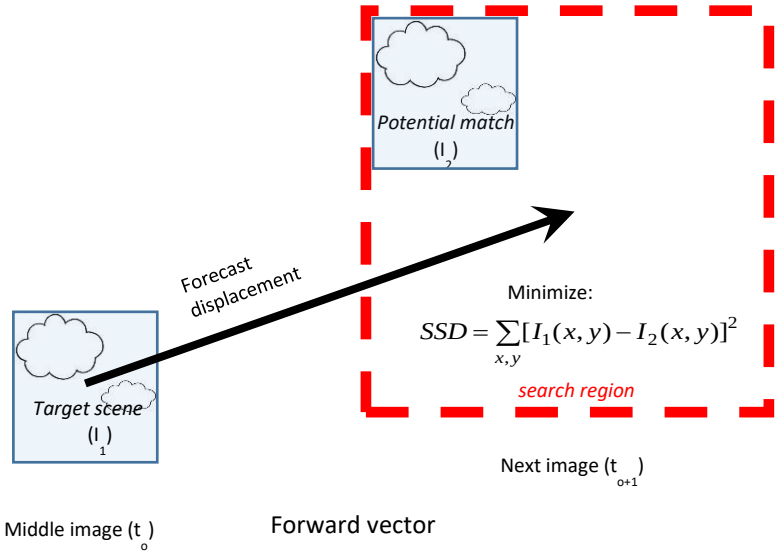

FIG. 7. Schematic showing the basic concepts associated with the feature tracking algorithm. Targets are selected from the middle image of a three-image loop and tracked forward and backward in time via the SSD method. The two displacements are averaged to produce a final motion estimate. Only the forward vector is shown in the figure.

represent the motion of the target over the time interval spanned by the image triplet. This average vector is assigned to the middle image target location. This approach is what we will refer to as the conventional feature tracking approach. This approach is used when tracking clear-sky water vapor features when using the ABI water vapor channels 8 (6.15um), 9 (7.0um), and 10 (7.4um).

When tracking cloud features, however, an approach referred to as nested tracking (Daniels and Bresky, 2010) is used. Nested tracking uses the SSD method to compute local motions nested within a larger target scene together with a clustering algorithm, to arrive at a superior motion solution for the larger target scene. The details of this approach are described below in Section 3.4.2.2.2.

A short term GFS model forecast wind is used in the feature tracking step to center the location of the search area in the other images. This is done for two reasons. First, it minimizes computational time required for tracking and secondly, minimizes the number of false solutions generated by the SSD method. It should be emphasized that the search region must be sufficiently large to allow for substantial departures from the forecast. It has been shown by Merrill (1989) that the derived wind is inherently constrained to the forecast wind by the following relationship:

$$(u - u_g) \leq \frac{(L-2)x}{2t} \tag{10}$$

where u (m/s) is the east-west component of the satellite wind, u_g (m/s) is the east-west component of the forecast wind, L is referred to as the lag size and is the max displacement of a target scene within a given search box, t is the time interval (in seconds) between images and x is the resolution of the imagery in meters. A similar relationship holds for the north-south component, but is omitted for brevity. For a given image sequence time interval and pixel resolution, the ratio given by the right hand side of equation (10) yields a value that represents the maximum departure of the feature tracking wind solution from the forecast wind. It is important that this ratio be sufficiently large to minimize the dependency of the forecast wind in the tracking step. Furthermore, the magnitude of this ratio must be considered when different size target scenes and/or sequence time intervals are used. For example, for a given image resolution, if smaller image time intervals are desired, then a corresponding reduction in the lag size must be made in order to keep the magnitude of the ratio constant. By specifying a maximum forecast departure of 30 m/s in Equation (10), the equation for keeping the lag size constant is given by:

$$\frac{60}{x}t + 2 = L \tag{11}$$

By specifying the desired time interval between images to use and the resolution of the imagery in Equation 11), the lag size can be computed. Once the lag size is known, the size of the search scene can be computed from:

$$S = T + (L/2) * 2 \tag{12}$$

Where: S is the search scene size in pixels
T is the target scene size in pixels

L is the lag size in pixels

In summary, the step by step procedure for tracking is as follows:

1. Compute forecast displacement, in pixels, using the forecast wind valid at the target lat/lon and interpolated to the initial height estimate.
2. Use forecast displacement to center search box.
3. Fill search box with data from image buffer
4. Find matching scene in the first and third images and compute AMV displacement via the conventional or nested tracking algorithm (displacement is a real value not an integer value).
5. Compute end point of AMV displacement vector in pixel coordinates
6. Compute earth location (lat/lon) of end point
7. Compute U/V components using the beginning (target center pixel) and ending (match location) lat/lon values

3.4.2.2.1 Sum-of-Squared Difference (Euclidean Distance) Method

The sum-of-squared-differences method (SSD) is the correlation routine used by the DMW algorithm. In the SSD routine the following sum is minimized:

$$\sum_{x,y}[I_1(x,y) - I_2(x,y)]^2 \tag{13}$$

where: I_1 is the brightness temperature at pixel (x,y) of the target scene, I_2 is the brightness temperature at pixel (x,y) of the search window, and the summation is performed over two dimensions. In practice, the region over which the search is conducted is substantially larger than the size of the target scene and the above summation is carried out for all target box positions within the search region. The array of positions that the target box can assume in the search region is often referred to as the "lag coefficient" or "lag" array and the field of values is referred to as the correlation surface. The size of the search and lag arrays are given by Equations (11) and (12) in the previous section.

To speed up the search for the minimum SSD value, the tracking algorithm first constructs a table (a square array) of values specifying the order of positions to search within the lag matrix. This is illustrated in Figure 8. The first point in the table corresponds with the middle of the lag matrix, which also corresponds with the center of the search region, which also corresponds with the location predicted by the forecast. The search then "spirals" outward in a clockwise fashion about the central point. By starting the search in the middle of the search region we are hopefully maximizing our chance of

finding a match sooner than if we were to start in the top left corner of the search region. The spiral search, when used in conjunction with the practice of terminating the SSD summation early once a current minimum has been exceeded, can significantly reduce the number of computations required during the tracking step of the DMW algorithm.

	7	8	9	10
	6	1	2	11
	5	4	3	12
				13

Figure 8. Table (a square array) of values specifying the order of positions to search within the lag matrix as part of the spiral search algorithm.

A typical correlation surface for the SSD method is shown in Figure 9. Each pixel in this figure represents a SSD value for a potential matching scene in the search region. The cool colors (blues) indicate minimum values while the warm colors (yellows) indicate relative maxima. The minimum SSD solution value results in a discrete, pixel displacement being identified as a possible DMW tracer. Unaltered, these integer displacements would cause an artificial binning of the satellite derived wind estimates. To avoid this effect, the SSD values of the four points surrounding the minimum SSD are used to linearly interpolate to sub-pixel accuracy. The following equation is used to compute the fractional element displacement:

$$\Delta = \frac{(l_1 - l_3)}{2(l_1 + l_3 - 2l_2)} \tag{14}$$

where l_1 is the lag array value at (x-1, y), l_2 is the lag array value at (x, y) (i.e., the minimum SSD value) and l_3 is the lag array value at (x+1, y).

The fractional value is added to the integer displacement to produce a Real (ie., non-integer) estimate of the displacement.

A similar equation is used for the fractional line displacement, but it uses the lag array values above (x, y-1) and below (x, y+1) the minimum lag location.

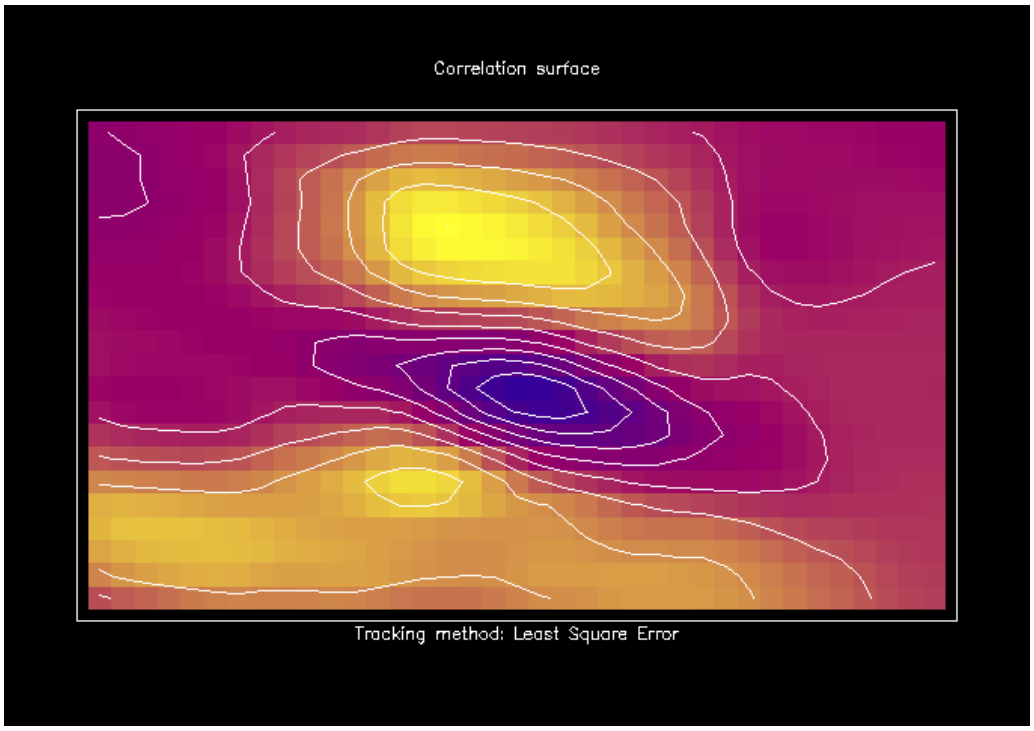

Figure 9. Example of a typical correlation surface for the Sum-of-Squared Difference (SSD) tracking method. The cool (blue) colors indicate minimum values while the warm (yellows) colors indicate relative maxima.

3.4.2.2.2 Nested Tracking

When tracking cloudy target scenes a technique referred to as "nested tracking" is employed. This approach involves nesting smaller (5x5 pixels) target scenes within a larger target scene (ie., whose size is specified in Table 5) so that a field of local motion vectors can be derived over the interior pixels.

A schematic of this approach is shown in Figure 10 alongside one example of the vector field produced by the approach. Differences in orientation and magnitude can arise between the local motion vectors if more than one cloud layer is being tracked or if multiple scales of motion are being detected. Outliers vectors – those vectors that differ greatly from most of the sample – can result if the cloud is evolving or if the smaller box is insufficiently large to resolve the true motion. The second contributor to vector outliers is often referred to as the aperture effect and is discussed at length in the field of

computer vision (Trucco and Verri, 1998). The red vector shown in Figure 9 makes it clear that averaging conflicting motion within a target scene can produce a slow wind speed estimate. The challenge is to derive a dominant motion vector from a subset of all possible solutions that best represents the flow of the larger target scene. This can be accomplished by analyzing all of the local displacements within the larger target scene with a cluster analysis program. More specifically, a cluster analysis of the line and element displacements is done to produce clusters that represent unique displacements.

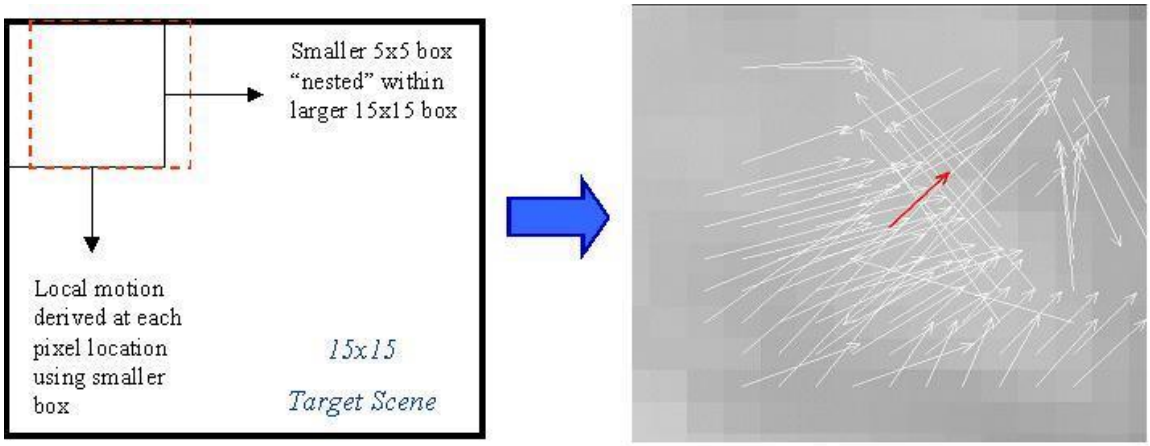

Figure 10. Schematic of the nested tracking approach. The white vectors show the local motion vectors successfully derived for each possible 5x5 box within a larger 15 x 15 target scene. The red vector on the right is the resulting motion vector if one were to take an average of all the successfully derived local motion vectors.

The justification for using a cluster analysis algorithm to analyze the local motion field is twofold. First, as was discussed above, the local motion field can be quite noisy. The field of vectors often reveals motion associated with two or more cloud layers and/or spatial scales. Removing noise and separating the sample into coherent motion clusters can prevent the excessive averaging of motion occurring at multiple levels or for different scales that can lead to a slow speed bias. Second, identifying clusters in the local motion field provides a means for directly linking the tracking step with the height assignment step. In other words, the pixels belonging to the coherent clusters allow us to limit the sample of pixels used for height assignment.

For the DMW algorithm we selected a cluster analysis program called DBSCAN (Ester et. al., 1996), a density-based algorithm for identifying clusters in spatial databases with noise. It was selected because it is very effective at identifying clusters of varying shapes and, unlike other methods such as K-means (Lakshmanan et al., 2009a, 2009b, 2003), does not require the user to specify apriori the number of clusters to find. Two parameters must be specified before running DBSCAN: the minimum number of points in a cluster (currently set at 4) and the radius around the point to search for neighbors in the cluster (currently set at 0.5 pixels). Basically, DBSCAN steps through each point (each point being a displacement in line and element space) and classifies it in one of three ways. A

"core" cluster point has at least 4 neighbors within its neighborhood (radius). A boundary point has fewer than 4 neighbors but is still connected to a cluster by at least one other point. The third possibility is that the point does not belong to any cluster and is "noise." Output from DBSCAN consists of a list of clusters found and the number of points in each cluster.

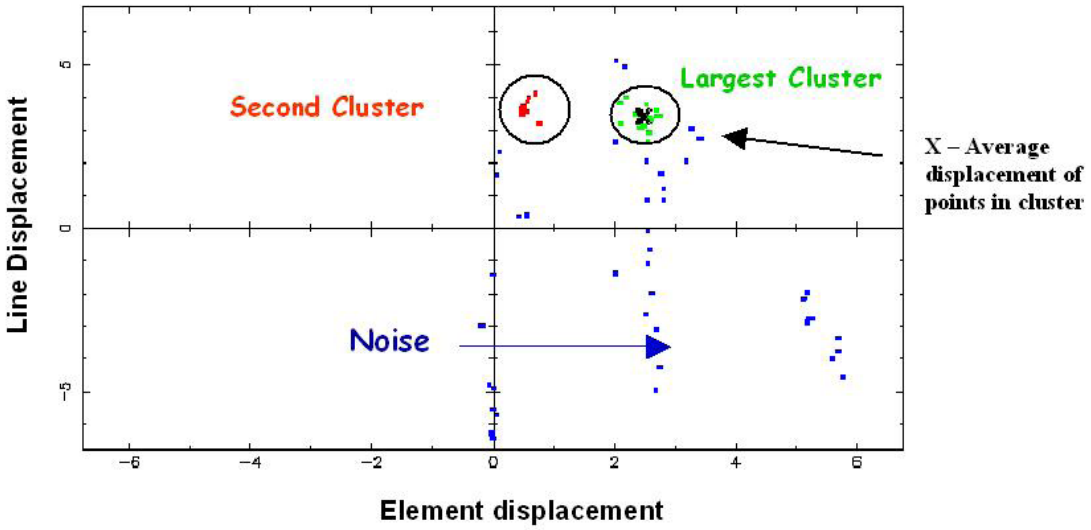

Figure 11. Motion clusters identified by DBSCAN clustering routine. Green dots indicate line and element displacements belonging to the largest cluster. Red dots indicate line and element displacements belonging to the second largest cluster. Blue dots represent incorrect or noisy line and element displacements.

One example of output from DBSCAN is shown in Figure 11. This figure shows that noisy motions have been removed from the scene leaving two distinct motion clusters. The DMW algorithm selects the largest cluster to represent the dominant motion and computes a final derived motion vector by averaging the displacements belonging to the largest cluster. Figure 12 shows the vector field that remains after the analysis is complete.

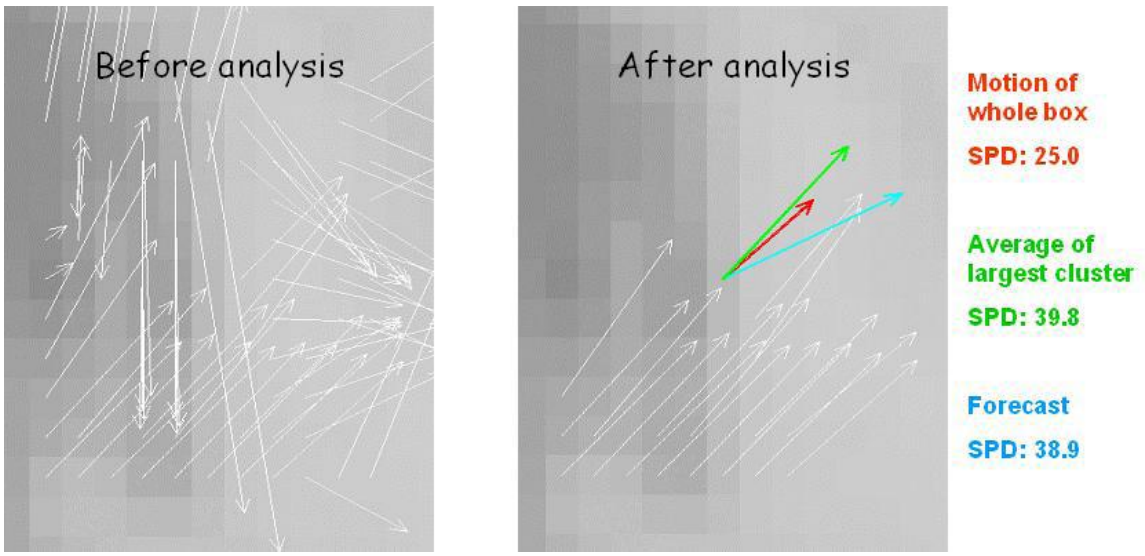

Figure 12. Example of the vector field produced with nested tracking before (left) and after (right) DBSCAN is applied to find the largest cluster. The forecast vector (blue) is shown for comparison.

3.4.2.2.3 Feature Tracking Gross Error Tests

All retrieved wind values undergo a series of quality control tests to determine if the derived wind is valid. This series of tests are described below. If a retrieved wind fails any one of these tests, it is deemed to be an invalid wind and is flagged appropriately. Each failure is associated with a unique "flag" value which is saved in the DMW output file. These unique flag values are listed in Table 6.

The tests are applied in the following order:

1. Match on boundary check
2. Correlation check
3. u-component acceleration check
4. v-component acceleration check
5. u- and v-component acceleration check
6. Slow wind speed check
7. Pressure limit checks on cloud type
8. Channel-specific NWP wind speed and direction comparison tests

Correlation Test

As mentioned in Section 3.2, one of two correlation tests is applied when matching the feature of interest to the original target scene. When nested tracking is employed, each matching 5x5 sub-scene must have a correlation score of 0.8 or higher. Otherwise, the displacement associated with the match is discarded and will not be analyzed by the cluster analysis routine. When conventional tracking is used instead of nested tracking, a

lower threshold of 0.6 is applied. In this case, the correlation scores of each of the intermediate (i.e., the reverse and forward) matching scenes (derived from the SSD method described in Section 3.4.2.3.1) are checked to see if they exceed the minimum threshold value of 0.60. If either scene fails this correlation test, the DMW product is flagged as unacceptable in the output file.

A higher correlation threshold is used for nested tracking because the scene being matched is much smaller and this increases the likelihood of finding a false positive. The higher threshold is a way of accounting for the higher variance in the estimated displacement and is used to remove gross errors from the matching process.

.

u/v-acceleration Test

If the DMWA is performing as intended, it is reasonable to expect that the wind estimates derived from each image pair of the image triplet will be similar to one another. While real accelerations are certainly plausible, especially in certain weather regimes (near jet streams, for example) testing for unrealistic accelerations is prudent, especially given the time and space scales we are concerned with. The existence of an unrealistic acceleration in either the u-component or v-component of the DMW is likely to be the result of a false positive in the tracking step. Large, unrealistic u- or v-accelerations are dealt with by imposing an upper limit of 10 m/s on the difference between the two individual u and v-components of DMWs derived for any of the spectral channels except the visible channel, where a 5 m/s limit is imposed. Any DMW that fails the u/v acceleration test is flagged.

Slow Wind Speed Test

The speed of every DMW is checked against a minimum speed threshold of 3 m/s. If any DMW is slower than this speed threshold, then the DMW is flagged.

Cloud Type Pressure Limit Test

Pressure limit checks are performed for each DMW assigned to the cloud types of thick ice, cirrus, supercooled or liquid cloud scenes and flagged as a Gross Error Failure if the thresholds are exceeded. All DMWs assigned to the mixed cloud type are flagged, as well. The thresholds, applied only to cloud-track winds, are as follows:

Cloud Type	*Test Threshold*
Thick Ice and Cirrus	DMW flagged if median pressure > 500 hPa
Supercooled and Liquid Water	DMW flagged if median pressure < 500 hPa
Mixed	DMW flagged

Correlation Boundary Test

If either of the intermediate matching scenes derived from the SSD method described in Section 3.4.2.3.1 are found on the boundary of the search scene, then the match scene is flagged. This condition may indicate the true matching solution is located beyond the domain of the search scene. In terms of the lag array, this implies that the tracer is rejected if the minimum SSD value is found along the edges of the lag array. Likewise, when nested tracking is used, any matches found on the boundary of the lag array are discarded from influencing the dominant motion calculation.

It should be noted that when tracking the entire target scene with the conventional approach, the correlation boundary test results in a failed tracer. This is not true when nested tracking is employed. In this case, the match is rejected, and the algorithm moves to the next pixel where it attempts to compute another local motion vector. In other words, the small 5x5 sub-target is discarded, not the entire target scene.

NWP Vector Difference Test

An additional quality control component of the derived motion winds is the removal of wind estimates that differ significantly from a short-term numerical weather prediction (NWP) forecast wind. The goal of this test is to remove those winds that are grossly different from the forecast due to a poor motion estimate, a poor height assignment, or both. Previously this test examined the difference between the speed and direction components of the wind vector separately but has since been combined into a single vector difference threshold that is band dependent. The threshold was determined, more or less quantitatively, by examining the relationship between the product accuracy (relative to ground truth radiosonde observations), as defined by the mean vector difference and the standard deviation about the mean, and the maximum vector difference. The upper limit was identified as the vector difference value at which the precision specification dropped sufficiently below the requirement (4.2 m/s set forth in the F&PS document) but did not reduce the coverage (i.e., sample size) excessively. The plot used to determine the vector difference threshold for the LWIR winds is shown below in Figure 13.

Although the standard deviation curve (red) first dips below the precision specification value when a vector difference threshold of 16 m/s is selected, it is clear from the diagram that the sample size isn't adversely impacted until the limit drops below 10 m/s. For this reason, a threshold of 10 m/s was selected as the upper limit for the LWIR winds, meaning any wind having a vector difference from the forecast of more than 10 m/s is rejected. This threshold is applied as a final check on the AMV before it is classified a good wind. In a similar fashion, vector difference thresholds were determined for all wind product bands. Table 8 summarizes the various band-dependent vector thresholds in current use by the DMW algorithm.

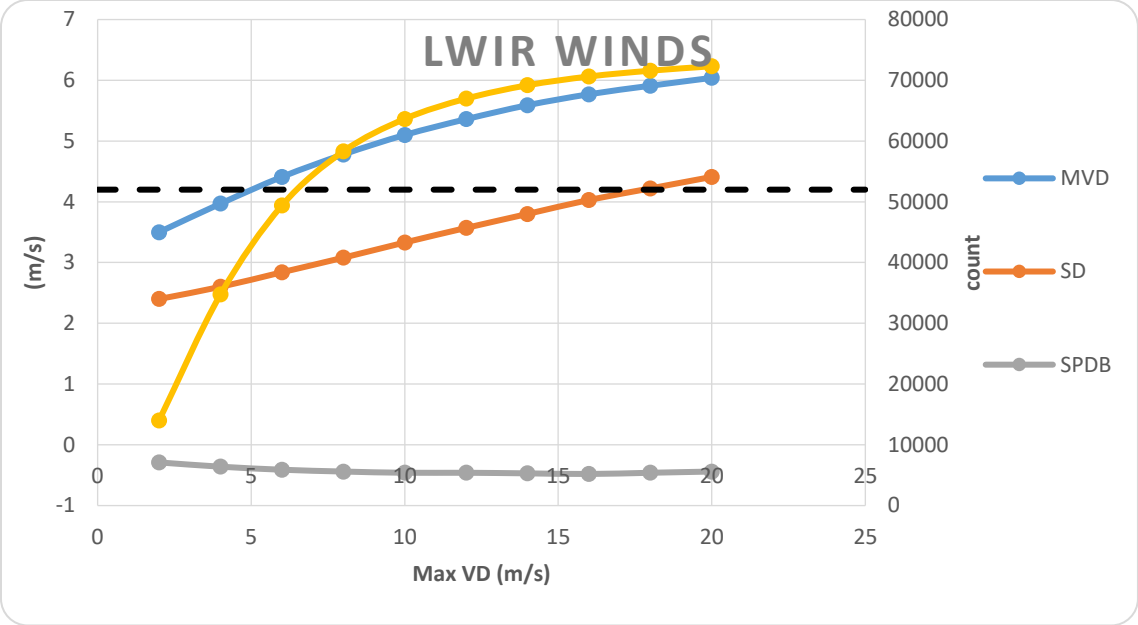

Figure 13. GOES-16 AMV-radiosonde wind verification statistics for the ABI LWIR winds for the period November 1, 2017- January 23, 2018. The Mean Vector Difference (MVD) statistic is used to determine the accuracy of the wind whereas the standard deviation is used to quantify the precision. Note that the accuracy specification (7.5 m/s) is not shown in this figure.

Table 8. Summary of the vector difference thresholds used in the DMW algorithm.

Channel Number	*Tracer Type*	*Vector Difference Threshold (m/s)*
2	Cloud-top	6.0
7	Cloud-top	7.0
8	Cloud-top	10.0
8	Clear-sky water vapor	12.0
9	Clear-sky water vapor	12.0
10	Clear-sky water vapor	12.0
14	Cloud-top	10.0

3.4.2.3 Target Height Assignment

Each suitable target (ie., those passing all of the target selection tests described in Section 3.4.2.1.1) is assigned a height using information from the middle image of the loop sequence. The cloudy or clear designation for each target scene (per the fractional cloud cover test described in Section 3.4.2.1.1) has implications on how a representative height assignment is computed for each target scene.

The process of assigning a representative height to the DMW tracer involves selecting the appropriate sample of pixels from the target scene and using these pixels to compute a representative height for the target scene being processed. The following factors drive the selection of the appropriate sample of pixels to use, as well as the approach, to compute a representative height for each target:

- Target is deemed clear or cloudy
- Cloud height quality flag check
- Channel used to derive the wind
- Whether or not the nested tracking methodology is used

Cloudy Target Scenes

When winds are generated from cloudy target scenes, input pixel-level cloud-top pressures derived using NESDIS' Enterprise Cloud Height Algorithm (Enterprise Cloud Height ATBD for details) are used to compute a representative height for the target scene. Since the nested tracking approach is used when using these channels, only cloud-top pressures associated with pixels belonging to the largest cluster (as defined in the nested tracking discussion in Section 3.4.2.2.2) are used to derive a representative height. Because two unique large clusters are identified – one for the reverse time step and one for the forward time step – the cloud-top pressure samples from both of these clusters are combined and the median cloud-top pressure value is assigned as the representative height for this target.

A key benefit of this approach is that the assigned height is inherently linked to the tracking solution since the same sample of pixels contributes to each of these derived quantities. Figure 14 highlights the fact that this approach will usually produce a lower height assignment in the atmosphere (higher pressure) than the traditional method of assigning the height based on an arbitrary cold sample (typically 20%) of pixels.

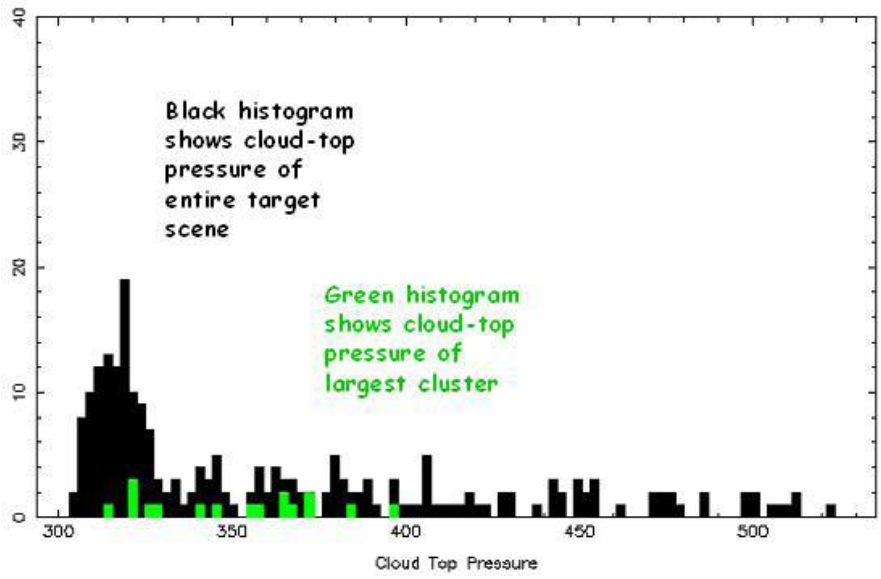

Figure 14. Cloud-top pressure distribution for a single target scene. The values associated with the largest cluster are shown in green.

In situations where a low-level cloudy target scene over ocean is partially or totally located in an area experiencing a low-level temperature inversion, the DMWA must apply a different approach to compute a representative height assignment to the target scene.
Low-level temperature inversions occur frequently over the ocean in the vicinity of the subtropical high where large-scale subsidence contributes to their formation. These regions are often covered by extensive sheets of marine stratocumulus cloud located at the base of the temperature inversion (see Figure 15). Cloud height algorithms often overestimate the height of these cloud layers by 200 hPa or greater (Gustafsson and Lindberg, 1999). The problem arises when there are two elevations in the temperature profile at which the cloud temperature is reached. In this scenario the actual cloud layer is found at the bottom of the inversion.

The DMWA uses the low-level temperature inversion flag output by the cloud height algorithm to identify those pixels in a target scene where a low-level temperature inversion is present. In these situations, the DMWA keeps track of pixels within the largest nested tracking clusters, whose heights are derived at the base of the inversion versus those derived radiometrically via the cloud height algorithm. The DMWA uses only the cloud heights (pressures) belonging to the larger of these two samples to assign a height to the derived wind. The representative height assigned to the derived motion wind is the median pressure of the larger sample.

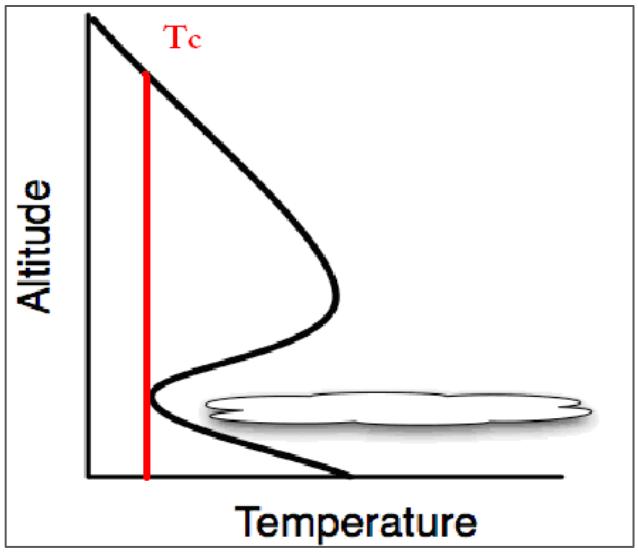

Figure 15. Idealized temperature profile highlighting the cloud height assignment problem posed by low-level temperature inversions.

Clear Target Scenes

When ABI channels 8 (6.15um, clear sky), 9 (7.0um), or 10 (7.4um) are used for targeting clear-sky target scenes (i.e. elevated moisture gradients are being tracked), only clear pixels in the target scene are used. Specifically, a histogram of the target scene brightness temperature values is constructed from all of the clear pixels in the target scene. Next, the 20% coldest pixels of this histogram are identified and the median brightness temperature is calculated. This median brightness temperature is then converted to a height (in pressure) value through linear interpolation of the associated GFS forecast temperatures that bound this brightness temperature.

Initial Cold Sample Height

Regardless of whether nested tracking or traditional tracking is being used an initial "cold sample" height assignment must be computed. The primary purpose of computing an initial height is to use it as a look up index to obtain the forecast wind from a profile. The forecast wind is subsequently used to center the search box in the subsequent (or previous) image. Depending on the channel being processed either a histogram BT values or cloud top temperature values is used to construct a 1-D histogram. The following steps are carried out in constructing the histogram:

1. Loop through each pixel in the target scene and check the cloud mask, temperature (BT or CTT), low-level inversion flag and cloud height quality flag. For clear sky tracers retain all clear and probably clear pixels. For cloudy tracers retain all pixels having a valid cloud top pressure (not missing) and

'good retrieval' quality flag. Next, check that the temperature value is in the range 150 – 340 K and exclude those outside of the range. Lastly, determine how many pixels are located in a low-level inversion region (low-level inversion flag=1) and how many pixels are outside a low-level inversion region (low-level inversion flag=0). Determine which sample is larger.

2. Using the larger sample, a histogram is constructed for the range 150 K – 340 K. With a scale factor of 10 the range of the histogram is actually 1500 – 3400. Each CTT or BT from the larger sample is placed in a slot on the histogram rounding up or down to the nearest bin.

3. A point cutoff is computed using the cold threshold:

Point_Cutoff = NINT(REAL(Histogram_Points) * Cold_Threshold)

where 'Histogram_Points' is the size of the screened sample from step 1 and Cold_Threshold is:

Band 2	0.25
Band 7	0.25
Band 8	0.20 clear sky, 0.99 cloud top
Band 9	0.20 clear sky, 0.99 cloud top
Band 10	0.20 clear sky
Band 14	0.25

4. Starting from the cold end scan the histogram to find the cutoff slot. One of three conditions must be met:

```
DO BrtTemp = Lower_Bound, Upper_Bound   (threshold_loop)

 Cold_Sample = Cold_Sample + Histogram(BrtTemp)

 IF (Histogram(BrtTemp) .GT. 0) Number_Of_Bins = Number_Of_Bins + 1

 IF (Cold_Sample .GT. Point_Cutoff .AND. Number_Of_Bins .GT. 1) THEN

        Cold_Sample = Cold_Sample - Histogram(BrtTemp)
        Cold_Slot_Threshold = BrtTemp - 1
        EXIT

 ! Keep at least one histogram bin
 ELSE IF (Cold_Sample .GT. Point_Cutoff .AND. Number_Of_Bins .EQ. 1) THEN
        Cold_Sample = Cold_Sample
        Cold_Slot_Threshold = BrtTemp
```

```
                EXIT

        ELSE IF (Cold_Sample .LE. Point_Cutoff .AND. BrtTemp .EQ. Upper_Bound) THEN

            Cold_Sample = Cold_Sample
            Cold_Slot_Threshold = BrtTemp
            EXIT

        ENDIF

       END DO  (threshold_loop)
```

Cold sample arrays of BT or CTT, cloud top pressure and cloud top height are created using the cold slot threshold as the highest value allowed

3.4.2.3.1 Derived Motion Wind Height Assignment Quality Tests

All retrieved wind height (in pressure) values undergo a couple of quality control tests to determine if the derived heights are valid. These tests are described below. If a retrieved height fails any one of these tests, it is deemed to be invalid and is flagged appropriately. Each failure is associated with a unique "flag" value which is saved in the DMW output file. These unique flag values are also listed in Table 6.

Acceptable Height Assignment Check

An acceptable height assignment check is done for each derived motion wind that is attempted. The derived height is checked to determine if it falls within an acceptable height (in pressure) range. The minimum and maximum pressures belonging to this range are a function of which channel is being used to derive the wind and shown in Table 9.

Table 9. Acceptable height range to use as a function of channel used and tracer type

Channel Number	Tracer Type	Acceptable Height Range (hPa)
ABI		
2	Cloud-top	700 - 1000
7	Cloud-top	700 - 1000
8	Cloud-top	100 – 350
8	Clear-sky water vapor	100 - 1000
9	Clear-sky water vapor	100 - 1000
10	Clear-sky water vapor	450 - 700
14	Cloud-top	100 - 1000
AHI		
3	Cloud-top	700 - 1000
7	Cloud-top	700 - 1000
8	Cloud-top	100 – 350

8	Clear-sky water vapor	100 - 1000
9	Clear-sky water vapor	100 - 1000
10	Clear-sky water vapor	450 - 700
14	Cloud-top	100 - 1000
VIIRS		
M11	Cloud-top	300 - 1000
M15	Cloud-top	100 - 1000
AVHRR-3		
4	Cloud-top	100 - 1000

Height Consistency Check

When nested tracking is performed, a height consistency checked is performed between the median pressure computed from the largest cluster belonging to the first and second image pairs, respectively. If the difference in these two pressures exceeds 100 hPa, then the derived motion wind is flagged as bad.

Cloud Height Quality Flag Check

The pixel level ABI cloud height quality flag, produced by the upstream cloud algorithm, is used to filter pixels based on the value of this quality indicator. This check is invoked when building the Initial Cold Sample Height (described above) and during the nested tracking height assignment step. The values for this flag are:

Category	*Value*
Good Retrieval	0
Marginal Retrieval	1
Retrieval Attempted	2
Bad Retrieval	3
Opaque Retrieval	4

3.4.2.4 Product Quality Control

Quality control of the retrieved DMWs is performed in two ways. The first is through the application of target selection, feature tracking, and height assignment error checks as described in the previous sections. The second way involves the calculation of two quality indicators for each of the DMWs using two different, but related, algorithms: the Quality Indicator (QI) (Holmlund, 1998; Holmlund et al., 2001) and the Expected Error (EE) (LeMarshall et al., 2004; Berger et al. 2008).

3.4.2.4.1 Quality Indicator (QI) Method

The statistically-based quality indicator (QI) developed at EUMETSAT estimates the reliability of each derived DMW based on several quality control tests (Holmlund, 1998, Holmlund et. al 2001). These tests not only analyze the consistency in space and time of each of the intermediate DMW vector components, but also the height and temperature of the tracers used in the vector determination, the symmetry of vector pairs achieved from tracking tracers between consecutive images, differences with surrounding vectors, and differences from a forecast field (optional). There are a total of seven individual components that contribute to the final QI score that is appended to each DMW. A weighted average value is computed for the final quality test function value $f_i(x)$ for each vector. In order to combine the results of the different test functions, each result must be normalized into a specific range. This is done using a tanh-based function:

$$\phi_i(x) = 1 - \tanh\left\{\left[f_i(x)\right]\right\}^{a_i} \tag{15}$$

After normalization of all of the tests, QI values will be distributed from zero (poor quality) to one (perfect quality).

Direction Consistency Check

This calculation is a measure of the direction consistency of the DMW. A quality tracer should provide sub-vectors that are similar in direction. In function space it is calculated as:

$$\text{Direction:} \quad |D_2(x,y) - D_1(x,y)| / A * \exp^{-((V_2(x,y)+V_1(x,y))/B)+C)} \tag{16}$$

$D_i(x, y)$, $V_i(x, y)$ are the direction (degrees) and speed (m/s) derived from the first image ($i = 1$) pair (image 1 and image 2) or the second imager ($i = 2$) pair (image 2 and image 3) of an image triplet at location (x, y).

The normalized component used in the software is constructed as such:

$$QI_{dir} = 1 - (\tanh(|D_2(x, y)-D_1(x, y)|/(A*\exp(-vel/B)+C)))^{**}D \tag{17}$$

Where:

$vel = (V_1(x, y) + V_2(x, y))/2$

The values of the constants are:

A	20
B	10
C	10
D	4

Speed Consistency Check

This calculation is a measure of the speed consistency of the DMW. Intermediate DMWs should show agreement in speed. In function space it is calculated as:

$$\text{Speed:} \qquad |V_2(x, y)-V_1(x, y)|/(A*(V_2(x, y)+(V_1(x, y))+B) \tag{18}$$

$V_i(x, y)$ is the speed (m/s) derived from the first image ($i = 1$) pair (image 1 and image 2) or the second image ($i = 2$) pair (image 2 and image 3) of an image triplet at location (x, y).

The normalized component used in the software is constructed as such:

$$QI_{spd} = 1 - (\tanh(|V_2(x, y)-V_1(x, y)|/(A*vel+B)))**C \tag{19}$$

Where:

$vel = (V_1(x, y) + V_2(x, y))/2$

The values of the constants are:

A	0.2
B	1.0
C	3.0

Vector Consistency Check

This calculation is a measure of the vector consistency of the DMW. This test looks at the vector pairs that make up the final DMW. It should reject acceleration errors, but allow for real acceleration changes (jet entrance and exit regions). In function space it is calculated as:

$$\text{Vector:} \qquad |S_2(x, y)-S_1(x, y)|/(A*(V_2(x, y)+(V_1(x, y))+B) \tag{20}$$

$S_i(x, y)$ is the vector (m/s) derived from the first image ($i = 1$) pair (image 1 and image 2) or the second image ($i = 2$) pair (image 2 and image 3) of an image triplet at location (x, y).

The normalized component used in the software is constructed as such:

$$QI_{vec} = 1 - (\tanh(|S_2(x, y)-S_1(x, y)|/(A*vel+B)))**C \tag{21}$$

Where:

$vel = (V_1(x, y) + V_2(x, y))/2$

The values of the constants are:

A	0.2
B	1.0
C	3.0

Spatial Consistency Check (i.e. Best Buddy Check)

This calculation is a measure of the spatial wind consistency of the DMW with its best neighbor. To do this, the DMW values are compared with the DMWs computed at the neighboring grid points.

In function space it is calculated as:

$$\text{Spatial:} \quad |S(x, y)-S(x-i, y-j)|/(A*(|S(x, y)+(S(x-i, y-j)|)+B) \tag{22}$$

Here, $S(x, y) = S_1(x, y) + S_2(x, y)$. $S(x-i, y-j)$ refers to the vectors (m/s) in the surrounding locations. This spatial test is only applied to vectors within a predefined pressure range (50 hPa), and location range (within 1 degree).

The normalized component used in the software is constructed as such:

$$QI_{spatial} = 1 - (\tanh(|S(x-i, y-j)-S(x, y)|/(A*|S(x, y)+(S(x-i, y-j)| +B)))**C \tag{23}$$

The values of the constants are:

A	0.2
B	1.0
C	3.0

Forecast Check

This is currently set as an optional test, and is a measure of the consistency of the satellite DMW with the forecast wind at the height of the satellite DMW. The vector difference of the DMW values and the forecast vector interpolated to the same location and pressure level is computed to calculate it. In function space it is represented as:

$$\text{Forecast:} \quad |S_2(x, y)-F_1(x, y)|/(A*(|S_2(x, y)+(F_1(x, y)|)+B) \tag{24}$$

Where $S_2(x, y)$ is the vector (m/s) from the final DMW at location (x, y). $F_1(x, y)$ is the interpolated forecast vector (m/s) at location (x, y).

The normalized component used in the software is constructed as such:

$$QI_{fc} = 1 - (\tanh(|S_2(x, y)-F_1(x, y)|/(A*fc\_spd+B)))^{**}C \quad (25)$$

In practice, fc_spd is the speed (m/s) of the forecast at the DMW location. The values of the constants are:

A	0.4
B	1.0
C	2.0

U-Component Consistency Check

This calculation is a measure of the DMW's u-component (m/s) consistency from each intermediate vector. In function space it is calculated as:

$$\text{U-component:} \quad |u_2(x, y)-u_1(x, y)|/((A*|u_2(x, y)+(u_1(x, y)|)+B) \quad (26)$$

The normalized component used in the software is constructed as such:

$$QI_{uc} = 1 - (\tanh(|u_2(x, y)-u_1(x, y)|/(A*|u_2(x, y)+u_1(x, y)|+B)))^{**}C \quad (27)$$

The values of the constants are:

A	1.0
B	1.0
C	2.0

V-Component Consistency Check

This calculation is a measure of the DMW's v-component (m/s) consistency from each intermediate vector. In function space it is calculated as:

$$\text{V-component:} \quad |v_2(x, y)-v_1(x, y)|/((A*|v_2(x, y)+(v_1(x, y)|)+B) \quad (28)$$

The normalized component used in the software is constructed as such:

$$QI_{vc} = 1 - (\tanh(|v_2(x, y)-v_1(x, y)|/(A*|v_2(x, y)+v_1(x, y)|+B)))^{**}C \quad (29)$$

The values of the constants are:

A	1.0
B	1.0
C	2.0

To achieve a single QI value to represent the quality of each DMW, a weighted average of each normalized QI component is computed:

$$QI = \Sigma \text{ (Test Weight * Normalized QI Component test)} / \Sigma \text{ Test Weights} \quad (30)$$

The test weights used for each normalized QI component is shown in Table 10.

Table 10. Test weights used for each normalized QI component test.

Direction Component	1.0
Speed Component	1.0
Vector Component	1.0
Spatial Component	2.0
Forecast Component	1.0
U Component	0.0
V Component	0.0

Figure 16 shows an example of the final (weighted) QI distribution for winds generated from the 12 UTC 04 August 2006 Meteosat-8/SEVIRI proxy dataset. DMWs that possess QI values less than 0.60 are currently flagged as unacceptable quality.

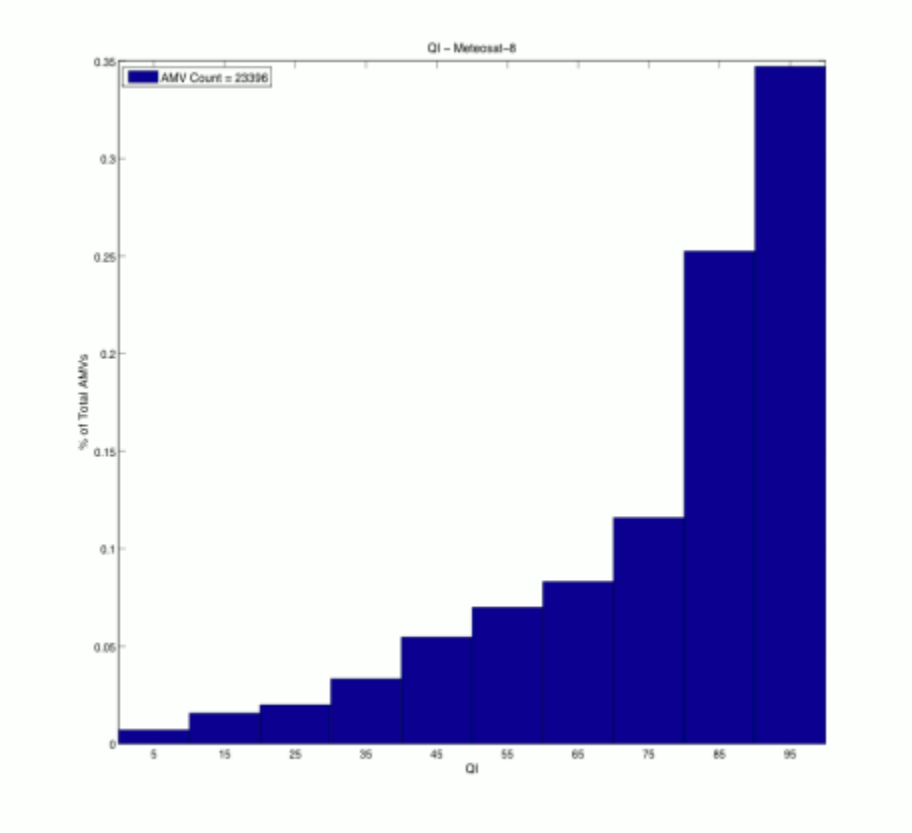

Figure 16. Histogram of the final (weighted) QI values for Meteosat-8 DMWs at 12 UTC on 04 August 2006.

3.4.2.4.2 Expected Error Method

The Expected Error (EE) algorithm, originally developed at the Australian Bureau of Meteorology (LeMarshall et al, 2004) is an extension of the QI algorithm described in the previous section. It is designed to express quality in terms of a physical vector error metric (meters/second, m/s), rather than a normalized score such as the QI. A slightly modified version of the EE algorithm described in Berger et al. 2008 has been adopted for use with the GOES-R DMWA. As shown in (31), the algorithm regresses several DMW variables against the natural logarithm of the EE, which represents the vector difference (in m/s) between a large sample of collocated DMWs and radiosonde winds.

$$a_0 + a_1 x_1 + a_2 x_2 + \ldots a_9 x_9 = \log(EE + 1) \tag{31}$$

where EE is the expected (or estimated) error, a_0 is a constant, and a_n values are regression coefficients multiplied by their corresponding predictors (x_n). The coefficients are applied in real time to compute and assign an EE to each DMW using:

$$EE = e^{(a_0 + a_1 x_1 + a_2 x_2 + \ldots a_9 x_9)} - 1 \tag{32}$$

The (-1) term constrains the minimum EE value to be zero. The current predictors are:

1. Constant (spectrally dependent)
2. QI Speed Test
3. QI Direction Test
4. QI Vector Difference
5. QI Local Consistency Test
6. QI Forecast Test
7. DMW Speed
8. Assigned DMW Pressure Level (height)
9. NWP Wind Shear (200 hPa Above – 200 hPa below DMW height)
10. NWP Temperature Gradient (200 hPa Above – 200 hPa below DMW height)

Table 11. Expected Error coefficients and predictors for different Meteosat-8 channels derived from the period August – October 2007.

Predictor	**Band-1 (0.60um)**	**Band-4 (3.9um)**	**Band-5 (6.2um)**	**Band-6 (7.3um)**	**Band-9 (10.8um)**
CONST	3.073	3.13	2.42	2.42	2.871
QI Speed Check	0.176	0.003	0.0660	0.0660	-0.0664

QI Direction Check	0.290	-0.171	0.199	0.199	0.1394
QI Vector	-0.101	-0.0471	-0.331	-0.331	-0.176
QI Local Consistency	-0,280	0.244	-0.173	-0.173	-0.252
QI Forecast Check	-0.585	-1.46	-0.552	-0.552	-0.509
DMW Speed	0.014	-3.61×10^{-3}	7.10×10^{-3}	7.10×10^{-3}	6.26×10^{-3}
DMW Pressure	-1.63×10^{-3}	-9.43×10^{-4}	-6.79×10^{-4}	-6.79×10^{-4}	-7.42×10^{-4}
NWP Wind Shear	0.011	0.015	7.80×10^{-3}	7.80×10^{-3}	9.81×10^{-3}
NWP Temp Gradient	0.011	-7.47×10^{-3}	6.89×10^{-3}	6.89×10^{-3}	0.0126

Table 11 shows a set of predictors and their respective coefficients used to calculate EE for different bands from the SEVIRI instrument (proxy to the ABI) onboard the Meteosat-8 satellite, generated from a dataset containing collocated Meteosat-8 DMWs and radiosonde wind observations that covered the period August – October 2007.

Synergistic Use of the EE and QI Quality Indicators

The outputted EE and QI quality indicators associated with each DMW estimate can be used synergistically in order to optimize the quality and geographic coverage of the final DMW dataset passed onto the user community. The synergistic use of these quality indicators is designed to take advantage of the strengths of each. The EE is superior at identifying the quality of relatively slow DMWs, whereas the QI is better at identifying the quality of relatively fast DMWs. A study conducted under the GOES-R Risk Reduction (Berger et al. 2008) sought to identify thresholds for each parameter that could serve as a potential starting point for users to use, if so desired, in any process they may have established to select a subset of the highest quality DMWs. Table 12 summarizes what these thresholds are, and shows that they vary as a function of the channel used to derive the DMW and the DMW speed. DMWs whose speeds are slower than the indicated speed thresholds are considered higher quality if their respective EE quality indicators are less then or equal to the EE threshold shown in Table 11. DMWs whose speeds exceed the speed thresholds are considered higher quality DMWs if their respective QI indicators exceed the QI thresholds shown in Table 12.

Table 12. Recommended thresholds for synergistic use of the QI and EE indicators

Channel	EE (m/s) <	OR (QI >	& Speed (m/s) >
1 (0.64um)	5.5	95	30
4 (3.90um)	5.0	95	30
5 (6.15um)	5.0	95	30
6 (7.30um)	5.0	95	30
9 (10.8um)	4.5	90	25

In order to validate the established thresholds in Table 12, Meteosat-8 DMWs were generated for an independent dataset covering February 2007 and compared to collocated radiosonde wind observations. The EE values were calculated using the generated coefficients from Table 11, and the QI was calculated as described in the previous section. Table 13 shows an example of DMW-RAOB verification statistics looking at QI > 0.6, QI > 0.8 and the specific EE/QI threshold for IR DMWs from Table 12. The statistics are for all available DMW heights in the dataset. A 0.8 QI threshold produces a lower RMSE, mean vector difference, and standard deviation than the 0.6 threshold (as expected). However, the QI/EE combination threshold results in the lowest RMSE error, mean-vector difference and speed bias of the three quality indicator choices. Use of the combined QI/EE thresholds generally results in the retention of more (less) DMWs when using the QI > 0.8 (0.60) threshold alone. These findings also hold for the other channel DMWs.

Table 13: Comparison statistics (m/s) between DMWs computed from the SEVIRI IR-Window channel (10.8um) and collocated radiosonde winds during Feb 2007.

QC	QI > 0.6	QI > 0.8	EE<=4.5 .OR. (QI>90 and Speed>25 m/s
RMSE	7.62	7.30	6.14
Bias	-1.62	-1.19	-1.02
Number of matches	23692	17501	16861
Mean Vector Difference	6.08	5.82	5.03
Standard Deviation	4.60	4.39	3.53
Avg. DMW Speed	17.16	18.48	17.21

3.4.3 Algorithm Output

Derived motion winds are generated separately by the band selected. The contents of the output of the DMWA are described in the following subsections.

3.4.3.1 Product Output

ID	Description
1	Time of wind from the middle image in image triplet (secs since 1970-01-01 00:00:00) Time
2	Latitude (degrees north) Latitude
3	Longitude (degrees east) Longitude
4	Speed of wind vector (m/s) Wind_Speed
5	Direction of wind vector (degrees) Wind_Dir
6	Pressure assignment of tracer (hPa) MedianPress (hPa)
7	Temperature associated with the pressure assignment of tracer (K) MedianBT
8	Local Zenith Angle (degrees) SatZen
9	Time interval between image pairs (minutes) TimeInterval

3.4.3.2 Diagnostic Information

ID	Description
1	u-component of vector 1 (m/s) [backward in time] UComponent1
2	v-component of vector 1 (m/s) [backward in time] VComponent1
3	u-component of vector 2 (m/s) [forward in time] UComponent2
4	v-component of vector 2 (m/s) [forward in time] VComponent2
5	Speed of forecast wind (m/s) at pressure assigned to satellite wind Fcst_Spd
6	Direction of forecast wind (degrees) at pressure assigned to satellite wind Fcst_Dir

7	Tracking correlation of vector 1 [backward in time] CorrCoeff
8	Tracking correlation of vector 2 [forward in time] CorrCoeff2
9	Standard deviation of cloud top pressure values in target scene (hPa) VariancePress
10	Cold sample counter in brightness temperature histogram PointIndex
11	Latitude of vector 1 (degrees north) [backward in time] LatMatch
12	Longitude of vector 1 (degrees east) [backward in time] LonMatch
13	Latitude of vector 2 (degrees north) [forward in time] LatMatch2
14	Longitude of vector 2 (degrees east) [forward in time] LonMatch2
15	Standard deviation of largest 5x5 cluster (sample 1 – reverse vector) StdDevMVD1
16	Standard deviation of largest 5x5 cluster (sample 2 – forward vector) StdDevMVD2
17	Standard deviation of sample 1 divided by magnitude of average displacement PctOfAvg1
18	Standard deviation of sample 2 divided by magnitude of average displacement PctOfAvg2
19	Number of distinct motion clusters from DBSCAN analysis (sample 1 – reverse vector) NumClusters1
20	Size of largest DBSCAN cluster (sample 1 – reverse vector) MaxClusterSize1
21	Number of distinct motion clusters from DBSCAN analysis (sample 2 – forward vector) NumClusters2
22	Size of largest DBSCAN cluster (sample 2 – forward vector) MaxClusterSize2
23	Height assignment of tracer (m) Altitude
24	Date of 1st image (year and Julian day) PriorImageDate
25	Time of 1st image (hour and minute) PriorImageTime
26	Date of 3rd image (year and Julian day) NextImageDate
27	Time of 3rd image (hour and minute) NextImageTime

28	Minimum cloud-top pressure (hPa) in largest cluster MinCTP
29	Maximum cloud-top pressure (hPa) in largest cluster MaxCTP
30	Minimum cloud-top temperature (K) in largest cluster MinCTT
31	Maximum cloud-top temperature (K) in largest cluster MaxCTT
32	Dominant cloud phase of target scene CloudPhase
33	Dominant cloud type of target scene CloudType
34	NWP vertical temperature gradient (K) [+/- 200 hPa about pressure assignment of tracer] TempGrad
35	NWP vertical wind shear (m/s) [+/- 200 hPa about pressure assignment of tracer] Wind_Speed_Shear
36	Land mask LandFlag
37	Low-level inversion flag InversionFlag

3.4.3.3 Product Quality Information

ID	Description
1	Product Quality Flag (0DMW product passes all quality tests; > 0 DMW product fails quality tests. *(See Table 6 in Section 3.4.2.1.1 for description of DMW failure codes)* Flag
2	Expected Error estimate of derived wind (m/s) ExpectedErr
3	Quality Indicator (QI) of derived wind with forecast term applied (0-100, with 100 being the best) QI
4	Quality Indicator (QI) of derived wind without forecast term applied (0-100, with 100 being the best) QINF
5	QI Test 1 value (speed consistency) QISpdFlag
6	QI Test 2 value (direction consistency) QIDirFlag
7	QI Test 3 value (vector consistency) QIVecFlag

8	QI Test 4 value (local consistency) QILocConsistencyFlg
9	QI Test 5 value (forecast consistency) QIFcstFlag
10	Representative height error (hPa) CombinedMedianHgtErr
11	Representative temperature error (K) CombinedMedianTempErr

3.4.3.4 Metadata Information

ID	Description
1	Satellite ID SatID
2	Number of ABI channels NumOfChn
3	ABI channel number AMVChannel
4	Target box size (in pixels) BoxSize
5	Lag size (in pixels) LagSize
6	Nested tracking flag (0=nested tracking disabled, 1= nested tracking enabled) NestedTrackingFlg
7	Target type (0 = clear; 1 = cloudy) Target_Type
8	Number of QC flag values: 23 NumQAVals
9	Percent of targets associated with a QC flag value 0 *Good wind; passes all QC checks* QA_Value_0
10	Percent of targets associated with a QC flag value 1 *Maximum gradient below acceptable threshold* QA_Value_1
11	Percent of targets associated with a QC flag value 2 *Target located on earth edge* QA_Value_2
12	Percent of targets associated with a QC flag value 3 *Cloud amount failure (less than 10% cloud cover for cloud track winds or greater than 0% cloud cover for water vapor clear sky winds)* QA_Value_3
13	Percent of targets associated with a QC flag value 4 *Median pressure failure* QA_Value_4

14	Percent of targets associated with a QC flag value 5 *Bad or missing brightness temperature in target scene* QA_Value_5
15	Percent of targets associated with a QC flag value 6 *More than 1 cloud layer present* QA_Value_6
16	Percent of targets associated with a QC flag value 7 *Target scene too coherent (not enough structure for reliable tracking)* QA_Value_7
17	Percent of targets associated with a QC flag value 8 *Tracking correlation below 0.6 (not used for nested tracking)* QA_Value_8
18	Percent of targets associated with a QC flag value 9 *u-component acceleration greater than 5 m/s (for winds generated from visible channel) or 10 m/s (for winds generated from any other channel)* QA_Value_9
19	Percent of targets associated with a QC flag value 10 *v-component acceleration greater than 5 m/s (for winds generated from visible channel) or 10 m/s (for winds generated from any other channel)* QA_Value_10
20	Percent of targets associated with a QC flag value 11 *u- and v- component accelerations greater than 5 m/s (for winds generated from visible channel) or 10 m/s (for winds generated from any other channel)* QA_Value_11
21	Percent of targets associated with a QC flag value 12 *Derived wind slower than 3 m/s* QA_Value_12
22	Percent of targets associated with a QC flag value 13 *Target scene too close to day/night terminator (visible and SWIR only)* QA_Value_13
23	Percent of targets associated with a QC flag value 14 *Median pressure used for height assignment outside acceptable pressure range (channel dependent)* QA_Value_14
24	Percent of targets associated with a QC flag value 15 *Match found on boundary of search region* QA_Value_15
25	Percent of targets associated with a QC flag value 16 *Gross difference from forecast wind (channel dependent)* QA_Value_16
26	Percent of targets associated with a QC flag value 17 *Median pressure of largest cluster for first image pair is too different from median pressure of largest cluster for second image pair – only valid for nested tracking* QA_Value_17

27	Percent of targets associated with a QC flag value 18 *Search region extends beyond domain of data buffer* QA_Value_18
28	Percent of targets associated with a QC flag value 19 *Expected Error (EE) too high* QA_Value_19
29	Percent of targets associated with a QC flag value 20 *Missing data in search region* QA_Value_20
30	Percent of targets associated with a QC flag value 21 *No winds are available for the clustering algorithm* QA_Value_21
31	Percent of targets associated with a QC flag value 22 *No clusters were found* QA_Value_22
32	Total targets identified NumTargets_Total
33	Mean wind speed (m/s) for all good derived winds WndSpdMean
34	Minimum wind speed (m/s) for all good derived winds WndSpdMin
35	Maximum wind speed (m/s) for all good derived winds WndSpdMax
36	Standard deviation about mean wind speed (m/s) for all good derived winds WndSpdStdDev
37	Number of Atmospheric Layers NumOfAtmosLayers
38	Number of good winds in atmospheric layer 1 *(100 - 399.9 hPa)* NumGoodWnds_Layer1
39	Number of good winds in atmospheric layer 2 *(400 – 699.9 hPa)* NumGoodWnds_Layer2
40	Number of good winds in atmospheric layer 3 *(700 – 1000 hPa)* NumGoodWnds_Layer3
41	Mean height (hPa) assigned to good derived winds in atmospheric layer 1 CldHgtMean_Layer1
42	Standard deviation about mean height (hPa) assigned to good derived winds in atmospheric layer 1 CldHgtStdDev_Layer1
43	Minimum height (hPa) assigned to good winds in atmospheric layer 1 CldHgtMin_Layer1
44	Maximum height (hPa) assigned to good winds in atmospheric layer 1

	CldHgtMax_Layer1
45	Standard deviation about mean wind speed (m/s) for all good derived winds in atmospheric layer 1 WndSpdStdDev_Layer1
46	Mean height (hPa) assigned to good derived winds in atmospheric layer 2 CldHgtMean_Layer2
47	Standard deviation about mean height (hPa) assigned to good derived winds in atmospheric layer 2 CldHgtStdDev_Layer2
48	Minimum height (hPa) assigned to good winds in atmospheric layer 2 CldHgtMin_Layer2
49	Maximum height (hPa) assigned to good winds in atmospheric layer 2 CldHgtMax_Layer2
50	Standard deviation about mean wind speed (m/s) for all good derived winds in atmospheric layer 2 WndSpdStdDev_Layer2
51	Mean height (hPa) assigned to good derived winds in atmospheric layer 3 CldHgtMean_Layer3
52	Standard deviation about mean height (hPa) assigned to good derived winds in atmospheric layer 3 CldHgtStdDev_Layer3
53	Minimum height (hPa) assigned to good winds in atmospheric layer 3 CldHgtMin_Layer3
54	Maximum height (hPa) assigned to good winds in atmospheric layer 3 CldHgtMax_Layer3
55	Standard deviation about mean wind speed (m/s) for all good derived winds in atmospheric layer 3 WndSpdStdDev_Layer3
56	Percent good winds generated GoodWndClrCld

4 DMW OUTPUTS AND VERIFICATION

4.1 Output from GOES-R L1B Data

The DMW product is generated routinely for GOES-16 and 17 for all sectors and wind types as described in previous sections. The following figures 17 through 29 show examples of cloud-drift and water vapor winds generated from tracking either cloud or water vapor features observed in GOES-16 and 17 L1B imagery for a variety of channels and sectors.

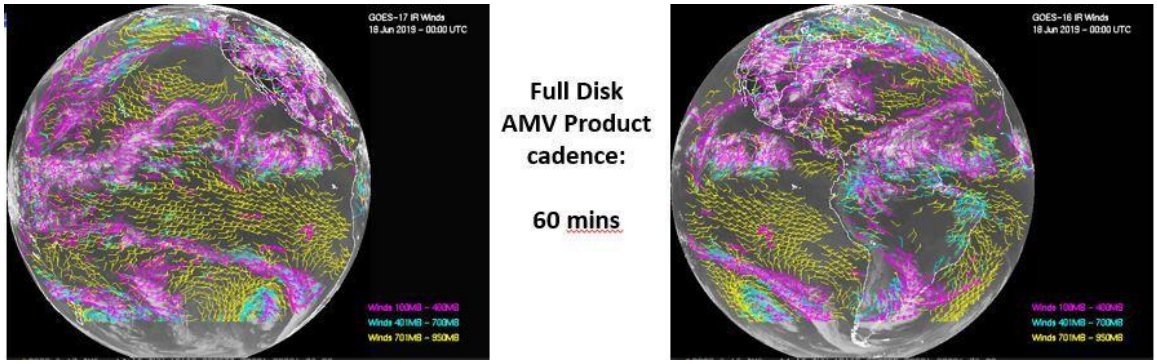

Figure 17. GOES-16 and 17 cloud-drift winds derived from Full Disk 10-minute 11.2um ABI data for 00 UTC on 18 June 2019. These winds are derived from tracking cloud features using the 11.2um channel. High level (100-400 hPa) winds are shown in violet; mid-level (400-700 hPa) winds are shown in cyan; and low-level winds (below 700 hPa) are shown in yellow.

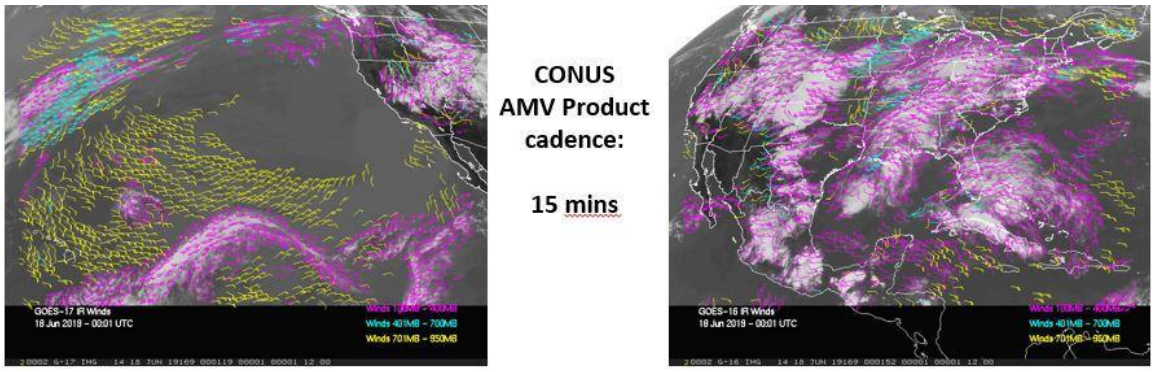

Figure 18. GOES-16 and 17 cloud-drift winds derived from CONUS 5-minute 11.2um ABI data for 00 UTC on 18 June 2019. These winds are derived from tracking cloud features using the 11.2um channel. High level (100-400 hPa) winds are shown in violet; mid-level (400-700 hPa) winds are shown in cyan; and low-level winds (below 700 hPa) are shown in yellow.

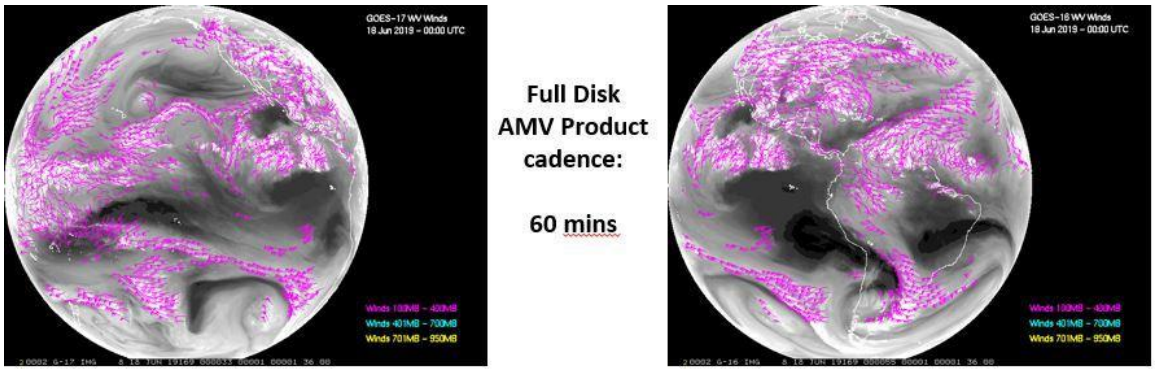

Figure 19. GOES-16 and 17 cloud-drift winds derived from Full Disk 10-minute 6.2um ABI data for 00 UTC on 18 June 2019. These winds are derived from tracking cloud features using the 6.2um channel. High level (100-400 hPa) winds are shown in violet; mid-level (400-700 hPa) winds are shown in cyan; and low-level winds (below 700 hPa) are shown in yellow.

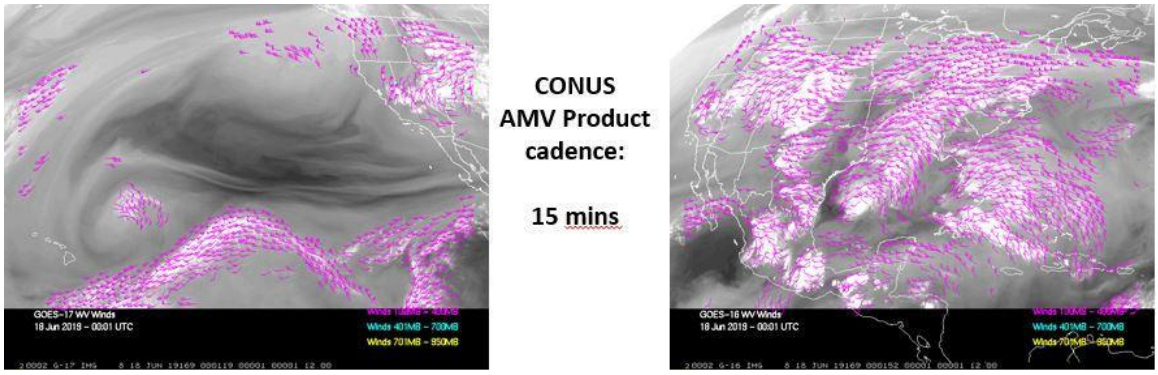

Figure 20. GOES-16 and 17 cloud-drift winds derived from CONUS 5-minute 6.2um ABI data for 00 UTC on 18 June 2019. These winds are derived from tracking cloud features using the 6.2um channel. High level (100-400 hPa) winds are shown in violet; mid-level (400-700 hPa) winds are shown in cyan; and low-level winds (below 700 hPa) are shown in yellow.

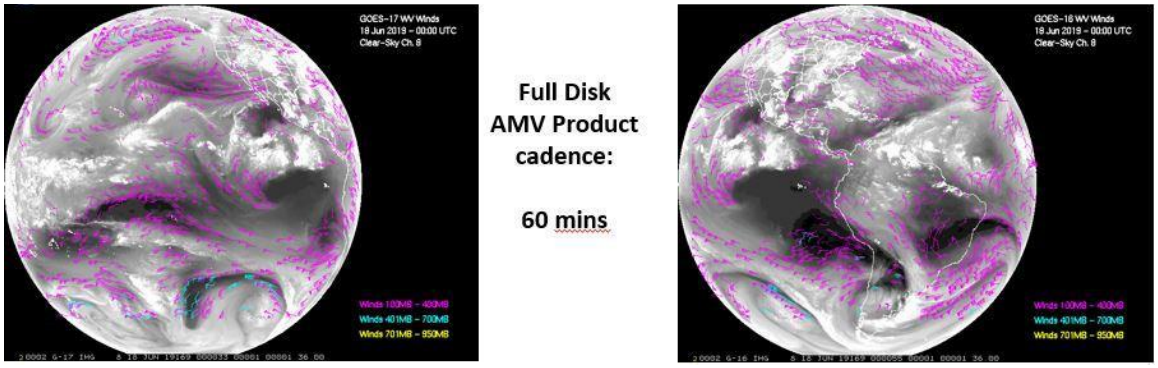

Figure 21. GOES-16 and 17 clear-sky water vapor winds derived from Full Disk 30-minute 6.2um ABI data for 00 UTC on 18 June 2019. These winds are derived from tracking water vapor features using the 6.2um channel. High level (100-400 hPa) winds are shown in violet; mid-level (400-700 hPa) winds are shown in cyan; and low-level winds (below 700 hPa) are shown in yellow.

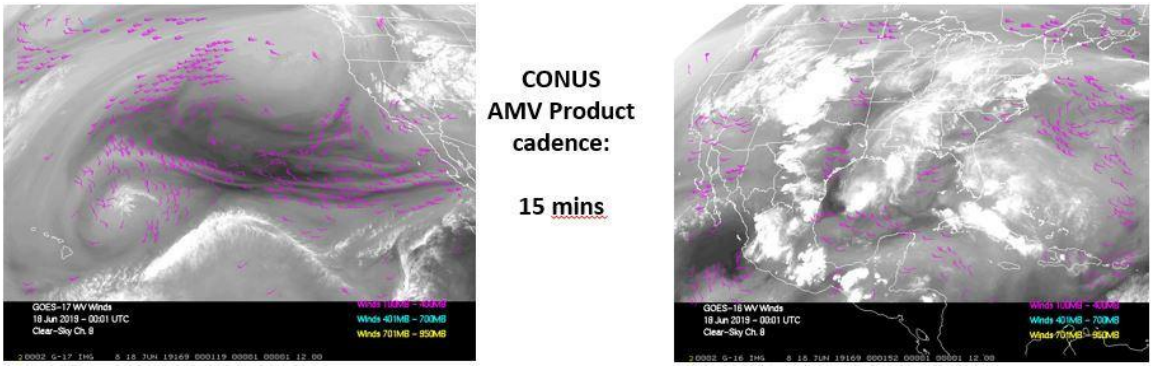

Figure 22. GOES-16 and 17 clear-sky water vapor winds derived from CONUS 30-minute 6.2um ABI data for 00 UTC on 18 June 2019. These winds are derived from tracking water vapor features using the 6.2um channel. High level (100-400 hPa) winds are shown in violet; mid-level (400-700 hPa) winds are shown in cyan; and low-level winds (below 700 hPa) are shown in yellow.

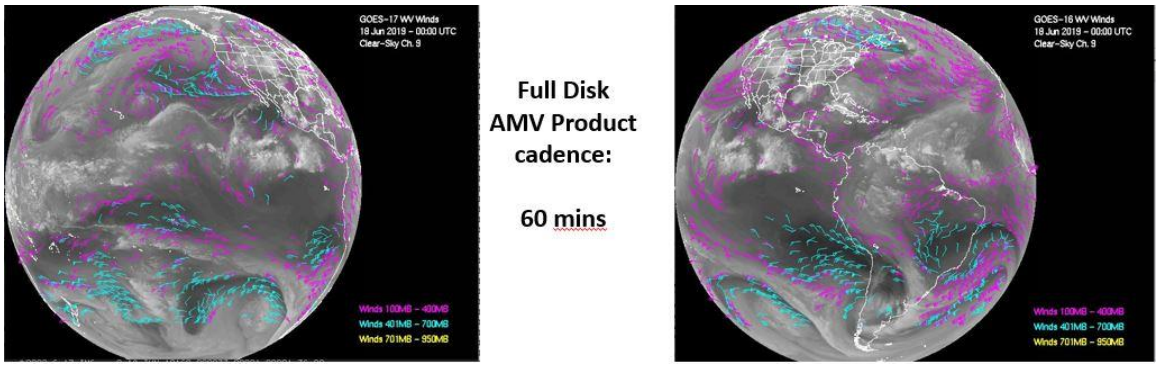

Figure 23. GOES-16 and 17 clear-sky water vapor winds derived from Full Disk 30-minute 6.9um ABI data for 00 UTC on 18 June 2019. These winds are derived from tracking water vapor features using the 6.9um channel. High level (100-400 hPa) winds are shown in violet; mid-level (400-700 hPa) winds are shown in cyan; and low-level winds (below 700 hPa) are shown in yellow.

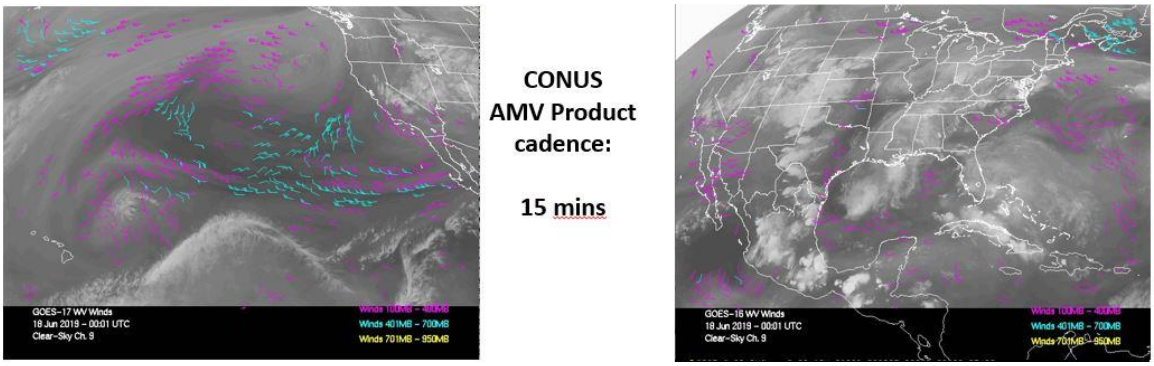

Figure 24. GOES-16 and 17 clear-sky water vapor winds derived from CONUS 30-minute 6.9um ABI data for 00 UTC on 18 June 2019. These winds are derived from tracking water vapor features using the 6.9um channel. High level (100-400 hPa) winds are shown in violet; mid-level (400-700 hPa) winds are shown in cyan; and low-level winds (below 700 hPa) are shown in yellow.

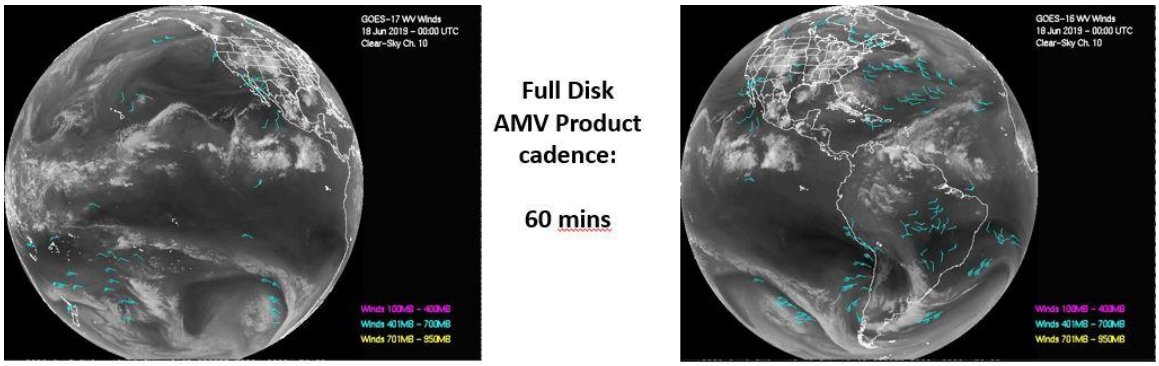

Figure 25. GOES-16 and 17 clear-sky water vapor winds derived from Full Disk 30-minute 7.3um ABI data for 00 UTC on 18 June 2019. These winds are derived from tracking water vapor features using the 7.3um channel. High level (100-400 hPa) winds are shown in violet; mid-level (400-700 hPa) winds are shown in cyan; and low-level winds (below 700 hPa) are shown in yellow.

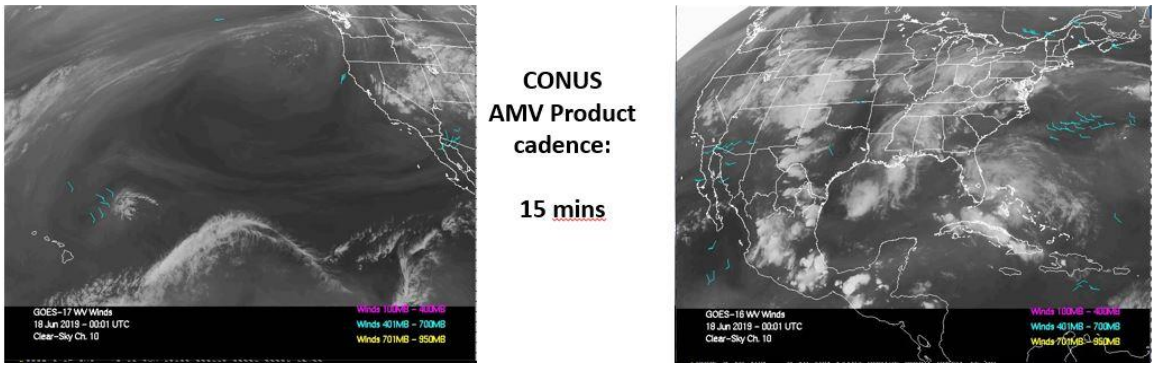

Figure 26. GOES-16 and 17 clear-sky water vapor winds derived from CONUS 30-minute 7.3um ABI data for 00 UTC on 18 June 2019. These winds are derived from tracking water vapor features using the 7.3um channel. High level (100-400 hPa) winds are shown in violet; mid-level (400-700 hPa) winds are shown in cyan; and low-level winds (below 700 hPa) are shown in yellow.

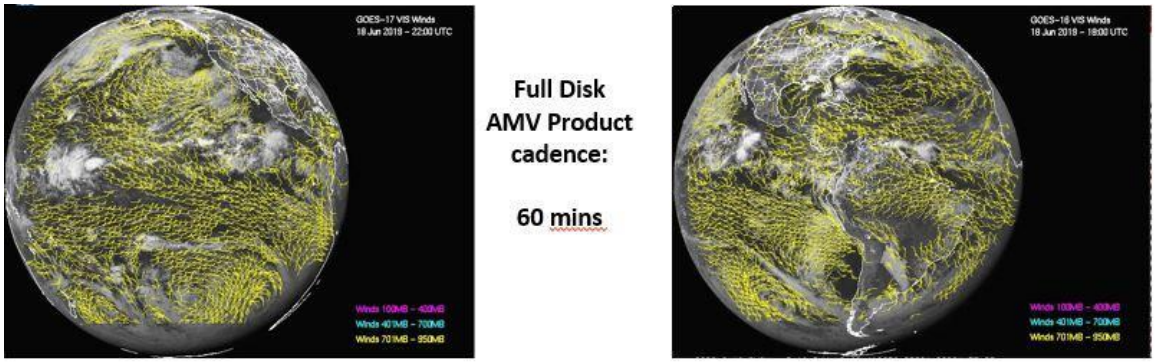

Figure 27. GOES-16 and 17 cloud-drift winds derived from Full Disk 10-minute 0.64um ABI data for 22 UTC on 18 June 2019. These winds are derived from tracking cloud features using the 0.64um channel. High level (100-400 hPa) winds are shown in violet; mid-level (400-700 hPa) winds are shown in cyan; and low-level winds (below 700 hPa) are shown in yellow.

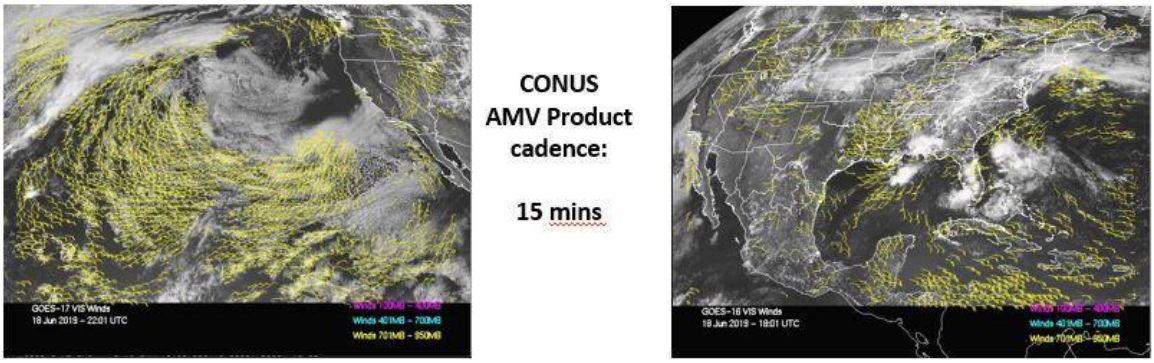

Figure 28. GOES-16 and 17 cloud-drift winds derived from CONUS 5-minute 0.64um ABI data for 22 UTC on 18 June 2019. These winds are derived from tracking cloud features using the 0.64um channel. High level (100-400 hPa) winds are shown in violet; mid-level (400-700 hPa) winds are shown in cyan; and low-level winds (below 700 hPa) are shown in yellow.

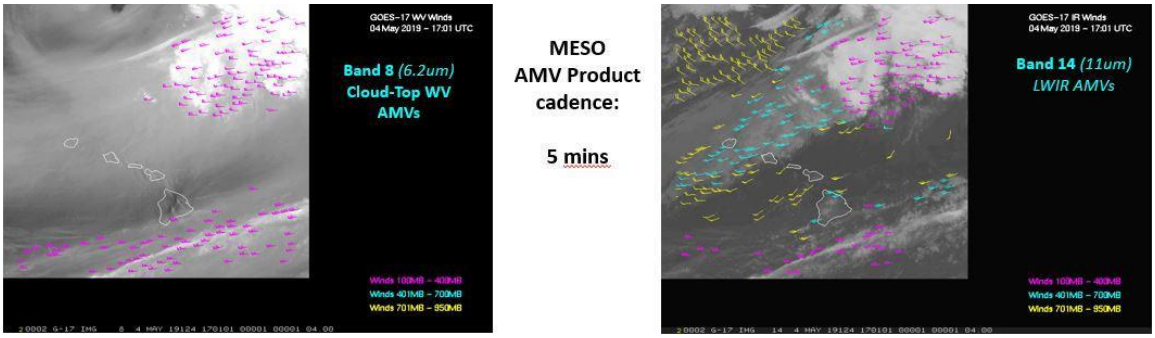

Figure 29. GOES-17 cloud-drift winds derived from MESO sector 5-minute ABI 6.2um (left) and 11.2um (right) data for 17 UTC on 04 May 2019. High level (100-400 hPa) winds are shown in violet; mid-level (400-700 hPa) winds are shown in cyan; and low-level winds (below 700 hPa) are shown in yellow.

4.2 *Output from Himawari L1B Data*

The DMW product is generated routinely for Himawari Full Disk sectors as described in previous sections. The following figures 30 through 36 show examples of cloud-drift and water vapor winds generated from tracking either cloud or water vapor features observed in Himawar-8 L1 imagery for a variety of channels and sectors.

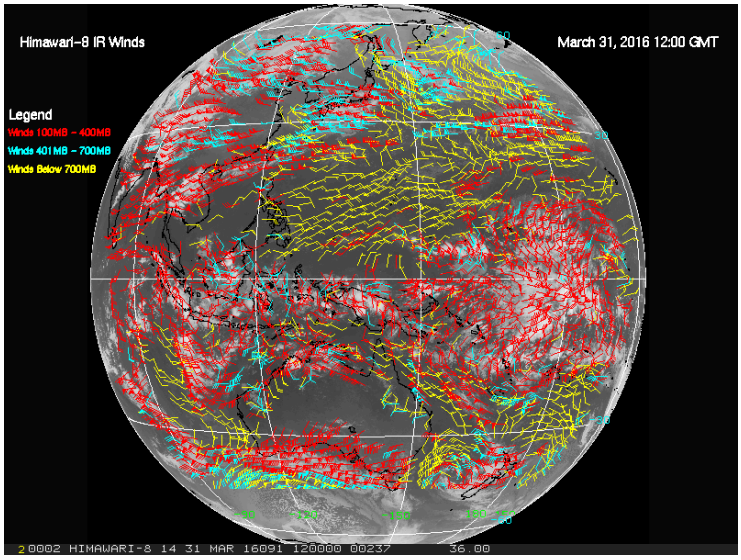

Figure 30. Himawari-8 cloud-drift winds derived from Full Disk 10-minute 11.2um AHI data for 12 UTC on 31 March 2016. These winds are derived from tracking cloud features using the 11.2um channel. High level (100-400 hPa) winds are shown in red; mid-level (400-700 hPa) winds are shown in cyan; and low-level winds (below 700 hPa) are shown in yellow.

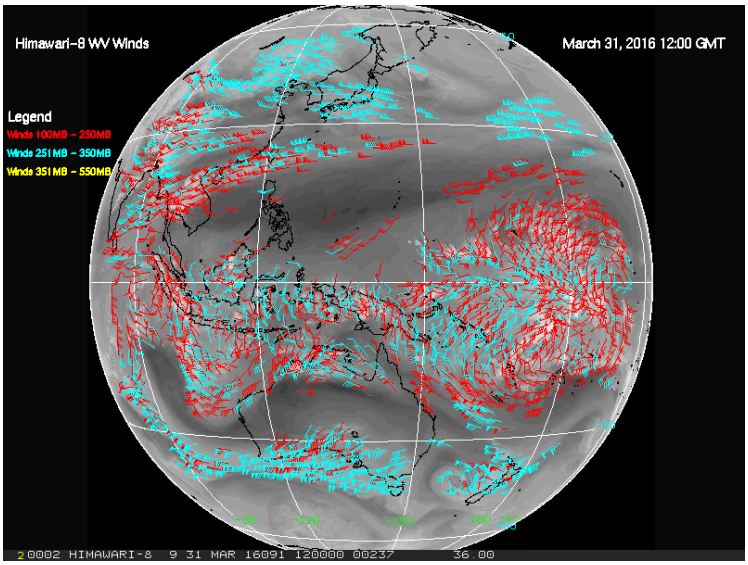

Figure 31. Himawari-8 cloud-top water vapor winds derived from Full Disk 10-minute 6.2um AHI data for 12 UTC on 31 March 2016. These winds are derived from tracking cloud features using the 6.2um channel. High level (100-400 hPa) winds are shown in red and mid-level (400-700 hPa) winds are shown in cyan.

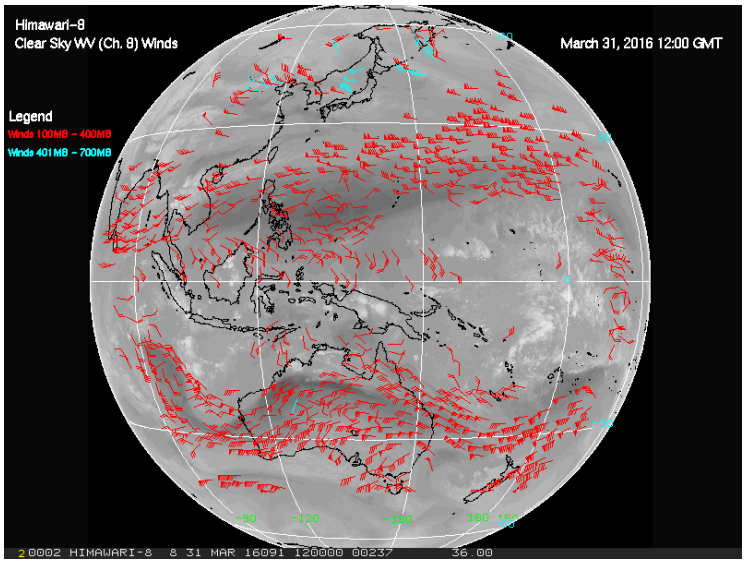

Figure 32. Himawari-8 clear-sky water vapor winds derived from Full Disk 10-minute 6.2um AHI data for 12 UTC on 31 March 2016. These winds are derived from clear-sky water vapor gradients features using the 6.2um channel. High level (100-400 hPa) winds are shown in red and mid-level (400-700 hPa) winds are shown in cyan.

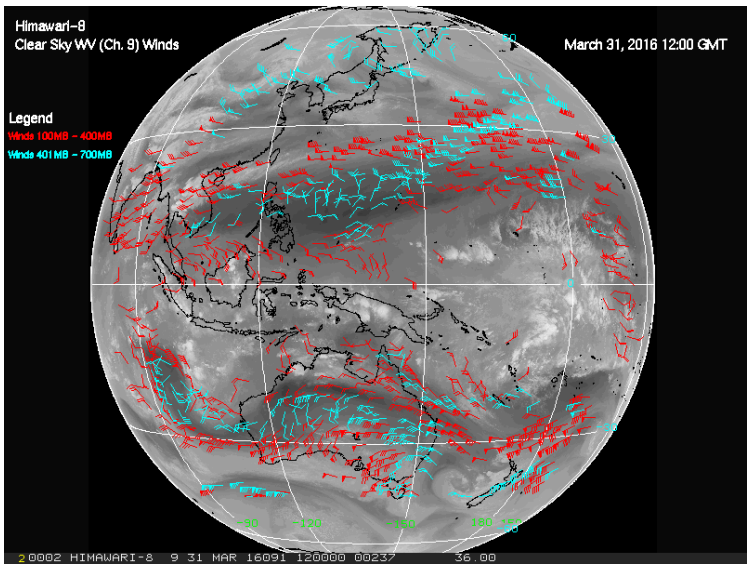

Figure 33. Himawari-8 clear-sky water vapor winds derived from Full Disk 10-minute 6.9um AHI data for 12 UTC on 31 March 2016. These winds are derived from clear-sky water vapor gradients features using the 6.9um channel. High level (100-400 hPa) winds are shown in red and mid-level (400-700 hPa) winds are shown in cyan.

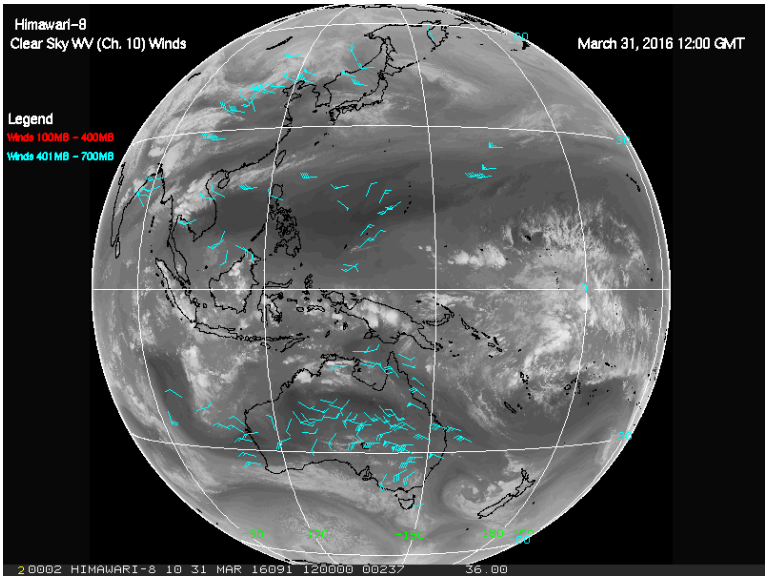

Figure 34. Himawari-8 clear-sky water vapor winds derived from Full Disk 10-minute 7.3um AHI data for 12 UTC on 31 March 2016. These winds are derived from clear-sky water vapor gradients features using the 7.3um channel. Mid-level (400-700 hPa) winds are shown in cyan.

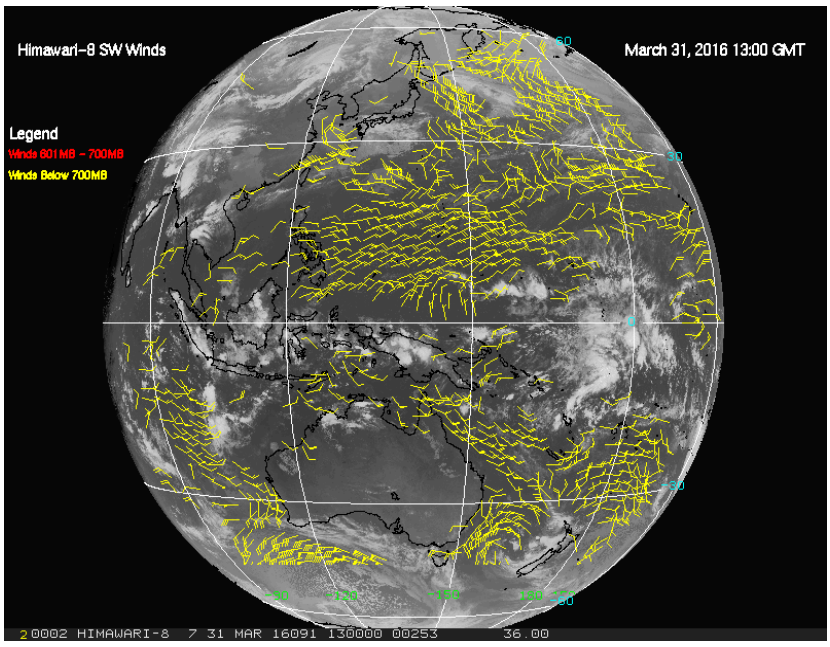

Figure 35. Himawari-8 cloud-top water vapor winds derived from Full Disk 10-minute 3.9um AHI data for 13 UTC on 31 March 2016. These winds are derived from tracking cloud features using the 3.9um channel. High level (100-400 hPa) winds are shown in red; mid-level (400-700 hPa) winds are shown in cyan; and low-level winds (below 700 hPa) are shown in yellow.

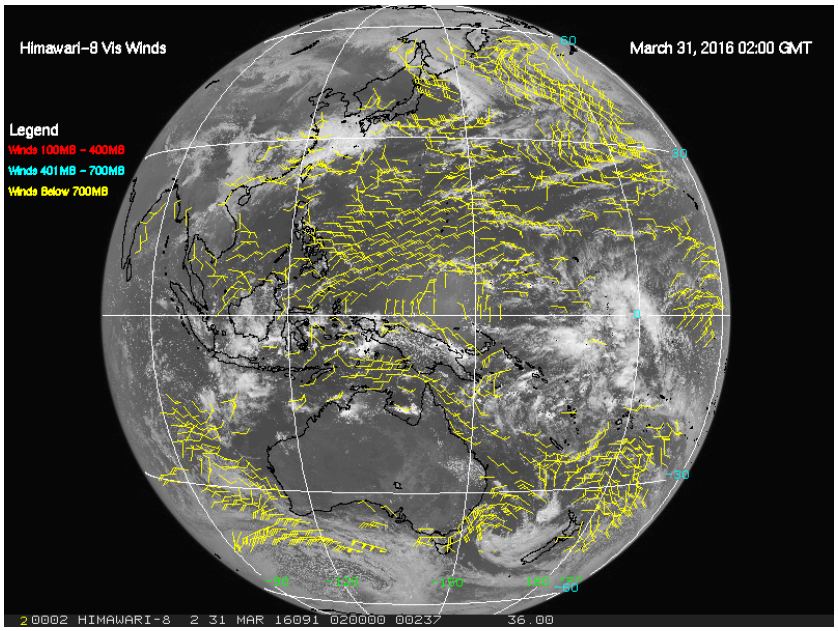

Figure 36. Himawari-8 cloud-top water vapor winds derived from Full Disk 10-minute 0.64um AHI data for 13 UTC on 31 March 2016. These winds are derived from tracking cloud features using the 0.64um channel. High level (100-400 hPa) winds are shown in red; mid-level (400-700 hPa) winds are shown in cyan; and low-level winds (below 700 hPa) are shown in yellow.

4.3 *Output from VIIRS Level-1 SDR Data*

The DMW product is generated routinely from VIIRS Level-1 Sensor Data Record (SDR) data over the Arctic and Antarctic as described in previous sections. The following figures 37 through 38 show examples of cloud-drift winds observed in S-NPP and NOAA-20 VIIRS Level-1 SDR Band M15 data.

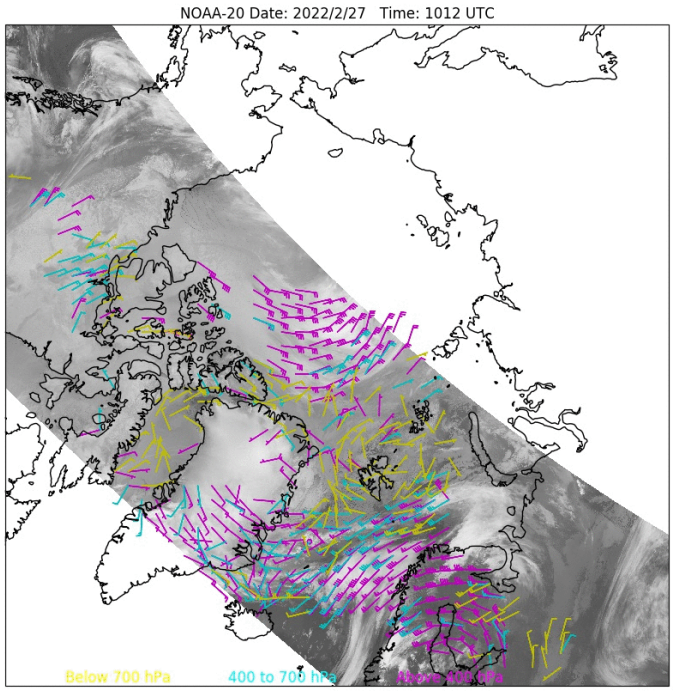

Figure 37. NOAA-20 cloud-drift winds derived in the Arctic from VIIRS Level-1 SDR 10.8um data for 1012 UTC on 27 February 2022. High level (100-400 hPa) winds are shown in violet; mid-level (400-700 hPa) winds are shown in cyan; and low-level winds (below 700 hPa) are shown in yellow.

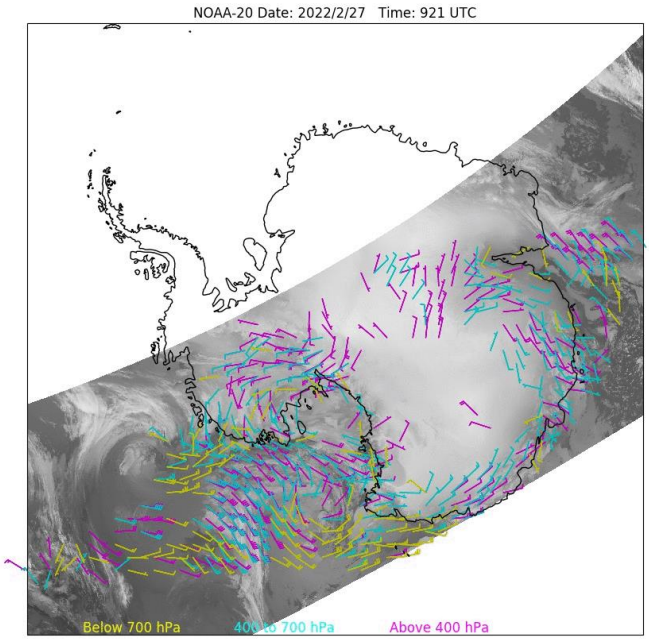

Figure 38. NOAA-20 cloud-drift winds derived in the Antarctic from VIIRS Level-1 SDR 10.8um data for 0921 UTC on 27 February 2022. High level (100-400 hPa) winds are shown in violet; mid-level (400-700 hPa) winds are shown in cyan; and low-level winds (below 700 hPa) are shown in yellow.

4.4 Output from AVHRR-3 L1B Data

The DMW product is generated routinely from AVHRR-3 L1b over the Arctic and Antarctic as described in previous sections. The following figures 39 through 40 show examples of cloud-drift winds observed in Metop-C AVHRR-3 L1b Band 4 data.

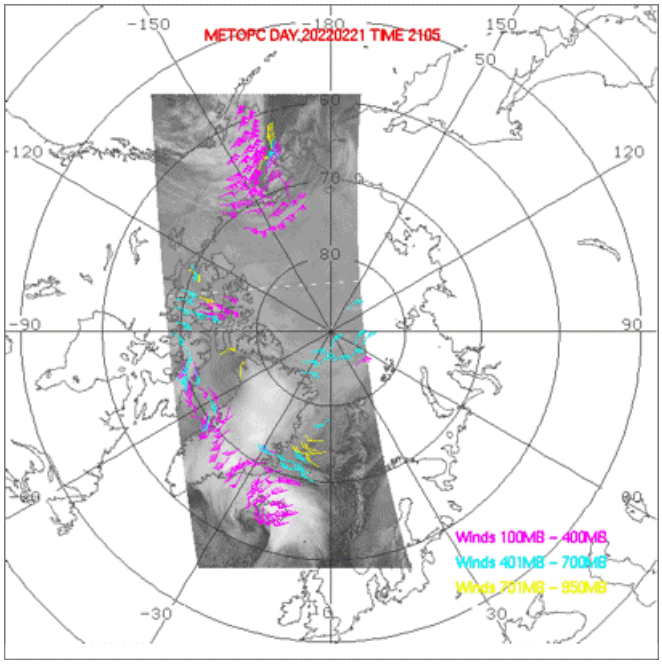

Figure 39. Metop-C cloud-drift winds derived in the Arctic from AVHRR-3 L1b 10.8um data for 2105 UTC on 21 February 2022. High level (100-400 hPa) winds are shown in violet; mid-level (400-700 hPa) winds are shown in cyan; and low-level winds (below 700 hPa) are shown in yellow.

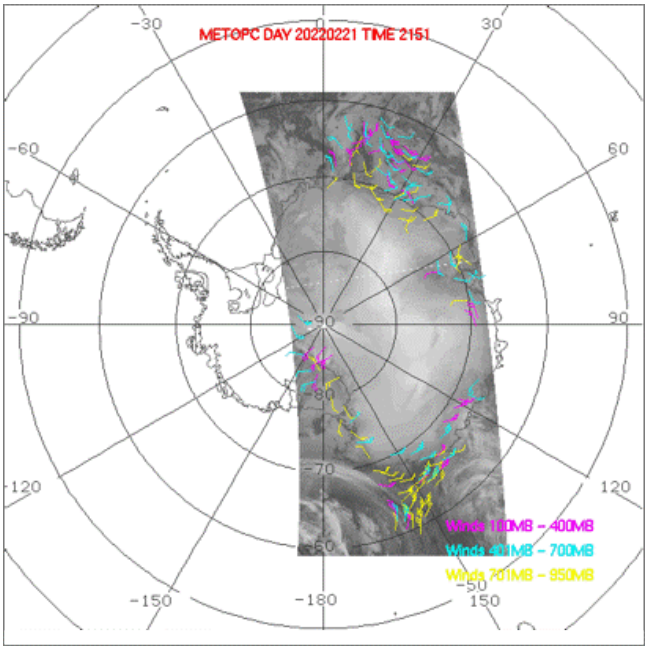

Figure 40. Metop-C cloud-drift winds derived in the Antarctic from AVHRR-3 L1b 10.8um data for 2151 UTC on 21 February 2022. High level (100-400 hPa) winds are shown in violet; mid-level (400-700 hPa) winds are shown in cyan; and low-level winds (below 700 hPa) are shown in yellow.

4.5 Precision and Accuracy Estimates

This section describes the predicted performance and product quality of the DMWA relative to the DMW specifications found within the GOES-R Functional and Performance Specification Document (F&PS). To estimate the precision and accuracy of the DMW product requires coincident measurements of reference ("truth") atmospheric winds values for the full range of observing geometry and environmental conditions that cover multiple seasons.

The reference ("truth") datasets used include radiosonde wind observations and Global Forecast System (GFS) analyses winds. The radiosonde wind observations are used primarily to validate the DMW product over land and coastal regions. A DMW/radiosonde wind collocation is considered a valid match if the radiosonde observation is within one hour in time within 150km in the horizontal, and within 50 hPa in the vertical of the DMW. The GFS model analysis wind fields are used to measure the performance of the DMW product over oceanic regions. Here, the analysis winds must be within 30 minutes of the DMW, and are spatially (horizontally and vertically) interpolated to the DMW location. An advantage of this approach is that a DMW/Analysis wind collocation match can be generated for every DMW produced.

The accuracy and precision estimates for the DMW products are determined by computing the Mean Vector Difference (MVD) and Standard Deviation (SD) metrics. The mean vector difference between retrieved and reference ("truth") wind representing the *accuracy (average error)* of the GOES-R ABI wind product is computed from:

$$MVD = 1/N \sum_{i=1}^{N} (VD)_i \tag{33}$$

where:

$$VD_i = \sqrt{(u_i - u_r)^2 + (v_i - v_r)^2} \tag{34}$$

u_i = u-component of satellite wind
v_i = v-component of satellite wind
u_r = u-component of the reference wind
v_r = v-component of the reference winds
N = size of collocated sample

The Standard Deviation (SD) about the mean vector difference between the retrieved GOES-R ABI DMW product and the reference wind data represents *the precision (random error)* of the ABI DMW product and is computed from:

$$SD = \sqrt{1/N \sum_{i=1}^{N} [(VD_i) - (MVD)]^2} \tag{35}$$

Certainly, assessment of algorithm performance depends on the validation samples from which the comparison statistics are derived. For example, validation of DMW products performed at different locations, heights in the atmosphere, different wind speeds, or local zenith angle could generate different accuracy and precision values for the same algorithm. The accuracy and precision of the DMW product will depend largely on a number things that include: (1) Calibration and navigation accuracy of the ABI measurements, (2) ABI band that is used for feature tracking, (3) Height of the DMW in the atmosphere, and (4) Accuracy and precision of the input ABI cloud mask and cloud height products.

Comparisons of GOES-16/17 ABI DMW Products to Radiosonde Wind Observations

Tables 14-20 show the seasonal Full Disk DMW product validation results as a function ABI band used for the time period December, 2018 to November, 2019 when using collocated 00 and 12 UTC radiosonde wind observations as reference/ground truth. These tables include the accuracy and precision metrics and speed bias metric, which is of particular interest to the NWP user community.

Seasonal comparison statistics for the low level DMWs computed using the visible band are shown in Table 14. These statistics indicate that these visible DMWs possess some small seasonal dependence. The accuracy and speed bias metrics displayed here indicate that visible DMWs are of high quality at levels of the atmosphere below 700 hPa and will contribute to improving NWP forecast performance when properly assimilated into NWP data assimilation systems.

Table 14. Seasonal comparison statistics between GOES-16/GOES-17 Full Disk Band 2 (0.64um) DMWs and radiosonde wind observations for Winter (Nov 2018 - Feb 2019), Spring (Mar 2019 - May 2019), Summer (Jun 2019 - Aug 2019) and Fall (Sept 2019 - Nov 2019).

Low Level *(P > 700hPa)*	***GOES-16 Visible (0.64um) Winds vs. Radiosonde Winds***				***GOES-17 Visible (0.64um) Winds vs. Radiosonde Winds***			
	Winter	**Spring**	**Summer**	**Fall**	**Winter**	**Spring**	**Summer**	**Fall**
Accuracy*(m/s)*	3.41	3.27	3.14	3.33	3.57	3.62	3.74	3.62
Precision *(m/s)*	2.43	2.23	2.14	2.25	2.45	2.37	2.50	2.43
Spd bias*(m/s)*	0.83	0.31	0.27	0.76	0.89	1.06	1.17	1.03
Speed *(m/s)*	8.76	8.73	8.46	8.13	8.90	7.94	7.82	8.13
Sample	67852	165191	250326	172362	85929	175731	253191	160377

The comparison statistics for the low level DMWs computed using the SWIR band are shown in Table 15. Like the visible DMWs, the SWIR winds are derived at low levels of

the atmosphere below 700 hPa. Their performance in terms of accuracy and precision is very similar to the performance of the visible DMWs. This is an important result as these two datasets are complimentary given that the visible DMWs are generated during daytime and the SWIR DMWs are generated during nighttime. This behavior is very important in terms of their use and potential impact in NWP data assimilation systems.

Table 15. Seasonal comparison statistics between GOES-16/GOES-17 Full Disk Band 7 (3.9um) DMWs and radiosonde wind observations for Winter (Nov 2018 - Feb 2019), Spring (Mar 2019 - May 2019), Summer (Jun 2019 - Aug 2019) and Fall (Sept 2019 - Nov 2019).

Low Level *(P > 700hPa)*	***GOES-16 SWIR (3.9um) Winds vs. Radiosonde Winds***				***GOES-17 SWIR (3.9um) Winds vs. Radiosonde Winds***			
	Winter	**Spring**	**Summer**	**Fall**	**Winter**	**Spring**	**Summer**	**Fall**
Accuracy*(m/s)*	3.27	3.36	3.17	3.29	3.81	3.65	3.86	3.76
Precision *(m/s)*	2.21	2.25	2.12	2.20	2.39	2.34	2.36	2.45
Spd bias*(m/s)*	-0.26	0.22	0.12	-0.05	0.42	0.89	1.46	0.93
Speed *(m/s)*	10.22	9.33	9.32	9.22	9.53	7.82	8.10	8.17
Sample	35603	14940	13038	26522	12554	10437	12086	11598

The comparison statistics for the DMWs computed using the LWIR band are shown in Table 16. The comparison statistics are shown for all levels of the atmosphere and are also broken down as a function of height in the atmosphere. The DMW metrics shown indicate some seasonal dependence, but this is not unexpected and reflects the seasonal changes in average wind speeds. When the LWIR DMW performance is evaluated as a function of height in the atmosphere, the magnitudes of the accuracy and precision metrics are observed to be smallest in the lower atmosphere and increase with height. This also indicates that the performance of the DMWs vary as a function of wind speed.

Table 16. Seasonal comparison statistics between GOES-16/GOES-17 Full Disk Band 14 (11.2um) DMWs and radiosonde wind observations for Winter (Nov 2018 - Feb 2019), Spring (Mar 2019 - May 2019), Summer (Jun 2019 - Aug 2019) and Fall (Sept 2019 - Nov 2019).

All Levels *(100-1000 hPa)*	***GOES-16 LWIR (11.2um) Winds vs. Radiosonde Winds***				***GOES-17 LWIR (11.2um) Winds vs. Radiosonde Winds***			
	Winter	**Spring**	**Summer**	**Fall**	**Winter**	**Spring**	**Summer**	**Fall**
Accuracy*(m/s)*	5.06	5.00	4.72	4.90	4.97	4.78	4.60	4.89
Precision*(m/s)*	3.50	3.38	3.16	3.27	3.28	3.19	3.02	3.21
Spd bias*(m/s)*	-0.59	-0.50	-0.40	-0.71	-0.04	-0.09	-0.10	-0.47
Speed *(m/s)*	21.78	19.62	15.55	18.07	22.04	18.72	14.46	18.75
Sample	431815	526418	649222	637964	206048	223802	313256	294072

High Level *(100-400 hPa)*								
	Winter	**Spring**	**Summer**	**Fall**	**Winter**	**Spring**	**Summer**	**Fall**
Accuracy*(m/s)*	5.63	5.39	5.11	5.25	5.29	5.12	4.91	5.22
Precision *(m/s)*	3.65	3.48	3.28	3.36	3.32	3.28	3.14	3.27
Spd bias*(m/s)*	-0.94	-0.70	-0.53	-1.00	-0.25	-0.20	-0.30	-0.77
Speed *(m/s)*	26.52	22.66	17.48	20.26	27.87	23.72	16.68	22.12
Sample	270798	369345	471872	453795	121220	133985	217518	195491
Mid Level *(400-700 hPa)*								
	Winter	**Spring**	**Summer**	**Fall**	**Winter**	**Spring**	**Summer**	**Fall**
Accuracy*(m/s)*	5.03	4.76	4.08	4.67	5.27	5.01	4.35	4.88
Precision *(m/s)*	3.41	3.24	2.72	3.18	3.53	3.37	2.90	3.32
Spd bias*(m/s)*	0.16	-0.09	-0.27	-0.09	0.02	-0.29	-0.05	-0.27
Speed *(m/s)*	18.06	15.61	12.03	16.37	17.75	14.53	11.47	15.86
Sample	74045	79740	84286	91831	44761	44380	38935	49563
Low Level *(700-1000 hPa)*								
	Winter	**Spring**	**Summer**	**Fall**	**Winter**	**Spring**	**Summer**	**Fall**
Accuracy*(m/s)*	3.34	3.42	3.31	3.40	3.69	3.52	3.56	3.55
Precision *(m/s)*	2.33	2.38	2.30	2.34	2.46	2.30	2.35	2.39
Spd bias*(m/s)*	-0.14	0.03	0.10	0.06	0.52	0.44	0.67	0.53
Speed *(m/s)*	10.18	9.26	8.97	9.04	9.21	8.08	8.04	8.24
Sample	86972	77333	93064	92338	40067	45437	56803	49018

The comparison statistics for the cloud-top water vapor DMWs computed using the 6.2um band are shown in Table 17. The comparison statistics are shown only for upper levels of the atmosphere above 400 hPa since these winds are only generated above 400 hPa. The DMW metrics indicate some seasonal dependence. More importantly, the statistics indicate these vectors are of good quality and the performance of these cloud-top DMWs is likely to contribute to improving NWP forecast performance when properly assimilated into NWP data assimilation systems.

Table 17. Seasonal comparison statistics between GOES-16/GOES-17 Full Disk Band 8 (6.2um) Cloud-top DMWs and radiosonde wind observations for Winter (Nov 2018 - Feb 2019), Spring (Mar 2019 - May 2019), Summer (Jun 2019 - Aug 2019) and Fall (Sept 2019 - Nov 2019).

High Level *(100-400 hPa)*	***GOES-16 Cloud-top Water Vapor (6.2um) Winds vs. Radiosonde Winds***				***GOES-17 Cloud-top Water Vapor (6.2um) Winds vs. Radiosonde Winds)***			
	Winter	**Spring**	**Summer**	**Fall**	**Winter**	**Spring**	**Summer**	**Fall**
Accuracy*(m/s)*	5.57	5.27	5.11	5.11	5.36	5.24	5.02	5.19
Precision *(m/s)*	3.59	3.40	3.27	3.28	3.29	3.25	3.15	3.24
Spd bias*(m/s)*	-0.35	0.00	0.17	-0.29	0.31	0.56	0.49	0.08
Speed *(m/s)*	27.56	23.75	18.40	20.67	29.39	25.77	17.85	22.67
Sample	290686	381274	499010	495560	99511	109922	193632	164064

The comparison statistics for the clear-sky water vapor DMWs computed using the 6.2um, 6.9um, and 7.3um bands are shown in Tables 18 - 20. The comparison statistics for the 6.2um clear-sky DMWs are shown only for upper levels of the atmosphere above 400 hPa since these winds are only generated above 400 hPa. The comparison statistics for the 6.9um clear-sky DMWs are shown for the atmospheric layer above 400 hPa and the layer between 400 hPa and 700 hPa, since these are the layers over which these winds are generated and most representative. The comparison statistics for the 7.3um clear-sky DMWs are shown only for the atmospheric layer between 400 hPa and 700 hPa, since this is the layer over which these winds are generated and most representative.

All sets of clear-sky DMW metrics indicate the performance of the clear-sky DMWs will vary by season with the most challenging season being winter when the atmosphere is much drier. It is clear from these statistics that the clear-sky DMWs are the most challenging to derive. The primary reason for this is that the feature being tracked in these cases is a clear-sky moisture gradient which lacks a sharp radiometric signal typically observed with clouds. Complicating matters further is the fact that the radiometric signal being tracked emanates from a rather broad layer of the atmosphere. Thus, the motion retrieved from tracking clear-sky water vapor features is more representative of the average motion over a broad atmospheric layer. Statistical comparisons of these DMWs versus single level reference/ground truth wind observations like radiosondes, then, reflect this phenomenon with the result being slightly worse performance (e.g., lower accuracy and reduced precision).

Table 18. Seasonal comparison statistics between GOES-16/GOES-17 Full Disk Band 8 (6.2um) Clear-Sky DMWs and radiosonde wind observations for Winter (Nov 2018 - Feb 2019), Spring (Mar 2019 - May 2019), Summer (Jun 2019 - Aug 2019) and Fall (Sept 2019 - Nov 2019).

High Level *(100 - 400 hPa)*	***GOES-16 Clear-sky Water Vapor (6.2um) Winds vs. Radiosonde Winds***				***GOES-17 Clear-sky Water Vapor (6.2um) Winds vs. Radiosonde Winds***			
	Winter	**Spring**	**Summer**	**Fall**	**Winter**	**Spring**	**Summer**	**Fall**
Accuracy*(m/s)*	5.61	5.38	5.16	5.08	5.87	5.57	5.16	5.30
Precision *(m/s)*	3.80	3.71	3.67	3.54	4.10	3.78	3.55	3.77
Spd bias*(m/s)*	-0.54	-0.78	-0.63	-0.74	-0.85	-0.38	-0.38	-0.61
Speed *(m/s)*	19.66	17.79	15.63	16.83	21.53	19.61	16.65	17.83
Sample	36746	39443	63396	65103	15922	17064	30291	27724

Table 19. Seasonal comparison statistics between GOES-16/GOES-17 Full Disk Band 9 (6.9um) Clear-Sky DMWs and radiosonde wind observations for Winter (Nov 2018 - Feb 2019), Spring (Mar 2019 - May 2019), Summer (Jun 2019 - Aug 2019) and Fall (Sept 2019 - Nov 2019).

HighLevel *(100 - 400 hPa)*	***GOES-16 Clear-sky Water Vapor (6.9um) Winds vs. Radiosonde Winds***				***GOES-17 Clear-sky Water Vapor (6.9um) Winds vs. Radiosonde Winds***			
	Winter	**Spring**	**Summer**	**Fall**	**Winter**	**Spring**	**Summer**	**Fall**
Accuracy*(m/s)*	5.09	4.84	4.55	4.53	5.44	5.26	4.85	4.95
Precision*(m/s)*	3.29	3.19	3.09	3.00	3.41	3.38	3.26	3.22
Spd bias*(m/s)*	0.26	0.23	-0.03	-0.12	0.41	0.39	0.23	0.17
Speed *(m/s)*	16.95	15.69	13.95	14.73	20.99	18.22	14.64	16.69
Sample	17138	19021	56265	49400	13052	15291	37543	30261
Mid level *(400 -700 hPa)*								
	Winter	**Spring**	**Summer**	**Fall**	**Winter**	**Spring**	**Summer**	**Fall**
Accuracy*(m/s)*	5.62	5.64	5.52	5.54	5.94	5.58	5.09	5.68
Precision *(m/s)*	3.85	3.83	3.75	3.82	4.13	3.77	3.52	4.08
Spd bias*(m/s)*	-0.76	-0.94	-0.75	-0.96	-1.23	-0.87	-0.94	-1.22
Speed *(m/s)*	17.47	16.25	14.94	16.89	16.93	15.54	12.93	14.98
Sample	32144	26667	16812	24169	14687	11747	6089	10531

Table 20. Seasonal comparison statistics between GOES-16/GOES-17 Full Disk Band 10 (7.3um) Clear-Sky DMWs and radiosonde wind observations for Winter (Nov 2018 - Feb 2019), Spring (Mar 2019 - May 2019), Summer (Jun 2019 - Aug 2019) and Fall (Sept 2019 - Nov 2019).

Mid Level *(400 - 700hPa)*	***GOES-16 Clear-sky Water Vapor (7.3um) Winds vs. Radiosonde Winds***				***GOES-17 Clear-sky Water Vapor (7.3um) Winds vs. Radiosonde Winds***			
	Winter	**Spring**	**Summer**	**Fall**	**Winter**	**Spring**	**Summer**	**Fall**
Accuracy*(m/s)*	5.28	4.87	4.74	4.73	5.66	4.98	4.71	5.12
Precision *(m/s)*	3.33	3.15	3.20	3.04	3.61	3.13	3.00	3.15
Spd bias*(m/s)*	-0.61	-0.54	-0.54	-0.55	-1.14	-0.73	-1.81	-1.37
Speed *(m/s)*	15.50	13.27	12.56	14.52	17.48	14.64	8.78	13.35
Sample	8862	9890	8690	12918	1829	1956	1817	2326

Comparisons of GOES-16/17 ABI DMW Products to GFS Analysis Winds

Tables 21-27 show Full Disk DMW product validation results as a function of ABI band used broken down by season (Winter: Dec 2018 - Feb 2019, Spring: Mar 2019 - May 2019, Summer: Jun 2019 - Aug 2019 and Fall: Sept 2019 - Nov 2019) when using collocated NCEP GFS analysis winds as reference/ground truth. These tables include the accuracy and precision metrics and speed bias metric which is of particular interest to the NWP user community. It needs to be noted that use of NCEP GFS analysis winds as the reference/ground truth wind observations leads to smaller magnitudes in the accuracy and

precision metrics as compared to the magnitudes of these metrics when using radiosonde wind observations. Two reasons likely contribute to this. First, the horizontal and temporal resolution of the GFS analysis wind field is much coarser than the radiosonde wind observations and second, the GFS analysis wind field is influenced by a number of satellite-derived winds as these are assimilated operationally by NCEP. Despite this, these comparison statistics still provide a useful measure of the performance of the DMWA.

The comparison statistics for the low level DMWs computed using the visible band are shown in Table 21. The accuracy and precision values of these DMWs shown in the table indicate the visible DMWs possess a very small seasonal dependence which is consistent with what was observed when comparing these winds to radiosonde wind observations.

The comparison statistics for the low level DMWs computed using the SWIR band are shown in Table 22. Like the visible DMWs, the SWIR winds are derived at low levels of the atmosphere below 700 hPa. Their performance in terms of accuracy and precision is very similar to the performance of the visible DMWs. As previously mentioned, this is an important result as these two datasets are complimentary given that the visible DMWs are generated during daytime and the SWIR DMWs are generated during nighttime. This behavior is very important in terms of their use and potential impact in NWP data assimilation systems.

Table 21. Seasonal comparison statistics between GOES-16/GOES-17 Full Disk Band 2 (0.64um) DMWs and NCEP GFS Analysis winds for Winter (Dec 2018 - Feb 2019), Spring (Mar 2019 - May 2019), Summer (Jun 2019 - Aug 2019) and Fall (Sept 2019 - Nov 2019).

Low Level *(P > 700hPa)*	***GOES-16 Visible (0.64um) Winds vs. GFS Analysis Winds***				***GOES-17 Visible (0.64um) Winds vs. GFS Analysis Winds***			
	Winter	**Spring**	**Summer**	**Fall**	**Winter**	**Spring**	**Summer**	**Fall**
Accuracy *(m/s)*	1.48	1.54	1.45	1.47	1.43	1.58	1.51	1.42
Precision *(m/s)*	1.01	1.06	1.02	0.98	0.99	1.07	1.01	0.96
Speed bias*(m/s)*	0.10	0.18	0.12	0.08	0.12	-0.05	-0.07	0.03
Speed *(m/s)*	9.10	8.82	8.66	8.86	9.33	9.56	7.76	8.23
Sample *(m/s)*	12124642	7285533	11809327	13906206	8163821	3518028	3497952	1308351

Table 22. Seasonal comparison statistics between GOES-16/GOES-17 Full Disk Band 7 (3.9um) DMWs and NCEP GFS Analysis winds for Winter (Dec 2018 - Feb 2019), Spring (Mar 2019 - May 2019), Summer (Jun 2019 - Aug 2019) and Fall (Sept 2019 - Nov 2019).

Low Level *(P > 700hPa)*	***GOES-16 SWIR (3.9um) Winds vs. GFS Analysis Winds***				***GOES-17 SWIR (3.9um) Winds vs. GFS Analysis Winds***			
	Winter	**Spring**	**Summer**	**Fall**	**Winter**	**Spring**	**Summer**	**Fall**
Accuracy *(m/s)*	1.49	1.32	1.34	0.90	1.42	1.57	1.52	1.59
Precision *(m/s)*	1.06	0.96	1.00	2.90	1.01	1.08	1.02	1.09
Speed bias*(m/s)*	0.17	0.19	0.16	0.21	0.23	0.13	0.09	0.15
Speed *(m/s)*	9.50	8.77	10.15	8.78	9.25	9.37	9.52	8.63
Sample *(m/s)*	3991925	1315380	1354233	1348068	6569406	1901978	1502868	3046479

The comparison statistics for the DMWs computed using the LWIR band are shown in Table 23. The comparison statistics are shown for all levels of the atmosphere and are also broken down as a function of height in the atmosphere. Conclusions to be drawn from these statistics are similar to those drawn from statistics computed between these winds and radiosonde wind observations. The DMW metrics indicate some seasonal dependence which reflects the fact that the average wind speeds are higher in Winter than in Summer. When the LWIR DMW performance is evaluated as a function of height in the atmosphere, the magnitudes of the accuracy and precision metrics are observed to be smallest in the lower atmosphere and increase with height. This also indicates that the performance of the DMWs vary as a function of wind speed.

Table 23. Seasonal comparison statistics between GOES-16/GOES-17 Full Disk Band 14 (11.2um) DMWs and NCEP GFS Analysis winds for Winter (Dec 2018 - Feb 2019), Spring (Mar 2019 - May 2019), Summer (Jun 2019 - Aug 2019) and Fall (Sept 2019 - Nov 2019).

All Levels *(100-1000 hPa)*	***GOES-16 LWIR (11.2um) Winds vs. GFS Analysis Winds***				***GOES-17 LWIR (11.2um) Winds vs. GFS Analysis Winds***			
	Winter	**Spring**	**Summer**	**Fall**	**Winter**	**Spring**	**Summer**	**Fall**
Accuracy*(m/s)*	2.39	2.39	2.27	2.45	2.73	2.48	2.36	2.44
Precision *(m/s)*	1.92	1.97	1.96	2.19	2.33	1.98	1.86	2.04
Spd bias*(m/s)*	0.18	0.18	0.20	0.15	-0.19	0.17	0.21	-0.61
Speed *(m/s)*	15.91	15.96	13.72	14.22	20.58	15.46	12.76	13.90
Sample	9737169	6105279	13159440	12630615	14633289	3416027	3526524	16370733
High Level *(100-400 hPa)*								
	Winter	**Spring**	**Summer**	**Fall**	**Winter**	**Spring**	**Summer**	**Fall**
Accuracy*(m/s)*	3.14	2.95	3.02	3.07	3.58	3.41	3.20	3.33
Precision *(m/s)*	2.04	1.96	2.00	2.10	2.37	2.13	2.06	2.13
Spd bias*(m/s)*	0.17	0.21	0.34	0.23	-0.45	0.31	0.42	-0.27
Speed *(m/s)*	22.43	21.33	18.58	18.74	31.20	22.91	16.65	20.06
Sample	4207188	3135530	5267811	5766423	5978934	1335480	1280826	6299127

Mid Level *(400-700 hPa)*								
	Winter	**Spring**	**Summer**	**Fall**	**Winter**	**Spring**	**Summer**	**Fall**
Accuracy*(m/s)*	3.45	3.37	3.26	3.50	3.89	3.57	3.33	3.55
Precision *(m/s)*	2.19	2.21	2.13	2.52	2.46	2.30	2.13	2.32
Spd bias*(m/s)*	0.40	0.31	0.07	0.25	-0.43	0.77	0.44	-0.97
Speed *(m/s)*	18.15	16.09	14.45	16.78	21.00	18.68	15.71	17.82
Sample	894588	493638	1298280	1211577	1252746	314948	292525	1294944
Low Level *(700-1000 hPa)*								
	Winter	**Spring**	**Summer**	**Fall**	**Winter**	**Spring**	**Summer**	**Fall**
Accuracy*(m/s)*	1.50	1.49	1.47	1.59	1.64	1.58	1.66	1.65
Precision *(m/s)*	1.25	1.55	1.52	1.87	1.70	1.24	1.29	1.53
Spd bias*(m/s)*	0.14	0.11	0.12	0.05	0.10	-0.05	0.05	-0.79
Speed *(m/s)*	9.57	9.06	9.70	9.10	11.02	9.26	9.76	8.89
Sample	4635393	2476111	6593349	5652615	7401609	1765599	1954173	8776662

The comparison statistics for the cloud-top water vapor DMWs computed using the 6.2um band are shown in Table 24. The comparison statistics are shown only for upper levels of the atmosphere above 400 hPa since these winds are only generated above 400 hPa. The metrics here indicate little to no seasonal dependence with respect to the performance of the DMWs when using this channel to track clouds. Positive speed biases are evident from these comparison stats which indicate the DMWs are faster than the GFS analysis. The exact reasons for this are not known. Positive speed biases for these DMWs, however, were not evident in the DMW/radiosonde wind comparison statistics shown in Table 17.

Table 24. Seasonal comparison statistics between GOES-16/GOES-17 Full Disk Band 8 (6.2um) Cloud-top DMWs and NCEP GFS Analysis winds for Winter (Dec 2018 - Feb 2019), Spring (Mar 2019 - May 2019), Summer (Jun 2019 - Aug 2019) and Fall (Sept 2019 - Nov 2019).

High Level *(100-400 hPa*	***GOES-16 Cloud-top Water Vapor (6.2um) Winds vs. GFS Analysis Winds***				***GOES-17 Cloud-top Water Vapor (6.2um) Winds vs. GFS Analysis Winds***			
	Winter	**Spring**	**Summer**	**Fall**	**Winter**	**Spring**	**Summer**	**Fall**
Accuracy *m/s)*	3.36	3.15	3.19	3.69	3.29	3.44	3.46	3.48
Precision *(m/s)*	2.16	2.08	2.07	2.27	2.21	2.14	2.18	2.22
Spd bias*(m/s)*	1.02	0.97	1.02	1.00	0.93	0.78	1.03	0.82
Speed *(m/s)*	22.86	21.10	19.37	25.64	24.35	22.63	16.99	20.74
Sample	4582260	1238696	5508027	140253	2628324	1602736	1955476	718893

The comparison statistics for the clear-sky water vapor DMWs computed using the 6.2um, 6.9um, and 7.3um bands are shown in Tables 25 - 27. The comparison statistics

for the 6.2um clear-sky DMWs are shown only for upper levels of the atmosphere above 400 hPa since these winds are only generated above 400 hPa. The comparison statistics for the 6.9um clear-sky DMWs are shown for the atmospheric layer above 400 hPa and the layer between 400 hPa and 700 hPa, since these are the layers over which these winds are generated and most representative. The comparison statistics for the 7.3um clear-sky DMWs are shown only for the atmospheric layer between 400 hPa and 700 hPa, since this is the layer over which these winds are generated and most representative.

The DMW metrics indicate that the performance of the clear-sky DMWs will vary slightly by season with the most challenging season being winter when the atmosphere is much drier. It is clear from these statistics that the clear-sky DMWs are the most challenging to derive. As previously discussed, the primary reason for this is that the feature being tracked in these cases is a clear-sky moisture gradient which lacks a sharp radiometric signal typically observed with clouds. Complicating matters further is the fact that the radiometric signal being tracked emanates from a rather broad layer of the atmosphere. Thus, the motion retrieved from tracking clear-sky water vapor features is more representative of the average motion over a broad atmospheric layer. Statistical comparisons of these DMWs with single level reference/ground truth wind observations like radiosondes or even GFS analysis then, reflect this phenomenon with the result being slightly worse performance (e.g., lower accuracy and reduced precision).

Table 25. Seasonal comparison statistics between GOES-16/GOES-17 Full Disk Band 8 (6.2um) Clear-Sky DMWs and NCEP GFS Analysis winds for Winter (Dec 2018 - Feb 2019), Spring (Mar 2019 - May 2019), Summer (Jun 2019 - Aug 2019) and Fall (Sept 2019 - Nov 2019).

High Level *(100 - 400 hPa)*	***GOES-16 Clear-sky Water Vapor (6.2um) Winds vs. GFS Analysis Winds***				***GOES-17 Clear-sky Water Vapor (6.2um) Winds vs. GFS Analysis Winds***			
	Winter	**Spring**	**Summer**	**Fall**	**Winter**	**Spring**	**Summer**	**Fall**
Accuracy *(m/s)*	3.64	3.48	3.52	3.63	3.61	3.80	3.55	3.80
Precision *(m/s)*	2.53	2.47	2.52	2.55	2.49	2.60	2.44	2.58
Speed bias*(m/s)*	0.20	-0.34	-0.15	-0.16	0.17	-0.34	-0.04	-0.20
Speed *(m/s)*	17.76	16.60	15.94	16.94	17.75	18.57	15.55	17.21
Sample	592974	381804	1318725	1338984	620334	361793	316743	853809
Mid Level *(400-700 hPa)*								
	Winter	**Spring**	**Summer**	**Fall**	**Winter**	**Spring**	**Summer**	**Fall**
Accuracy *(m/s)*	4.12	4.54	4.01	4.10	4.32	4.85	4.33	4.89
Precision *(m/s)*	2.88	3.10	2.87	2.89	2.93	3.22	2.86	3.18
Speed bias*(m/s)*	-0.99	-1.45	-0.91	-1.13	-1.02	-1.49	-1.36	-1.72
Speed *(m/s)*	18.92	17.94	19.31	18.61	20.01	20.81	20.33	19.91
Sample	33831	14054	107751	84405	40134	36523	37497	59301

Table 26. Seasonal comparison statistics between GOES-16/GOES-17 Full Disk Band 9 (6.9um) Clear-Sky DMWs and NCEP GFS Analysis winds for Winter (Dec 2018 - Feb

2019), Spring (Mar 2019 - May 2019), Summer (Jun 2019 - Aug 2019) and Fall (Sept 2019 - Nov 2019).

High Level *(100 - 400 hPa)*	***GOES-16 Clear-sky Water Vapor (6.9um) Winds vs. GFS Analysis Winds***				***GOES-17 Clear-sky Water Vapor (6.9um) Winds vs. GFS Analysis Winds***			
	Winter	**Spring**	**Summer**	**Fall**	**Winter**	**Spring**	**Summer**	**Fall**
Accuracy *(m/s)*	3.57	3.30	3.20	3.51	3.46	3.76	3.30	3.61
Precision *(m/s)*	2.51	2.42	2.33	2.51	2.47	2.59	2.33	2.48
Speed bias*(m/s)*	0.75	0.44	0.32	0.40	0.65	0.64	0.38	0.32
Speed *(m/s)*	16.51	15.02	13.46	15.17	16.55	16.62	13.62	15.60
Sample *(m/s)*	511752	122074	1031586	879936	504810	312708	368352	757131
Mid Level *(400-700 hPa)*								
	Winter	**Spring**	**Summer**	**Fall**	**Winter**	**Spring**	**Summer**	**Fall**
Accuracy *(m/s)*	3.56	3.57	3.52	3.73	3.38	3.94	3.79	3.99
Precision *(m/s)*	2.58	2.79	2.48	2.81	2.54	2.78	2.57	2.75
Speed bias*(m/s)*	-0.13	-0.29	-0.15	-0.41	-0.24	-0.52	-0.49	-0.68
Speed *(m/s)*	16.58	16.71	16.95	16.79	16.50	16.76	17.16	16.33
Sample	468186	80117	523392	579129	543066	301567	273900	695481

Table 27. Seasonal comparison statistics between GOES-16/GOES-17 Full Disk Band 10 (7.3um) Clear-Sky DMWs and NCEP GFS Analysis winds for Winter (Dec 2018 - Feb 2019), Spring (Mar 2019 - May 2019), Summer (Jun 2019 - Aug 2019) and Fall (Sept 2019 - Nov 2019).

Mid Level *(400 - 700 hPa)*	***GOES-16 Clear-sky Water Vapor (7.3um) Winds vs. GFS Analysis Winds***				***GOES-17 Clear-sky Water Vapor (7.3um) Winds vs. GFS Analysis Winds***			
	Winter	**Spring**	**Summer**	**Fall**	**Winter**	**Spring**	**Summer**	**Fall**
Accuracy *(m/s)*	3.42	3.17	3.20	3.48	3.29	3.53	3.49	3.79
Precision *(m/s)*	2.41	2.30	2.29	2.43	2.37	2.35	2.24	2.37
Speed bias*(m/s)*	-0.03	-0.03	0.24	-0.11	0.27	0.01	-0.13	-0.43
Speed *(m/s)*	13.87	12.16	11.78	14.24	12.55	13.25	11.48	11.75
Sample	69405	62666	72684	93792	21486	23510	33915	48441

Comparisons of Himawari-8 AHI DMW Products to Radiosonde Wind Observations

Tables 28-29 show the Full Disk DMW product validation results as a function AHI band used for the time period March 24-31, 2021, 2018 when using collocated 00 and 12 UTC radiosonde wind observations as reference/ground truth. These tables include the accuracy and precision metrics and speed bias metric, which is of particular interest to the NWP user community.

Table 28 Himawari-8 Full Disk DMW product validation results as a function AHI bands used for cloudy target scenes for the time period March 24-31, 2021.

All Levels *(100-1000 hPa)*	**Band 14 (11.2um)**	**Band 8 (6.2um;WVCT)**	**Band 3 (0.64um)**	**Band 7 (3.9um)**
Accuracy *(m/s)*	5.16	5.12	4.33	3.79
Precision *(m/s)*	3.62	3.52	3.20	2.68
Speed bias *(m/s)*	-0.54	0.38	0.51	0.52
Speed *(m/s)*	14.40	16.55	9.34	8.18
Sample	98569	89944	75225	12420
High Level *(100-400 hPa)*				
Accuracy *(m/s)*	5.33	5.12	N/A	N/A
Precision *(m/s)*	3.68	3.52	N/A	N/A
Speed bias *(m/s)*	-0.66	0.38	N/A	N/A
Speed *(m/s)*	15.86	16.55	N/A	N/A
Sample	72646	89944	N/A	N/A
Mid Level *(400-700 hPa)*				
Accuracy *(m/s)*	5.50	N/A	N/A	N/A
Precision *(m/s)*	3.84	N/A	N/A	N/A
Speed bias *(m/s)*	-1.46	N/A	N/A	N/A
Speed *(m/s)*	13.50	N/A	N/A	N/A
Sample	8940	N/A	N/A	N/A
Low Level *(700-1000 hPa)*				
Accuracy *(m/s)*	4.27	N/A	4.33	3.79
Precision *(m/s)*	3.08	N/A	3.20	2.68
Speed bias *(m/s)*	0.45	N/A	0.52	0.52
Speed *(m/s)*	8.64	N/A	9.34	8.18
Sample	16983	N/A	75215	12418

Table 29 Himawari-8 Full Disk DMW product validation results as a function AHI bands used for clear-sky target scenes for the time period March 24-31, 2021.

All Levels *(100-1000 hPa)*	**Band 8 (6.2um)**	**Band 9 (6.9um)**	**Band 10 (7.3um)**
Accuracy *(m/s)*	5.17	4.97	5.50
Precision *(m/s)*	4.14	3.31	3.28
Speed bias *(m/s)*	-0.44	-0.14	-0.28
Speed *(m/s)*	15.33	14.93	12.14
Sample	5029	5423	1550
High Level *(100-400 hPa)*			
Accuracy *(m/s)*	5.17	4.88	N/A
Precision *(m/s)*	4.14	3.21	N/A
Speed bias *(m/s)*	-0.44	0.03	N/A
Speed *(m/s)*	15.33	15.77	N/A
Sample	5029	2697	N/A
Mid Level			

(400-700 hPa)			
Accuracy *(m/s)*	N/A	5.06	5.50
Precision *(m/s)*	N/A	3.41	3.28
Speed bias *(m/s)*	N/A	-0.32	-0.28
Speed *(m/s)*	N/A	14.09	12.14
Sample	N/A	2726	1550

Comparisons of S-NPP and NOAA-20 VIIRS DMW Products to Radiosonde Wind Observations

Table 30 shows the DMW product validation results for the time period July 5-29, 2018 using collocated 00 and 12 UTC radiosonde wind observations as reference/ground truth. These tables include the accuracy and precision metrics and speed bias metric, which is of particular interest to the NWP user community.

Table 30 S-NPP and NOAA-20 DMW (band M15; 10.8um) product validation results for the time period July 5-29, 2018.

All Levels *(100-1000 hPa)*	**S-NPP**	**NOAA-20**
Accuracy *(m/s)*	5.79	5.99
Precision *(m/s)*	3.58	3.64
Speed bias *(m/s)*	1.03	1.02
Speed *(m/s)*	20.44	20.19
Sample	4668	3860
High Level *(100-400 hPa)*		
Accuracy *(m/s)*	6.39	6.36
Precision *(m/s)*	3.76	3.82
Speed bias *(m/s)*	1.33	1.23
Speed *(m/s)*	23.85	23.71
Sample	2085	2073
Mid Level *(400-700 hPa)*		
Accuracy *(m/s)*	5.42	5.79
Precision *(m/s)*	3.40	3.47
Speed bias *(m/s)*	0.81	0.53
Speed *(m/s)*	18.85	17.93
Sample	2071	1190
Low Level *(700-1000 hPa)*		
Accuracy *(m/s)*	4.81	5.10
Precision *(m/s)*	3.13	3.16
Speed bias *(m/s)*	0.66	1.28
Speed *(m/s)*	12.56	12.47
Sample	512	597

Comparisons of Metop-B/C AVHRR DMW Products to Radiosonde Wind Observations

Table 31 shows the DMW product validation results for the time period March 24-31, 2021, using collocated 00 and 12 UTC radiosonde wind observations as reference/ground truth. These tables include the accuracy and precision metrics and speed bias metric, which is of particular interest to the NWP user community.

Table 31 Metop-C DMW (band 4; 10.8um) product validation results for the time period November 28 – December 26, 2021.

All Levels *(100-1000 hPa)*	**Metop-B**		**Metop-C**	
	Arctic	**Antarctic**	**Arctic**	**Antarctic**
Accuracy *(m/s)*	5.54	5.89	5.84	5.28
Precision *(m/s)*	3.20	3.71	3.39	2.94
Speed bias *(m/s)*	-0.06	-0.04	0.24	-0.57
Speed *(m/s)*	11.84	13.60	13.81	13.03
Sample	4164	1579	3416	2401
High Level *(100-400 hPa)*				
Accuracy *(m/s)*	5.81	6.34	6.17	5.51
Precision *(m/s)*	3.40	3.87	3.70	3.06
Speed bias *(m/s)*	-0.30	-1.66	-0.59	-0.83
Speed *(m/s)*	18.22	22.88	18.42	19.67
Sample	1343	357	1507	813
Mid Level *(400-700 hPa)*				
Accuracy *(m/s)*	5.68	5.07	5.50	5.04
Precision *(m/s)*	3.14	3.13	3.00	2.96
Speed bias *(m/s)*	-0.01	-0.43	1.33	-0.76
Speed *(m/s)*	12.23	13.22	12.87	11.27
Sample	671	578	776	760
Low Level *(700-1000 hPa)*				
Accuracy *(m/s)*	5.32	6.37	5.63	5.26
Precision *(m/s)*	3.07	3.97	3.49	2.79
Speed bias *(m/s)*	0.06	1.21	0.60	-0.14
Speed *(m/s)*	7.74	8.80	8.31	8.11
Sample	2150	644	1133	828

4.6 Error Budget

The DMW products are considered validated at the 100% level if the overall accuracy and precision of the wind product satisfies the specified accuracy and precision requirements specified within the appropriate satellite series requirement documents.

5 PRACTICAL CONSIDERATIONS

5.1 Numerical Computation Considerations

The pattern matching performed by the DMWA is the most computationally expensive aspect of the entire derivation process. It is natural then to focus on this step when considering ways to improve the overall performance of the algorithm.

Major efficiency upgrades have recently been made to the tracking portion of the AMV algorithm resulting in a 25% improvement in the processing times. One recent upgrade, the spiral search, terminates the sum-of-squared differences (SSD) calculation early once a current minimum value has been exceeded. The rationale for terminating the summation early is that any additional calculations would simply increase the summation value above the current minimum.

A second implemented upgrade has been to begin the search for the minimum SSD value at the forecast location and "spiral" outwards instead of starting at the top left corner of the search region where the SSD value is typically much larger. This has the effect of establishing a low threshold right from the start so that the SSD calculation can be terminated earlier resulting in fewer calculations.

5.2 Programming and Procedural Considerations

The current version of the DMWA includes a large data buffer that holds information (radiance, brightness temperature, cloud mask, etc) from adjacent line segments (also called swaths). Such a buffer makes it possible for the algorithm to track features that move out of the domain of the middle line segment, which is the only part of the buffer being processed for targets. With each new line segment read in, data in the buffer is shifted upwards so that the “oldest” data is always at the top of the buffer while the new segment data is added to the bottom of the buffer. This involves a substantial amount of copying from one segment of the buffer to another. It is anticipated that future versions of the algorithm will not have this buffer, as it is expected that the processing framework provided by the AIT will take care of this task. This will greatly simplify the algorithm and should significantly improve its performance.

The current version of the algorithm is also limited to processing three images of equal size. These limitations will need to be addressed in future versions. In addition to adding flexibility to the algorithm, having the ability to process images of varying size (mixing and matching) will improve the timeliness of the product.

As required by the AIT, a common variable type declaration statement has been used while writing the AMV algorithm.

5.3 Quality Assessment and Diagnostics

The following information should be monitored/trended for diagnosing the quality of the derived motion wind product:

Number of total targets attempted
Number of good winds generated
Percent of winds retrieved with specified QA flag values
Mean, Min, Max and StdDev of derived wind speed
Percent of retrievals with a QA flag value for specified atmospheric layers
Mean, Min, Max, and StdDev cloud height for specified atmospheric layers

5.4 Exception Handling

Exception handling is required for the development of robust and efficient numerical software. Requirements set forth by the AIT also stress the importance of exception handling. The main modules of the DMW program (target_selection.f90 and feature_tracking_utils.f90) use AIT-provided subroutine for error messaging.

For the most part, the DMWA assumes that all necessary image, forecast and ancillary data are available through the processing framework. The only data that the algorithm explicitly checks for is the temporal brightness temperature data, which is necessary for the tracking portion of the algorithm. If the temporal data is unavailable, the algorithm outputs an error message and control is returned to the processing framework.

As part of the target selection process, the DMWA checks for missing or unrealistic values within both the target and search regions. These values are specified in Section 3.4.2.1.1 (see Channel Validity Test). If either condition is met, the algorithm will flag the scene as bad and proceed to the next adjacent scene.

5.5 Algorithm Validation

Validation of the DMW products requires collocated measurements of reference ("truth") atmospheric wind values for the full range of ABI observing geometry and environmental conditions. From these collocated measurements, comparison metrics can be calculated that characterize the agreement between the satellite-derived DMWs and the reference values.

During the pre-launch phase of the GOES-R program, the product validation activities are aimed at characterizing the performance and uncertainties of the DMW products resulting from parameterizations and algorithmic implementation artifacts. During this phase, there is total reliance on the use of GOES-R ABI proxy and simulated datasets as described in Section 4.1. Post-launch validation will apply lessons learned to inter-comparisons of actual DMW products generated from real ABI measurements and reference ("ground-truth") wind observations. Validation methodologies and tools

developed and tested during the pre-launch phase will be automated and applied. More specific details on DMW product validation activities can be found in the Product Validation Document for the DMW product.

6 ASSUMPTIONS AND LIMITATIONS

The following sections describe the limitations and assumptions used in the current version of the DMWA.

6.1 Algorithm Performance

The following assumptions have been made in developing and estimating the performance of the DMWA.
ABI pixel level channel data (for each line segment) from all three images in the sequence are available along with accompanying meta-data (latitude, longitude, solar and local zenith angles, image scan times, quality flags). It is further assumed that the processing framework will handle any preprocessing needed to account for channel imagery whose resolutions may differ
Forecast temperature and wind profiles, surface skin temperature, and surface pressure are available and made available to the DMWA through the processing framework
The pixel level ABI cloud mask, cloud-top pressure, cloud-top temperature, estimated cloud height retrieval error, and cloud height quality flag(s) corresponding to each image in the image sequence are available through the processing framework
DMWA products are validated with reliable ground-based wind measurements and/or winds from a NWP model forecast/analysis
Proxy datasets and simulated ABI radiance fields from NWP models provide a suitable surrogate for estimating the DMWA performance/verification

6.2 Sensor Performance

It is assumed the GOES-R ABI sensor will meet its specifications as documented in the ABI PORD (417-R-ABIPORD-0017).

6.3 Pre-Planned Product Improvements

While development of the baseline DMWA continues, we expect to focus on the following issues.

6.3.1 Improve the Link between Pixels Dominating the Feature Tracking Solution and Target Height Assignment

Target height assignment has been identified as a major source of error for the DMW products. Deriving a representative height that is consistent with, and has ties to, the features being tracked is the goal of an upgraded wind derivation process. Studying and improving the link between the features being tracked and the heights assigned to these features is the major focus of this future effort.

6.3.2 Quality Control Indicators

The quality control indicators attached to each DMW vector are important to the users of these products. Proper interpretation and application of these quality control indicators helps the user community make optimal use of the DMW products. As such, improving these quality control indicators so that they more accurately represent the integrity and accuracy of the DMW product is vital. Of particular interest by the NWP community is a quality indicator that provides information about the estimated accuracy of the height assignment associated with the derived motion wind products. This will be an area of future study.

7 REFERENCES

Baum, Bryan , P. Yang, Yang, Ping; Heymsfield, Andrew J.; Platnick, Steven; King, Michael D.; Hu, Y.-X., and Bedka, Sarah T., 2005: Bulk scattering properties for the remote sensing of ice clouds, part II: Narrowband models. *Journal of Applied Meteorology*, Volume **44**, Issue 12, pp.1896-1911.

Berger, H., C. Velden, J. Daniels and S. Wanzong, 2008: Assessing the 'Expected Error' as a potential new quality indicator for atmospheric motion vectors. 9th International Winds Workshop, Annapolis, MD. Available online at: http://www.eumetsat.int/Home/OldWhoWeAre/Conference_and_Workshop_Proceedings/SP_1217939522789?l=en

Coakley, J.A, and F.P. Bretherton, 1982: Cloud cover from high resolution scanner data: Detecting and allowing for partially filled fields of view. *J. Geophys. Res.*, **87**, 4917−4932.

Daniels, J. and W. Bresky, 2010: A New Nested Tracking Approach for Reducing the Slow Speed Bias Associated With Atmospheric Motion Vectors (AMVS). Proceedings of the 10th International Winds Workshop, Tokyo, Japan.

EUMETSAT, 2005: The EUMETSAT wind vector automatic quality control scheme. EUM/OPS/TEN/05/1747, 10 pp.[Available online at http://www.eumetsat.int/Home/Main/Publications/Technical_and_Scientific_Documentation/Technical_Notes/SP_1124282585834?l=en .

Gustaffson J. and M. Lindberg, 1999: CMW low-level height assignment. Proc. EUMETSAT Satellite Data Users' Conf., Copenhagen, September 1999

Hamada, T., 1983: On the optimal time-interval of satellite image acquisition for operational cloud motion wind derivation. *Meteorology Center of Japan Meteorological Agency Tech. Note 7*, 79–87.

Hansen, M., R. DeFries, J.R.G. Townshend, and R. Sohlberg (1998), UMD Global Land Cover Classification, 1 Kilometer, 1.0, Department of Geography, University of Maryland, College Park, Maryland, 1981-1994.

Holmlund, K., 1998: The utilization of statistical properties of satellite-derived atmospheric motion vectors to derive quality indicators. *Weather and Forecasting*, Volume **13**, Issue 4,pp.1093-1104.

Holmlund, K, C. Velden, and M. Rohn: 2001: Enhanced automated quality control applied to high-density satellite-derived winds. *Monthly Weather Review*, Volume **129,** Issue 3, pp.517-529.

Huang, Allen and M. Goldberg, 2008: Overview of GOES-R Analysis Facility for Instrument Impacts on Requirements (GRAFIIR) planned activities and recent progress. *GOES Users' Conference*, 5th, New Orleans, LA, 20-24 January 2008. American Meteorological Society, Boston, MA, 2008, Manuscript not available for publication.

Jedlovek, G. and R. Atkinson, 1998: The Marshall automated wind algorithm: Error analysis, quality control and climate applications. *Proceedings 3rd International Winds Workshop,* Saanenmoser, Switzerland, pp. 247-254.

Lakshmanan, V., K. Hondl, and R. Rabin. 2009a: An efficient, general-purpose technique for identifying storm cells in geospatial images. J. Ocean. Atmos. Tech., 26, 523-537.

Lakshmanan, V. and T. Smith, 2009b: Data mining storm attributes from spatial grids. J. Ocean. Atmos. Tech, 26, 2353-2365.

Lakshmanan, V., R. Rabin, and V. DeBrunner, 2003: Multiscale storm identification and forecast. J. Atmos. Res., 67, 367-380.

LeMarshall, J. A., A. Rea, L. Leslie, R. Seecamp, and M. Dunn, 2004: Error characterization of atmospheric motion vectors. *Aust. Meteor. Mag.*, **53**, 123-131

Menzel, W.P., 1996: Report from the working group on verification statistics. *Proceedings 3rd International Winds Workshop,* Ascona, Switzerland, 10-12 June 1996, Pages 17-19.

Merrill, R.T., 1989: Advances in the automated production of wind estimates from geostationary satellite imagery. Preprints, *Fourth Conf. on Satellite Meteorology and Oceanography*, San Diego, CA, Amer. Meteor. Soc., 246−249.

Merrill, R.T., W. P. Menzel, W. Baker, J. Lynch, and E. Legg, 1991: A report on the recent demonstration of NOAA's upgraded capability to derive cloud motion satellite winds. *Bull. Amer. Meteor. Soc.*, **72**, 372–376.

Minnis P., P. Heck, D. Young, C. Fairall, and J. Snider, 1992: Stratocumulus cloud properties derived from simultaneous satellite and island-based instrumentation during FIRE. *J. Appl. Meteor*., **31**, 317-339.

Nieman, S.J., W.P. Menzel, C. Hayden, D. Gray, S. Wanzong, C. Velden, and J. Daniels, 1997: Fully Automated Cloud-Drift Winds in NESDIS Operations. *Bull. Amer. Meteor. Soc.*, **78**, 1121–1133

Nieman, S.J., J. Schmetz, and W.P. Menzel, 1993: A comparison of several techniques to assign heights to cloud tracers. *J. Appl. Meteor.*, **32**, 1559−1568.

Otkin, J. A., D. J. Posselt, E. R. Olson, H.-L. Huang, J. E. Davies, J. Li, and C. S. Velden, 2007: Mesoscale numerical weather prediction models used in support of infrared hyperspectral measurements simulation and product algorithm development. *J. Atmospheric and Oceanic Tech.*, 24, 585-601.

Otkin, J. A., and T. J. Greenwald, 2008: Comparison of WRF model-simulated and MODIS-derived cloud data. *Mon. Wea. Rev.*, in press.

Rossow, W.B., F. Mosher, E. Kinsella, A. Arking, M. DeBois, E. Harrison, P. Minnis, E. Ruprecht, G. Seze, C. Simmer, and E. Smith, 1985: ISCCP cloud algorithm intercomparison. *J. Climate Appl. Meteor.*, **24**, 877–903.

Schmetz, J., P. Pili, S. Tjemkes, D. Just, J. Kerkmann, S. Rota, and A. Ratier, 2002: An introduction ot Meteosat Second Generation (MSG). *Bull. Amer. Meteor. Soc.*, **83**, 977-992.

Schmetz, J.K., K. Holmlund, J. Hoffman, B. Strauss, B. Mason, V. Gartner, A. Koch, and L. van de Berg, 1993: Operational cloud-motion winds from Meteosat infrared imagery. *J. Appl. Meteor.*, **32,** 1206-1225.

Schmit, T., M. Gunshor, W.P Menzel, J.Gurka,, J. Li, and A. Bachmeier: 2005 Introducing the next-generation advanced baseline imager on GOES-R. *Bull. Amer. Meteor. Soc.*, Volume **86**, Issue 8, pp 1079-1096.

Shenk, W. E., 1991: Suggestions for improving the derivation of winds from geosynchronous satellites. *Global Planet. Change*, **4**, 165–171.

Simmer, C., E. Raschke, and E. Ruprecht, 1982: A method for determination of of cloud properties from two dimensional histograms. *Ann. Meteor.*, 18, 130-132.

Trucco, Emanuele and Alessandro Verri, 1998: "Introductory Techniques for 3-D Computer Vision", Prentice Hall.

Wang, Zhipeng X. Wu, F. Yu, J.P. Fulbright, E. Kline, H. Yoo, T.J. Schmit, M. Gunshor, M. Coakley, M. Black, D. Lindsey, H. Qian, X. Shao, R. Iacovazzi, 2020: On-orbit calibration and characterization of GOES-17 ABI IR bands under dynamic thermal condition. *Journal of Applied Remote Sensing*, **14**(3), 26pp. https://doi.org/10.1117/1.JRS.14.034527

Velden, C.S., and K.M. Bedka, 2009: Identifying the Uncertainty in Determining Satellite-Derived Atmospheric Motion Vector Height Assignments. Weather and Forecasting, Volume 24, Issue 1, pp.76-86.

Velden, C., J. Daniels, D. Stettner, D. Santek, J. Key, J. Dunion, K. Holmlund, G. Dengel, W. Bresky, W.P. Menzel, 2005: Recent innovations in deriving tropospheric winds from meteorological satellites. *Bull. Amer. Meteor. Soc*., 86, 205-221.

Velden, C., D. Stettner, and J. Daniels, 2000: Wind vector fields derived from GOES rapid-scan imagery. *Proc.10th Conf. on Satellite Meteor. and Oceanogr*., Long Beach California, Amer. Meteor. Soc., 20–23.

Appendix 1: Common Ancillary Data Sets

1. LAND_MASK_NASA_1KM

a. Data description

Description: Global 1km land/water used for MODIS collection 5
Filename: lw_geo_2001001_v03m.nc
Origin: Created by SSEC/CIMSS based on NASA MODIS collection 5
Size: 890 MB.
Static/Dynamic: Static

b. Interpolation description

The closest point is used for each satellite pixel:

Given ancillary grid of large size than satellite grid
In Latitude / Longitude space, use the ancillary data closest to the satellite pixel.

2. SFC_TYPE_AVHRR_1KM

a. Data description

Description: Surface type mask based on AVHRR at 1km resolution
Filename: gl-latlong-1km-landcover.nc
Origin: University of Maryland
Size: 890 MB
Static/Dynamic: Static

b. Interpolation description

The closest point is used for each satellite pixel:

Given ancillary grid of large size than satellite grid
In Latitude / Longitude space, use the ancillary data closest to the satellite pixel.

3. NWP_GFS

a. Data description

Description: NCEP GFS model data in grib format – 1 x 1 degree (360x181), 26 levels
Filename: gfs.tHHz.pgrbfhh
Where,
HH – Forecast time in hour: 00, 06, 12, 18
hh – Previous hours used to make forecast: 00, 03, 06, 09
Origin: NCEP

Size: 26MB
Static/Dynamic: Dynamic

b. Interpolation description

There are three interpolations are installed:

NWP forecast interpolation from different forecast time:

Load two NWP grib files which are for two different forecast time and interpolate to the satellite time using linear interpolation with time difference.

Suppose:

T1, T2 are NWP forecast time, T is satellite observation time, and
T1 < T < T2. Y is any NWP field. Then field Y at satellite observation time T is:

$Y(T) = Y(T1) * W(T1) + Y(T2) * W(T2)$

Where W is weight and

$W(T1) = 1 – (T-T1) / (T2-T1)$
$W(T2) = (T-T1) / (T2-T1)$

NWP forecast spatial interpolation from NWP forecast grid points. This interpolation generates the NWP forecast for the satellite pixel from the NWP forecast grid dataset.

The closest point is used for each satellite pixel:

1) Given NWP forecast grid of large size than satellite grid
2) In Latitude / Longitude space, use the ancillary data closest to the satellite pixel.

NWP forecast profile vertical interpolation

Interpolate NWP GFS profile from 26 pressure levels to 101 pressure levels

For vertical profile interpolation, linear interpolation with Log pressure is used:

Suppose:

y is temperature or water vapor at 26 levels, and y101 is temperature or water vapor at 101 levels. p is any pressure level between p(i) and p(i-1), with p(i-1) < p <p(i). y(i) and y(i-1) are y at pressure level p(i) and p(i-1). Then y101 at pressure p level is:

$$y101(p) = y(i-1) + \log(p[i] / p[i-1]) * (y[i] - y[i-1]) / \log (p[i] / p[i-1])$$